PARP1 Resolves DNA Replication Defects in PCNA-Associated DNA Repair Disorder



Lihao Wang

St Hugh's College

Nuffield Department of Medicine

University of Oxford

A thesis submitted for the degree of

Doctor of Philosophy in Clinical Medicine

Trinity Term 2019

PARP1 Resolves DNA Replication Defects in PCNA-Associated DNA Repair Disorder

Lihao Wang
St Hugh's College, University of Oxford, D.Phil, Trinity 2019

Abstract

Proliferating cell nuclear antigen (PCNA) is an essential cofactor for DNA replication and repair. The toroidal structure of a PCNA trimer makes it a sliding clamp protein, which utilizes its interdomain connecting loop (IDCL) interacting with PIP-box containing proteins to recruit these clients to sites of DNA replication to enable their functions. In 2014, the Crosby and Green laboratories reported a novel DNA repair disorder with clinical features including short stature, hearing loss, premature aging, telangiectasia, neurodegeneration, and photosensitivity, which results from a homozygous missense (p.Ser228Ile) alteration of PCNA so it is named PCNA-associated DNA repair disorder (PARD).

Previous structural studies have shown that the S228I alteration of PCNA results in a dramatic conformational change of the IDCL, and biochemical studies indicated a profound perturbation of PCNA's interaction with many of its interaction partners, including FEN1, LIG1, Cdt1, DNMT1 and XPG. Patient-derived cells exhibited marked abnormalities in response to UV irradiation, displaying substantial reductions in both UV survival and RNA synthesis recovery. However, no evidence for DNA replication defects has been found in these patient-derived cells. The aim of this thesis was to determine cellular pathways that are affected by the S228I alteration and to uncover mechanisms by which $PCNA^{S228I}$ cells tolerate the perturbed PCNA interactions in specific pathways.

An isogenic $PCNA^{S228I}$ knock-in hTERT RPE-1 cell line was generated using CRISPR-Cas9 technique. Phenotypes observed in patient-derived cells were recapitulated in the knock-in cell line. By applying survival assays with treatment of different chemical agents, we showed most DNA repair pathways unaffected, except that $PCNA^{S228I}$ cells were more sensitive to treatment with the PARP inhibitor olaparib than WT controls.

By comet assay as well as immunostaining of γH2AX, I showed that olaparib induced more DNA damage in cells with the $PCNA^{S228I}$ alteration, and FACS analysis showed perturbed cell cycle progression after PARP inhibition. By using an inhibitor of PARG, I detected high levels of PAR chains being formed at replication forks in $PCNA^{S228I}$ cells. Thus I proposed that the $PCNA^{S228I}$ mutation results in abnormal interactions between PCNA and key enzymes needed for normal Okazaki fragment maturation at replication forks. The resultant persistent single-strand breaks are processed via a back-up, PARP-dependent mechanism to ensure completion of lagging strand synthesis.

Overall, these data have implications both for the etiology of PCNA-associated repair disorder as well as suggesting novel circumstances in which PARP-inhibition might be of use in the cancer clinic.

Acknowledgements

First of all, I would like to say thanks to Dr Catherine Green for giving me the opportunity for doctoral studies in her laboratory, providing me with a fantastic environment to carry out scientific researches and being extremely supportive on every step I have moved forward. And this thesis would not exist without the guidance and advice of her.

Secondly, I would like to thank all of my colleagues in the Green's laboratory, both past and present, for being friendly and always helpful when I was in trouble. I want to thank Rose for collaboration in the $PCNA^{S228I}$ project, giving me lots of new ideas and helping me with new assays. I also want to thank Elsie, Daniela and Maciej for supportive advice. Also Mary – working with you is a real pleasure. I can't name everybody but I just want to say thanks to every member of the Green's laboratory. I would like to thank all the members of Chapman's laboratory, and especially Dr Ross Chapman, for giving me lots of helpful suggestions and creative ideas. I would also like to thank my joint supervisor, Professor Stephen Kearsey, for providing useful suggestions.

Importantly, I would like to thank my parents who are on the other side of the earth but always supportive on every decision I have made. I am grateful to all of my friends, both here in Oxford and back in China, for the company and emotional support. It is so lucky that I can always find someone when I need help.

Last but not least, I would like to say thanks to the China Scholarship Council as well as Nuffield Department of Medicine, University of Oxford for providing funding throughout my D.Phil study. I also want to thank my collaborator, Arnaud in Grigory's Laboratory, for acquiring fantastic data for comet assays for me.

I can't thank enough to everybody who has been mentioned above and also people that was not mentioned but did help me in any period of my life. The four years of doctoral study was an exciting journey with many memorable moments, and I feel really lucky that you are always around. Thank you.

Preface

This thesis is a collection of the research work undertaken by the author under the supervision of Dr Catherine Green and Professor Stephen Kearsey, University of Oxford from October 2015 to October 2019.

I declare that all results described in this thesis are original, though the work of others are clearly cited with appropriate references throughout. No part of this research has been submitted for a degree at the University of Oxford or any other University.

Some of the work described in this thesis has been published in the following paper:

Wilson, R. H., Biasutto, A. J., **Wang, L.**, Fischer, R., Baple, E. L., Crosby, A. H., ... & Green, C. M. (2017). PCNA dependent cellular activities tolerate dramatic perturbations in PCNA client interactions. DNA repair, 50, 22-35.

Contents

Abstract i

Acknowledgements ii

Preface iv

List of Figures x

List of Tables xiv

List of Abbreviations xv

Chapter 1: Introduction and literature review ..... - 1 -

1.1 DNA replication and repair ..... - 1 -

1.1.1 Process of DNA replication ..... - 1 -

1.1.1.1 Initiation of DNA replication ..... - 2 -

1.1.1.2 Elongation of DNA replication ..... - 4 -

1.1.1.2.1 Elongation on the leading strand ..... - 5 -

1.1.1.2.2 Elongation on the lagging strand ..... - 6 -

1.1.1.3 Termination of DNA replication ..... - 14 -

1.1.1.4 Post synthesis processes of DNA replication ..... - 16 -

1.1.2 DNA repair pathways ..... - 19 -

1.1.2.1 Single strand breaks (SSBs) and base excision repair ..... - 20 -

1.1.2.2 Bulky adducts and nucleotide excision repair (NER) ..... - 22 -

1.1.2.3 Double strand breaks (DSBs), non-homologous end joining (NHEJ) and homologous recombination (HR) ..... - 24 -

1.1.2.4 Interstrand crosslink (ICL) repair ..... - 27 -

1.1.2.5 DNA-protein crosslink (DPC) repair ..... - 29 -

1.1.2.6 DNA damage checkpoints ..... - 30 -

1.2 PCNA and its functions in DNA replication and repair ..... - 32 -
1.2.1 PCNA and its protein structure ..... - 33 -
1.2.2 PCNA-client interaction model ..... - 36 -
1.2.3 PCNA modifications ..... - 39 -
1.2.4 PCNA functions in DNA replication and repair ..... - 42 -
1.3 PCNA-associated DNA repair disorder (PARD) caused by a point mutation of PCNA p.Ser228Ile ..... - 48 -
1.3.1 PCNA variations among species ..... - 48 -
1.3.2 PCNA-associated DNA repair disorder ..... - 49 -
1.4 Functions of poly(ADP)ribosylation in DNA replication and repair ... - 52 -
1.4.1 Poly(ADP)ribosylation in DNA repair ..... - 53 -
1.4.2 PARP1 at replication forks ..... - 55 -
1.4.3 PARP inhibitors and cancer chemotherapy ..... - 58 -
1.5 Outline of Thesis ..... - 60 -
Chapter 2: Materials and Methods ..... - 62 -
2.1 Cell culture ..... - 62 -
2.1.1 Cell lines ..... - 62 -
2.1.2 Cell maintenance ..... - 62 -
2.1.2.1 Cell counting ..... - 63 -
2.1.3 Cell transfection ..... - 63 -
2.1.4 siRNA knock-down ..... - 64 -
2.1.5 Cell survival assay ..... - 65 -
2.1.6 FACS analysis ..... - 66 -
2.2 DNA analysis ..... - 67 -

2.2.1 DNA extraction ..... - 67 -
2.2.1.1 Bacteria ..... - 67 -
2.2.1.2 Cultured cells ..... - 68 -
2.2.2 Polymerase Chain Reaction (PCR) ..... - 69 -
2.2.3 Site-directed mutagenesis ..... - 71 -
2.2.4 DNA gel electrophoresis ..... - 73 -
2.2.5 DNA purification ..... - 73 -
2.2.5.1 DNA precipitation ..... - 73 -
2.2.5.2 DNA purification from agarose gels/PCR clean-up ..... - 74 -
2.2.6 DNA quantity determination and sequencing ..... - 74 -
2.2.7 Single-cell DNA gel electrophoresis (Comet assay) ..... - 75 -
2.3 DNA cloning ..... - 76 -
2.3.1 Restriction digestion ..... - 76 -
2.3.2 DNA ligation ..... - 76 -
2.3.3 Bacterial transformation ..... - 76 -
2.4 RNA analysis ..... - 77 -
2.4.1 RNA extraction ..... - 77 -
2.4.2 Reverse transcription of RNA into complimentary DNA (cDNA). - 78 -
2.5 Protein analysis ..... - 79 -
2.5.1 Whole cell extraction ..... - 79 -
2.5.2 Western blotting ..... - 80 -
2.5.3 Visualizing protein localization using immunofluorescence microscopy ..... - 81 -
2.5.4 Strep-tagged protein purification and mass spectrometry ..... - 84 -

Chapter 3: Construction of PCNA^{S228I} knock-in cell lines ..... - 85 -

3.1 Overview ..... - 85 -

3.2 Generation of PCNA^{S228I} knock-in cell lines through CRISPR-Cas9 technique ..... - 88 -

3.2.1 Constructing the targeting vector ..... - 89 -

3.2.2 Screening and clone genotyping ..... - 93 -

3.2.3 Phenotypic validation of PCNA^{S228I} knock-in cell lines ..... - 99 -

3.3 Discussion ..... - 107 -

Chapter 4: Cellular consequences of the PCNA^{S228I} mutation ..... - 111 -

4.1 Overview ..... - 111 -

4.2 S228I of PCNA is not a target of post translational modification ..... - 111 -

4.3 The PCNA^{S228I} mutation does not significantly affect the majority of cellular DNA repair pathways ..... - 112 -

4.4 PCNA^{S228I} cells are sensitive to Olaparib ..... - 115 -

4.5 Olaparib treatment generates DNA breaks in PCNA^{S228I} cells ..... - 117 -

4.6 Olaparib disrupts cell cycle progression in PCNA^{S228I} cells ..... - 119 -

4.7 Discussion ..... - 128 -

Chapter 5: The mechanism of olaparib sensitivity in PCNA^{S228I} cells ..... - 131 -

5.1 Overview ..... - 131 -

5.2 Olaparib sensitizes PCNA^{S228I} cells through inhibition of PARP1 function instead of PARP trapping ..... - 132 -

5.3 Perturbation in the repair of endogenous SSBs is not the reason for olaparib sensitivity in PCNA^{S228I} cells ..... - 134 -

5.4 PAR chains are detected at replication forks in PCNA^{S228I} cells ..... - 138 -

5.5 Discussion ..... - 145 -

Chapter 6: Discussion and future work ..... - 148 -

6.1 Discussion ..... - 148 -

6.1.1 PARP1-signalled alternative pathway for Okazaki fragment processing ..... - 150 -

6.1.2 PCNA^{S228I} and the pathology of PARD ..... - 151 -

6.1.3 PCNA^{S228I}-PARPi synthetic lethality and cancer chemotherapy- 154 -

6.2 Ongoing and future work..... - 156 -

Appendix A Karyotyping of hTERT RPE-1 cells ..... - 161 -

Appendix B Plasmid maps ..... - 162 -

Appendix C MFISH on knock-in RPE-1 cells ..... - 164 -

Appendix D Full Mass spectrometry results of PCNA ..... - 165 -

Appendix E Results of the survival assay against different damaging agents in lymphoblastoid cells..... - 166 -

Appendix F Results of DNA fibre assay upon PARGi treatment..... - 168 -

References..... - 169 -

List of Figures

Figure 1.1.2.2.2 Simplified process of lagging strand DNA synthesis ..... - 13 -

Figure 1.2.1 Crystal structure of PCNA in *S. cerevisiae* ..... - 34 -

Figure 1.2.2 Structure of human PCNA bound to PIP-box of p21 ..... - 38 -

Figure 1.3.2 $PCNA^{S228I}$ results in structural changes at the IDCL ..... - 51 -

Figure 1.4.1 The schematic representation of PARP1 and its domains.... - 54 -

Figure 3.2 The overall strategy of constructing $PCNA^{S228I}$ knock-in cell lines using CRISPR-Cas9 technique..... - 89 -

Figure 3.2.1A Assembly of the homology arm ..... - 91 -

Figure 3.2.1B Sequencing result of PAM removal site-directed mutagenesis..- 91 -

Figure 3.2.1C BspHI-NheI double digestion after site-directed mutagenesis to introduce the S228I mutation in the plasmid of HDR template..... - 92 -

Figure 3.2.1D The map of the HDR template vector ..... - 92 -

Figure 3.2.2A Primers designed for genotyping PCR of the knock-in clones...- 94 -

Figure 3.2.2B Genotyping results of some of the clones of WT ..... - 95 -

Figure 3.2.2C Genotyping results of some of the clones of S228I ..... - 96 -

Figure 3.2.2D Genotyping results of some of the clones of S228I ..... - 96 -

Figure 3.2.2E A proposed mechanism for the allele without PGK-Neo cassette recombination but containing S228I alteration ..... - 98 -

Figure 3.2.2F Sequencing result of the cDNA of the clone $S228I_{50\text{-}18}$ ..... - 98 -

Figure 3.2.3A Anti-PCNA Western blot of the whole cell lysate of the knock-in cell lines..... - 100 -

Figure 3.2.3B Immunofluorescence of knock-in cell lines against PCNA- 101 -

Figure 3.2.3C FACS cell cycle analysis of $PCNA^{S228I}$ knock-in RPE-1 cells.....- 102 -

Figure 3.2.3D FACS cell cycle analysis of EBV-transformed lymphoblastoid

cells derived from affected individuals ..... - 103 -
Figure 3.2.3E Quantitative fluorescence microscopy of knock-in cells after EdU pulse incorporation..... - 104 -
Figure 3.2.3F Immunofluorescence microscopy of knock-in cells against Cdt1 or p21..... - 106 -
Figure 3.2.3G T3 cytotoxicity to PCNA^{S228I} knock-in RPE-1 cells..... - 107 -
Figure 4.2 Mass spectrometry analysis of PCNA^{WT} shows no detectable PCNA phosphorylation at Ser228 in the unchallenged condition.....- 113 -
Figure 4.3 HU cytotoxicity to PCNA^{S228I} knock-in RPE-1 cells .....- 115 -
Figure 4.4A Olaparib cytotoxicity to lymphoblastoid cells .....- 116 -
Figure 4.4B Olaparib cytotoxicity to PCNA^{S228I} knock-in RPE-1 cells .....- 116 -
Figure 4.4C PCNA inhibitor T3 and olaparib led to cell death synergistically ...- 117 -
Figure 4.5A Alkaline COMET assay was performed after 24 hr treatment of olaparib in lymphoblastoid cells .....- 118 -
Figure 4.5B Immunofluorescence against γH2AX was performed in RPE-1 cells treated with olaparib for 24 hours ..... - 120 -
Figure 4.6A FACS cell cycle analysis after 6 hr olaparib treatment in lymphoblastoid cells..... - 121 -
Figure 4.6B FACS cell cycle analysis after 24 hr olaparib treatment in lymphoblastoid cells..... - 122 -
Figure 4.6C Average cell cycle proportions in lymphoblastoid cells after 24 hr olaparib treatment..... - 123 -
Figure 4.6D1 FACS cell cycle analysis after 24hr olaparib treatment in RPE-1 knock-in cells ..... - 125 -
Figure 4.6E Western blot of RPE-1 and lymphoblastoid cells whole cell lysates harvested after 24 hr treatment of olaparib ..... - 128 -
Figure 5.2A Niraparib and veliparib cytotoxicity to RPE-1 knock-in cells - 133 -
Figure 5.2B Western blot of RPE-1 cells transfected with siRNA against PARP1

..... - 135 -
Figure 5.2C Olaparib cytotoxicity in PARP1 knock-down RPE-1 cells ... - 135 -
Figure 5.2D RPE-1 cell viability after PARP1 knock-down ..... - 136 -
Figure 5.3A H_2O_2 cytotoxicity to lymphoblastoid cells ..... - 137 -
Figure 5.3B Results of comet assay showing the kinetics of DNA repair after H_2O_2 treatment..... - 137 -
Figure 5.3C Olaparib cytotoxicity to RPE-1 knock-in cells with low O_2 incubation ..... - 139 -
Figure 5.4A1 Two color flow cytometry, analyzing DNA content and the PARylation level ..... - 140 -
Figure 5.4A2 Two color flow cytometry, analyzing DNA content and the PARylation level ..... - 141 -
Figure 5.4B Immunofluorescence against PAR chains was performed in RPE-1 knock-in cells ..... - 143 -
Figure 5.4C Immunofluorescence against PAR chains was performed in RPE-1 knock-in cells (zoomed in)..... - 144 -
Figure 5.4D PARGi cytotoxicity to $PCNA^{S228I}$ knock-in RPE-1 cells ..... - 144 -
Figure 5.5 The model explaining the sensitivity of $PCNA^{S228I}$ cells to PARP inhibition..... - 147 -
Figure 6.1.1 Anti-p21 Western blot of the whole cell lysate of the knock-in cell lines ..... - 154 -
Figure A FISH karyotyping results of the parental hTERT RPE-1 cells .. - 161 -
Figure B1 Map of pSpCas9(BB)-2A-GFP plasmid with sgRNA cloned .. - 162 -
Figure B2 Map of the PL452 plasmid containing the PGK-Neo selection cassette ..... - 163 -
Figure C MFISH karyotyping results on RPE-1 knock-in cells ..... - 164 -
Figure D Full Mass Spec result of PCNA ..... - 165 -
Figure E1 $PCNA^{S228I}$ lymphoblastoid cells are not significantly more sensitive to many DNA damaging agents except HU at high doses ..... - 166 -

Figure E2 PCNA^{S228I} lymphoblastoid cells are not significantly more sensitive to IR ..... - 167 -
Figure F PCNA^{S228I} cells show slower DNA replication progression upon PARGi treatment..... - 168 -

List of Tables

Table 1.2.4 Common PCNA-binding proteins in various cellular pathways- 47 -

Table 1.3.1 PCNA mutants in *S. cerevisiae* and their phenotypes..... - 49 -

Table 2.1.3 Amount of cells and reagents for RPE-1 transfection using FuGENE®6 according to the plate size ..... - 64 -

Table 2.2.2A Standard master mix for PCR using the Phusion High Fidelity DNA Polymerase..... - 70 -

Table 2.2.2B Standard thermocycling conditions for a routine PCR..... - 70 -

Table 2.2.3A 25µl master mix for QuickChange II XL site-directed mutagenesis ..... - 72 -

Table 2.2.3B Standard thermocycling conditions for QuickChange II XL site-directed mutagenesis..... - 72 -

Table 2.4.2 Master mix and reaction conditions for reverse transcription of RNA into cDNA..... - 79 -

Table 2.5.2 Primary antibodies used for Western blotting in this thesis.... - 81 -

Table 2.5.3 Primary antibodies used for immunofluorescence microscopy in this thesis ..... - 83 -

Table 3.2.2 Targeting efficiency of CRISPR-Cas9 knock-in RPE-1 WT controls and S228I mutation cell lines ..... - 95 -

Table 4.6A Cell percentages summary for each population in Fig. 4.6B - 123 -

Table 4.6B1 Cell percentages summary for each population in Fig. 4.6D1- 125 -

Table 4.6B2 Cell percentages summary for each population in Fig. 4.6D2- 126 -

List of Abbreviations

53BP1	TP53 binding protein 1
8-oxoG	8-oxoguanine
AGS	Aicardi-Goutières syndrome
AP	Abasic sites
APIM	AlkB homolog 2 PCNA interacting motif
ARS	Autonomous replication sequence
AT	Ataxia Telangiectasia
ATM	Ataxia Telangiectasia mutated
ATP	Adenosine Triphosphate
ATR	Ataxia Telangiectasia and Rad3-related protein
ATRIP	ATR-interacting protein
BER	Base excision repair
BRCA	Breast cancer type 1 susceptibility protein
BrdU	5-bromo-2'-deoxyuridine
CAF1	Chromatin assembly factor 1
Cdc	Cell division cycle
CDK	Cyclin-dependent kinase
Cdt1	Chromatin licensing and DNA replication factor 1
ChIP	Chromatin immunoprecipitation
CMG	Cdc45, MCM2-7 and the GINS complex
CPD	Cyclobutane pyrimidine dimer
CPT	Camptothecin
CRISPR	Clustered Regularly Interspaced Short Palindromic Repeat
CS	Cockayne Syndrome
CtIP	CtBP-interacting protein
CV	Crystal violet
DAPI	4′,6-diamidino-2-phenylindole
DDK	Dbf4-dependent protein kinase
DDR	DNA damage response
DMEM	Dulbecco's Modified Eagle Medium
DMSO	Dimethyl sulfoxide
DNA	Deoxyribonucleic acid
DNMT1	DNA (cytosine-5)-methyltransferase 1
dNTP	Deoxynucleoside triphosphate
DPC	DNA-protein crosslink
DSB	Double-strand break
EBV	Epstein-Barr virus
EdU	5-Ethynyl-2'-deoxyuridine
ES cell	Embryonic stem cell
EU	5-Ethynyluridine
ExAC	Exome Aggregation Consortium

FA	Fanconi anemia
FACS	Fluorescence Activated Cell Sorting
FEN1	Flap endonuclease 1
FISH	Fluorescence in-situ hybridization
FOA	5-fluoro-orotic acid
G1	Gap 1
G2	Gap 2
GG-NER	Global genome nucleotide excision repair
GINS	go, ichi, ni and san
GST	Glutathione S-transferase
HDR	Homology-directed repair
HR	Homologous recombination
HU	Hydroxyurea
ICL	Interstrand crosslink
IDCL	Interdomain connecting loop
IR	Ionizing radiation
LIG1	DNA Ligase 1
MCM	Minichromosome Maintenance
MEF	Mouse embryonic fibroblast
MLH	MutL homologs
MMC	Mitomycin C
MMR	Mismatch repair
MMS	Methyl methanesulphonate
MNNG	Methylnitronitrosoguanidine
MRN	MRE11-RAD50-NBS1
MSH	MutS homologs
NAD	Nicotinamide adenine dinucleotide
NER	Nucleotide excision repair
NHEJ	Non-homologous end joining
OGG1	Oxoguanine glycosylase 1
ORC	Origin recognition complex
PALB2	Partner and localizer of BRCA2
PAM	Protospacer adjacent motif
PAR	Poly(ADP-ribose)
PARD	PCNA-associated DNA repair disorder
PARG	PAR glycohydrolase
PARGi	PARG inhibitor
PARP	Poly(ADP-ribose) polymerase
PARPi	PARP inhibitor
PARylation	poly(ADP)ribosylation
PBS	Phosphate buffered saline
PCNA	Proliferating cell nuclear antigen
PIP box	PCNA-interacting protein box
pLI	probability of loss-of-function intolerance

Pol	DNA polymerase
pre-RC	pre-replicative complex
RER	Ribonucleotide excision repair
RFC	Replication Factor C
RNA	Ribonucleic acid
ROS	Reactive oxygen species
RPA	Replication Protein A
RPE	Retinal pigmental epithilium
RPMI	Roswell Park Memorial Institute
RRS	RNA synthesis recovery
S phase	Synthesis phase
SCF	Skp, Cullin, and F-box containing complex
SDM	Site-directed mutagenesis
SLE	Systemic lupus erythematosus
SNV	Single nucleotide variation
SPR	Surface Plasmon Resonance
SPRTN	Spartan
SSB	Single strand binding protein or Single-strand break
T3	3,3’,5-triiodothyronine
TC-NER	Transcription coupled nucleotide excision repair
TDP	Tyrosyl-DNA phosphodiesterase
TERT	Telomerase Reverse Transcriptase
TLS	Translesion DNA synthesis
Tus	Terminus utilization substance
UBZ	Ubiquitin-binding zinc finger
UDS	Unscheduled DNA synthesis
UHRF1	Ubiquitin-like, containing PHD and RING finger domains 1
USP	Ubiquitin Specific Peptidase
UV	Ultraviolet
XAB2	XPA binding protein 2
XP	Xeroderma Pigmentosum
XPV	Xeroderma Pigmentosum Variant
XRCC1	X-ray repair cross-complementing protein 1

Chapter 1: Introduction and literature review

1.1 DNA replication and repair

DNA carries all of the genetic information in eukaryotic cells. Therefore, it is of great importance for cells to copy their genome in an error-free manner to maintain genome stability while they are proliferating. In order to transmit the genetic information accurately and efficiently, cells rely on complicated mechanisms to regulate DNA replication spatially and temporally [1]. Meanwhile, eukaryotic cells have evolved multiple pathways of DNA repair to deal with DNA damage generated from endogenous cell activity including DNA replication, as well as exogenous factors that induce DNA damage [2]. Compromised DNA replication or failures of DNA repair will drive genome instability, which is one of the major hallmarks of tumorigenesis [3] and aging [4].

1.1.1 Process of DNA replication

The discovery, by Watson and Crick, of how two antiparallel DNA strands pair together and form a double helix structure, gave an insight into DNA replication as a semi-conservative process [5], which was further confirmed by Meselson and Stahl in 1958 [6]. During the process of DNA replication, both strands act as templates and duplicate themselves separately. This requires the unwinding of double stranded DNA into two separate single strands which template their own DNA synthesis to produce two identical strands. Generally, DNA synthesis

can be split into three steps: initiation, elongation and termination.

1.1.1.1 Initiation of DNA replication

In *E. coli*, DNA replication initiates at a single specific sequence, *oriC*, in the circular chromosome and continues bidirectionally [7]. The initiation factor DnaA recognizes and binds to the DnaA box sequence in *oriC* [8], which guides the helicase DnaB-DnaC complex to the origin and unwinds the double helix bidirectionally with the help of single strand binding protein (SSB) and topoisomerase gyrase [9]. The DnaB generates a special DNA structure for binding of primase DnaG [10], which synthesizes RNA primers for further elongation by the DNA polymerase III Holoenzyme. Thus, the key steps of prokaryotic replication initiation include the recognition of a replication origin and assembly of a pre-priming complex with the helicase as well as recruitment of factors for further elongation.

In eukaryotic cells, these steps are also important, though the initiation process is more complex. Replication initiates at multiple origins in eukaryotic chromosomes. In *S. cerevisiae*, the origins contain specific DNA sequences, the autonomous replication sequences (ARS), which were proven to be replication origins in 1987 [11]. The origin recognition complex (ORC) recognizes and binds to ARS elements [12] and initiates further assembly of the pre-replicative complex (pre-RC). Although fission yeast, *S. pombe*, also contains similar AT-rich segments recognized by ORC [13], removal of such AT-

stretches significantly reduced, but did not completely abrogate replication firing, indicating less dependence on specific ARS sequences [14]. The origin sequence in metazoans, however, is much less specific than that in yeast. In *X. laevis* egg extracts, the exogenous DNA of SV40 can even replicate without the virus origin [15], showing the lack of requirement for specific origin sequences in the embryonic system of *X. laevis*. The characteristics that define replication origins in mammalian cells are still being discussed, and although there is still a lack of agreement, origin specification is widely accepted to be influenced by local DNA structure and accessibility, chromosomal structures and nucleotide availability [16]. Commonly in all eukaryotes, the ORC forms complex with Cdc6 at replication origins, functionally similar to DnaA in prokaryotes [17]. The heterohexameric complex MCM2-7 is bound first by Cdt1 and loaded onto DNA with the collaboration of Cdt1 and ORC-Cdc6 complex [18] [19]. The ORC, Cdc6, MCM2-7 and Cdt1 form an initiation intermediate which is known as the pre-replicative complex (pre-RC). The assembly of pre-RC starts from end of mitosis and lasts for the whole G1 phase, which is suppressed afterwards once cells enter into S phase [20]. This cell cycle-dependent activity is regulated by Cdc28 in *S. cerevisiae* (the CDK1 homolog) through phosphorylation of ORC, downregulation of Cdc6 and nuclear exclusion of MCM2-7 complex so as to limit pre-RC assembly strictly to the G1 phase to avoid re-initiation of DNA replication [21]. In multicellular eukaryotes, geminin was found active in S and G2 phase, which interacts tightly with Cdt1 and thus blocks binding of MCM

complex to origins of replication to inhibit re-replication [22]. In the pre-RC, the helicase activity of MCM2-7 is still inactive. At the G1/S transition, MCM4 and MCM6 are phosphorylated by DDK [23] [24], which facilitates the recruitment of Cdc45 and subsequent binding of GINS complex as well as DNA polymerase ε (Polε) in a CDK-dependent manner [25]. At this point, the active DNA helicase complex is formed, which consists of Cdc45, MCM2-7 and the GINS complex and is termed CMG helicase. Therefore, during S phase the CMG complex unwinds DNA double strands and drives the progression of replication forks [26].

The initiation of replication is so important that its disruption will lead to severe human diseases. The Meier-Gorlin syndrome was reported to be caused by mutation of ORC1/4/6 in the ORC complex or Cdc6 or Cdt1 which are all pre-RC components. The clinical manifestations of this disorder are profound growth retardation with short stature, microcephaly, bilateral microtia and dwarfism [27]. An MCM4 truncated mutation was also found to be responsible for an immunodeficiency syndrome with adrenal failure and short stature [28].

1.1.1.2 Elongation of DNA replication

The enzymes that catalyse the synthesis of double stranded DNA from ssDNA templates are called DNA polymerases. All DNA polymerases require a free 3′-hydroxyl (-OH) group to catalyse the formation of the phosphodiester bond when adding a new nucleotide to the growing end of the newly synthesized DNA. Therefore, DNA polymerases synthesize DNA in the direction of 5′ to 3′

specifically [29]. During replication fork progression, the CMG helicase opens antiparallel DNA double strands in an ATP-dependent manner [30], which have to be copied in opposite directions: one in the 3′ to 5′ direction and the other in the 5′ to 3′ direction. Therefore, considering the directional specificity of DNA polymerases, the two antiparallel strands have to be replicated asymmetrically. In other words, on the strand that is opened in the 3′ to 5′ direction, termed the leading strand, the DNA synthesis is continuous, while on the strand opened in an opposite direction, termed the lagging strand, the DNA has to be synthesized in short, discontinuous segments [31]. The asymmetry of DNA replication results in different mechanisms of DNA synthesis on both strands.

1.1.1.2.1 Elongation on the leading strand

In prokaryotes, cells depend on primase DnaG and DNA polymerase III Holoenzyme to elongate the DNA synthesis on both strands. In eukaryotic cells, the Polα/primase complex functions as the primase on both strands but Polε is the exclusive polymerase on the leading strand in most contexts [32], though there is evidence that at replication origins Polδ primes the synthesis of leading strands and is handed over to Polε afterwards for the elongation [33]. An RNA-DNA primer is needed to be synthesized only once on the leading strand as Polε is then able to synthesize DNA continuously in the same direction of CMG helicase movement. The mechanism of primer synthesis will be discussed in the next section (Section 1.1.1.2.2). Polε has an extremely low error rate on

undamaged DNA because its catalytic subunit has both polymerase and 3′ to 5′ DNA exonuclease proofreading activity [34]. In *S. cerevisiae*, the Dpb2 subunit of Polε interacts with GINS in the CMG helicase. This recruits Polε to the replication fork and keeps Polε moving with the CMG helicase while synthesizing DNA on the leading strand [35].

Mutations in the catalytic subunit of Polε often cause predisposition of colorectal cancers in human populations. It has been reported that mutations such as V411L, L424V and Y458F in the proofreading domain of Polε catalytic subunit lead to familial colorectal adenomas and carcinomas [36] [37]. Besides, a truncated mutation of amino acids 683-2286Δ of Polε catalytic subunit, losing its polymerase domain, was reported to cause developmental disorders with manifestations of intrauterine growth restriction, metaphyseal dysplasia, adrenal hypoplasia congenita, genital anomalies and immunodeficiency [38]. These indicate that functions of Polε is crucial to maintain genome stability as well as regulations of individual development.

1.1.1.2.2 Elongation on the lagging strand

On lagging strands, as was discussed above, DNA polymerases have to add new nucleotides in a direction opposite to that of the replication fork progression. Okazaki *et al*. proposed a discontinuous model to explain the asymmetry of the two strands synthesis, and detected nascent DNA fragments of 1000 to 2000 nucleotides during rapid replication in *E. coli* using ^{3}H-Thymidine labelling and

alkaline sucrose gradients [39] [40]. This nascent segment was named after the person who discovered it: the Okazaki fragment. In eukaryotic cells, however, these nascent fragments were shown to be much smaller, only 50 to 200 nucleotides [41] [42]. This difference in size was explained by a study in 2012 showing that the size of Okazaki fragments was determined by the size of nucleosome repeats in *S. cerevisiae*, suggesting a huge interconnection between Okazaki fragment synthesis and nucleosome assembly in eukaryotic cells [43]. DNA polymerases are unable to synthesize *de novo*, resulting in a requirement for priming for each Okazaki fragment synthesized. The mechanism of DNA lagging strand synthesis in prokaryotes was fully established in 1992 [44]. In *E. coli*, the primase DnaG is recruited by the helicase DnaB to synthesize RNA primers and initiate lagging strand synthesis before handing over to DNA Polymerase III Holoenzyme for the synthesis of Okazaki fragments. The prokaryotic single stranded DNA binding protein (SSB) is important during lagging strand synthesis as it stabilizes the ssDNA generated when the helicase extends in front of the active Okazaki fragment [45]. Once sufficient template is generated, an Okazaki fragment is initiated and elongated, displacing SSB, until they encounter the preceding Okazaki fragment. At this point DNA polymerase I is recruited, which removes the RNA primer using its nick translation activity and fills any gaps before fragment ligation by DNA ligase [46]. The process of prokaryote lagging strand synthesis highlights 3 important steps: (1) priming of the lagging strand synthesis, (2)

switching into DNA polymerases for Okazaki fragment elongation and (3) termination of Okazaki fragment synthesis and gap filling. In eukaryotes, different proteins with functionally equivalent activities are involved in similar processes.

The existence of RNA priming in eukaryotes was demonstrated by an elegant in vitro experiment using human lymphocyte lysates. This "nearest neighbour" method utilises the fact that a ^{32}P label from an exogenously supplied dNTP will transfer to a (2′)3′ ribonucleotide (and thus be released under alkaline lysis) only if the ribonucleotide is directly 5′ to the incorporated labelled dNTP [47]. The Polα-RNA primase complex, containing a primase subunit and another large p180 subunit with DNA polymerase activity, is known to initiate the *de novo* priming on both leading and lagging strands [48]. It has been reported in *S. cerevisiae* that Polα complex is recruited to and stabilized at replication forks through MCM10 after stimulation of CMG helicase [49]. And-1, the human homolog of Ctf4 in yeast, is loaded onto chromatin by MCM10 and further recruits the Polα complex for replication initiation [50]. Therefore, the Polε and Polα are both connecting with the CMG helicase, and this leads to the so-called trombone model enabling coordination of lagging and leading strand synthesis [51]. Structural studies of the human Polα complex revealed that the presence of the Polα polymerase subunit prevents the RNA primers from extending more than 10 ribonucleotides because of steric hindrance, which results in a

conformational change of the complex and switch from primase to Polα polymerase for DNA synthesis [52]. The primer-template DNA junction created by Polα is recognized and bound by Replication Factor C (RFC) in an ATP-dependent manner [53]. The RFC clamp loader interacts with amino acids 36-55 and 196-215 of human PCNA [54], and acts to open the PCNA sliding clamp trimer to enable the entry of DNA into the clamp [55]. The ATP hydrolysis catalytic subunits of RFC were reported to be essential for DNA replication: ATP hydrolysis is used to close the sliding clamp and enable processive DNA synthesis [56]. PCNA recruits DNA polymerase δ (Polδ) and greatly improves its processivity [57], which therefore competitively replaces the low-processivity Polα at the replication fork [58]. In addition, structural analysis has shown that yeast Polα has higher affinity to an RNA/DNA duplex, with its A-helix conformation. The elongation by Polα generates a B-form DNA double helix which has less affinity for Polα, leading to its dissociation [59]. Therefore, the combination of the competition from RFC-PCNA-Polδ and the low affinity of Polα for duplex DNA per se contributes to the outcome that Polδ takes over from Polα for the elongation of Okazaki fragments. Replication Protein A (RPA), the eukaryotic single stranded DNA binding protein, also plays an important role in lagging strand synthesis. As is in *E. coli*, it coats the ssDNA generated by the progression of the replicative helicase to stabilize and protect it. An interaction between RPA and RFC also helps to guide the clamp loader to the primed template structure for the Polα-Polδ handover [60].

Human Polδ contains 4 subunits: PolD1p125, PolD2p50, PolD3p66 and PolD4p12, with the 1-3 homologous to Pol3, Pol31 and Pol32 in *S. cerevisiae* [61]. In *S. cerevisiae* all 3 subunits of Polδ interact with PCNA to achieve high processivity for DNA replication [62]. The PolD1 in human, or Pol3 subunit in *S. cerevisiae*, is the catalytic subunit of Polδ, with functions of polymerase activity as well as 3′ exonuclease activity for proofreading. Similar to Polε, mutations in the proofreading domain of PolD1 such as S478N result in predisposition of colorectal cancers [36]. And patients with mutations in the polymerase domain of PolD1, i.e. R507C and S605del, were diagnosed with Werner Syndrome, with symptoms of premature aging, hearing loss and mandibular hypoplasia [63]. Interestingly, Polδ has strand displacement activity, generating flap structures when encountering the upstream RNA/DNA primers of the preceding Okazaki fragments. When this occurs the 3′ exonuclease activity inhibits over-displacement to keep the generated 5′ flap to a minimum size [64]. However, Polδ does not have flap endonuclease activity. RNaseH2 can degrade the 5′ RNA primers in eukaryotic cells, but this is a dispensable pathway for removal of RNA primers since deletion of RNase H in *S. cerevisiae* has only very subtle influences on cell viability and proliferation, suggesting the existence of an alternative pathway for primer removal [65]. Indeed, although first discovered in 1988 as a 5′ to 3′ exonuclease from HeLa cells able to remove RNA primers during SV40 *in vitro* DNA synthesis [66], Flap endonuclease 1 (FEN1) is now known as the key nuclease for removal of the 5′ flap before ligation of Okazaki

fragments in eukaryotic cells [67]. A free 5′ end is essential for FEN1 loading, as the binding of streptavidin at the 5′ end completely abrogated FEN1 binding and cleavage of unannealed tails [68]. Binding of streptavidin in the middle of unannealed single stranded DNA also prevented FEN1 cleavage, indicating that FEN1 has to traverse from the 5′ end of the single stranded flap to the annealed double stranded DNA where the cleavage occurs [68]. The majority of flaps shorter than 10 nucleotides are processed by this pathway, which is called the short flap pathway. However, Polδ occasionally goes into over-displacement for multiple reasons, such as lack of FEN1, when the flap grows to over 20 nucleotides and binds with RPA which prevents FEN1 loading. In this circumstance the Dna2 nuclease was found to trigger alternative pathways for Okazaki fragment processing, because overexpression of Dna2 in *S. cerevisiae* compensated for the phenotype of FEN1 deletion [69]. Dna2 was also reported to physically interact with FEN1 in HeLa cell extracts, indicating their functional association [70]. Dna2 acts to dissociate RPA from the single stranded flap and cleaves up to a terminal product flap length of about 5 nucleotides [71]. This length of flap is not sufficient for RPA binding and can be processed by FEN1. The Dna2 mediated pathway resolves flaps with length more than 20 nucleotides and is called long flap pathway. Both pathways of flap processing result in a nick between Okazaki fragments which can be sealed by DNA ligase I (LIG1) to generate continuous DNA double strands [72]. Noticeably, both FEN1 and LIG1 are PCNA binding proteins, and their PCNA binding capability

was reported critical for joining Okazaki fragments [73] [74], which indicates the importance of PCNA in Okazaki fragment processing. The F343AF344A (FFAA) mutant of FEN1 disrupts its PCNA interaction but retains its nuclease activities. The FFAA/FFAA knock-in mouse embryonic fibroblasts underwent slower DNA replication and division, and the FFAA/FFAA embryos displayed severe growth defect and finally led to newborn lethality [75]. This indicates the importance of PCNA-FEN1 interaction in DNA replication, and hence the growth and development of individuals.

The general process of DNA synthesis on lagging strands can be summarized in Fig. 1.1.2.2.2.

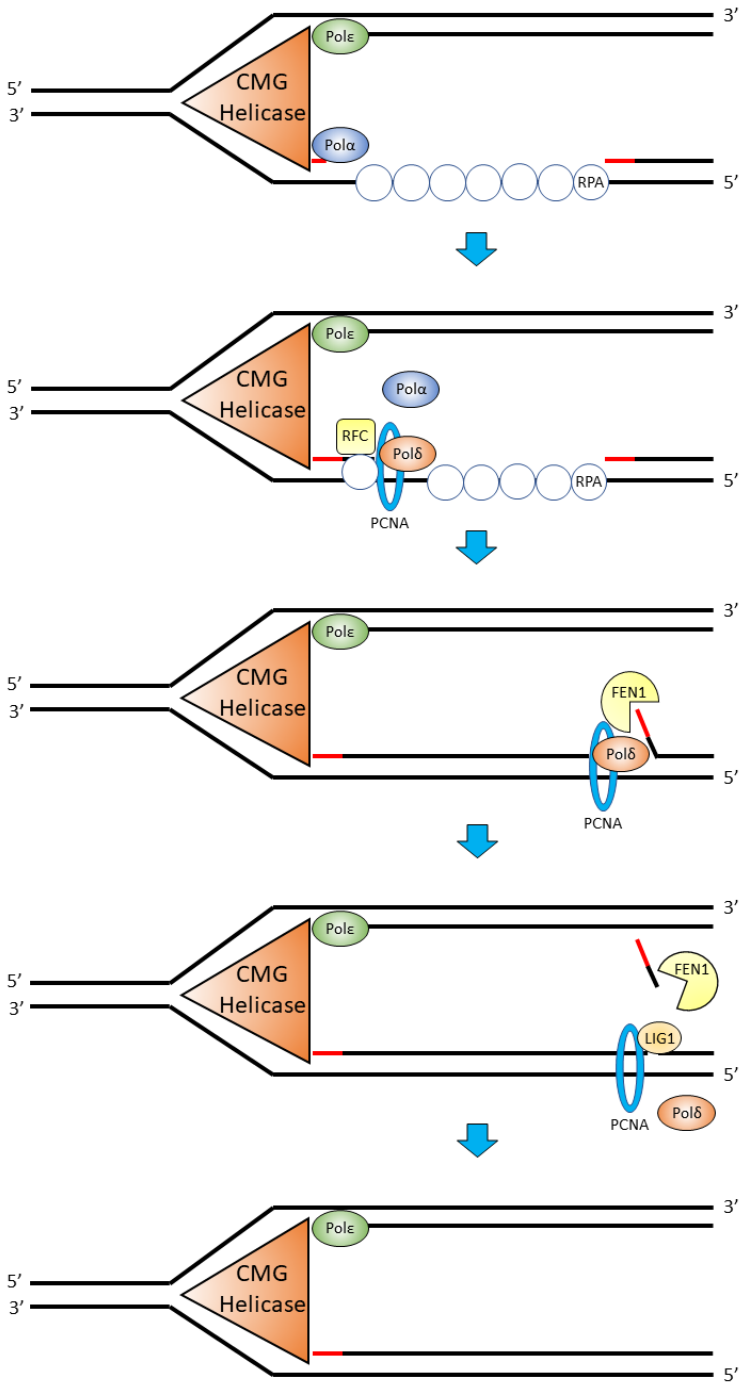


Figure 1.1.2.2.2 Simplified process of lagging strand DNA synthesis. The DNA strands are presented as black strand while the red strands indicate RNA primers.

1.1.1.3 Termination of DNA replication

When two congressing replication forks encounter each other during replication, the replisomes on both forks have to be dissembled to avoid re-replication and the DNA gaps between them have to be filled through processes similar to Okazaki fragment maturation. This process in DNA replication is termed termination [76]. In the circular *E. coli* chromosome, DNA replication initiates at *oriC* bidirectionally and two replication forks will encounter and terminate in a specific region opposite the origin. This region is flanked by ten polar *ter* sites which associate with the DNA replication terminus site-binding protein (Tus) to form oriented replication barriers [77]. The Tus-*ter* complexes block replication polarly, with the first five *ter* sequences allowing anticlockwise forks to pass but blocking the clockwise forks and vice versa [78]. This mechanism traps the two replication forks inside the termination region. However, the Tus-deleted strain was not observed to have any abnormal growth phenotypes [78], suggesting the Tus-*ter* system is not crucial for the termination machinery in prokaryotes. When two replication forks meet in wild type cells, a 3′ flap would be generated by the helicase function of DnaB, which, if not removed, would lead to re-replication at termination regions that was reported to be suppressed by Tus function [79]. Therefore, it is more likely that Tus-*ter* system functions as an inhibitor of re-initiation in the termination region of prokaryotes. DNA polymerase I with its 5′ to 3′ exonuclease activity is responsible for the gaping

filling and ligation process with similar mechanisms to Okazaki fragment processing in prokaryotes [80].

In eukaryotes, however, termination is more complicated because replication initiates at multiple origins on linear chromosomes and can terminate between these origins without the need for a specialized termination zone. This was confirmed by the deep sequencing of Okazaki fragments in budding yeast to determine fork merging zones in 2013 [81]. When two replication forks encounter each other, the CMG helicase on each leading strand will slide freely into the lagging strand of the converging fork. The MCM7 then becomes poly-ubiquitylated by SCF^{Dia2} or the $CRL2^{LRR1}$ ubiquitin ligases in *S. cerevisiae* and *X. laevis*, respectively [82] [83], which mediates the disassembly of CMG helicase through the Cdc48/p97 segregase. Notably, dissociation of the CMG helicase was found in *Xenopus* egg extracts to occur only after the ligation of two strands was completed, indicating that the CMG helicase dissociates from double stranded DNA and is not required for the completion of DNA synthesis [84]. Another question in eukaryotic termination is the gap filling process. When two replication forks congress, the leading strand will run into the 5′ end of the last Okazaki fragments of the other fork, and these strands need to be ligated. However, the leading strand polymerase Polε does not have strand displacement activity and is not able to cooperate with FEN1 for Okazaki fragment processing. It has therefore been proposed that Polε is removed from

the junction through interaction with the CMG helicase that moves forward into the converging lagging strand to make room for the Okazaki ligation machinery [85]. This event will have to be tightly regulated, as translocation of the CMG helicase onto an open 5′ flap of the incoming lagging strand will result in re-replication, as has been observed in *C. elegans* depleted of $CRL2^{LRR1}$ [86].

1.1.1.4 Post synthesis processes of DNA replication

DNA replication is more than DNA synthesis in eukaryotic cells, as there are post synthesis processes including error correction, DNA methylation and chromatin assembly and maturation.

DNA replication has an intrinsic basal error rate even if the DNA polymerases are of high fidelity, which is the main source of base mismatches in cells. This is because DNA polymerases do misincorporate incorrect nucleotides at a specific rate, and not all are detected by the proofreading exonuclease capacity. First proposed in the 1960s, the mismatch repair (MMR) is considered the main pathway in cells to deal with base mismatches arising after DNA replication [87]. The pathway involves two protein families: the MutS homologs (MSH) and the MutL homologs (MLH/PMS). The MSH complex and MLH/PMS complex recognize mismatches and initiate the 5′ and 3′ excision respectively, and EXO1 is the 5′ exonuclease that processes with MSH sliding clamp as well as digests the strand scissions resulting from activated MLH/PMS endonuclease [88]. After that, the gap filling DNA synthesis will also be processed by PCNA-Polε

machinery and eventually ligated through LIG1. MSH3 and MSH6 in the MSH complex are also PCNA binding proteins, showing the PCNA involvement in MMR (Section 1.2.4).

Apart from deoxynucleotides misincorporated by DNA polymerases, the abundant rNTPs in eukaryotes make ribonucleotides possibly the most common noncanonical nucleotides that are introduced into eukaryotic genome. In *S. cerevisiae*, for example, the cellular concentrations of rNTPs are 36- to 196-fold higher than their corresponding dNTPs, which largely increases the ribonucleotide incorporation rate of Polε to one rNMP per 1250 dNMPs, and Polδ one rNMP per 5000 dNMPs [89]. The persistence of ribonucleotides in the genome will lead to replicative stress and genome instability [90]. The ribonucleotide excision repair (RER) pathway is considered the most common eukaryotic pathway to remove ribonucleotides from the genome to maintain genome stability. Eukaryotic RER pathway is initiated by RNase H2, which recognizes the misincorporated ribonucleotides in the genome and incises the DNA 5′ to the ribonucleotide to generate DNA with 3′-hydroxyl and 5′-phospho-ribonucleotide ends [91]. This is therefore a similar substrate for Okazaki fragment processing machinery, in which Polδ catalyses the gap filling, with FEN1 excising 5′ flaps and LIG1 completing the ligation of strands. Importantly, the RNase H2B subunit directly interacts with PCNA, enabling the RNase H2 complex to scan the genome for ribonucleotides during the process of DNA

replication and enhancing the cleavage of ribonucleotides misincorporated in DNA duplexes as well [92]. Mutations in three subunits of RNase H2 in humans can result in Aicardi-Goutières syndrome (AGS), a neurological disorder with clinical manifestations of progressive microcephaly, spasticity, profound psychomotor retardation and altered interferon response [93]. This indicates the crucial role of RNase H2 in maintenance of genome stability.

Epigenetic maintenance is also important apart from faithful genetic inheritance during DNA replication. In mammalian cells DNMT1 is responsible for acting on hemimethylated CpG sites generated during DNA replication [94]. PCNA was found to interact with DNMT1 directly, coupling the maintenance of genomic methylation to the replication factories [95]. The highly transient interaction between PCNA and DNMT1 resolves the conflict of much slower turnover rate of DNMT1 compared to the replication speed [96]. However, the PCNA-binding deficient DNMT1 mutant was still able to restore methylation in DNMT1 knockout mouse ES cells, suggesting an alternative mechanism for recruiting DNMT1 [96]. Indeed, UHRF1 directly interacts with DNMT1 and the hemimethylated CpG sites as well as di- and trimethylated forms of histone H3K9 so can be responsible for tethering DNMT1 to the substrate [97] [98].

During DNA replication the chromatin must be assembled and epigenetic modifications on histones also require inheritance. The Chromatin assembly factor 1 (CAF1) assembles nucleosomes onto replicating DNA and regulates

histone modifications [99]. Depletion of CAF1 in human cells showed S phase arrest and slower DNA replication as well as defective chromatin assembly, suggesting that chromatin assembly mediated by CAF1 is crucial for human DNA replication [100]. PCNA also binds CAF1 directly [101], and mutant CAF1 defective for PCNA binding in *S. cerevisiae* displayed compromised nucleosome assembly activity, indicating that PCNA facilitates chromatin assembly during DNA replication by recruiting CAF1 [102].

1.1.2 DNA repair pathways

The integrity of DNA in cells is constantly challenged by endogenous metabolites and exogenous damaging agents. In order to maintain the genomic integrity, cells need to either remove the DNA damage through specific pathways, or activate checkpoints to arrest the cell cycle or even apoptosis if the damage is too serious to be repaired [103]. These repair pathways have to be coordinated with DNA replication because replication of damaged DNA or repair intermediates can lead to permanent changes to the nucleotide sequence (mutation). Cells have developed a variety of pathways to deal with different kinds of DNA damage, which are often dysfunctional in cancer cells and can be targeted for chemotherapy [2]. Here I will briefly introduce how cells response to different types of DNA lesions through a series of specific pathways.

1.1.2.1 Single strand breaks (SSBs) and base excision repair

DNA single strand breaks are usually not the direct consequence of damage agents, but are intermediates of base excision repair (BER) instead. Oxidative stress, or reactive oxygen species (ROS), can oxidize DNA bases. DNA bases can also be deaminated to generate uracil, and alkylated by drugs such as methyl methanesulphonate (MMS). Altered DNA bases are recognized and cleaved by DNA glycosylases, resulting in abasic (AP) sites in the DNA [104]. The AP sites are then further cleaved by APE1 endonuclease to generate one-nucleotide gaps as SSBs. These DNA SSBs can be sensed by PARP1/2 to catalyse ADP-ribosylation on itself as well as other acceptors at SSBs [105]. The poly(ADP-ribose) (PAR) chain recruits scaffold protein XRCC1 which further recruits DNA polymerase β (Polβ) and DNA Ligase 3 (LIG3) to initiate gap filling [106]. This is called short-patch base excision repair as it only replaces one nucleotide at a time. Alternatively, for example in the case when the AP sites are generated by the DNA glycosylase UNG2, the interaction between a glycosylase and PCNA results in the recruitment of Polδ which initiates base displacement synthesis for about 2-10 nucleotides [107]. Then PCNA recruits FEN1 to cut the 5′ flap as well as LIG1 to ligate the gap together, with very similar mechanisms to Okazaki fragment maturation [108]. This is called long-patch base excision repair as it replaces more than one nucleotide. The disruption of LIG1 with PCNA dramatically impaired the long-patch base

excision repair in human cells, suggesting an important function of PCNA in this pathway [74]. The SSB repair pathways are crucial for maintenance of genome stability. It was reported that an SSB repair defective cell line with XRCC1 mutation showed increased number of endogenous γH2AX and RAD51 foci which are markers for double strand break (DSB) signalling and repair [109]. This gives an idea that SSBs, if left unrepaired, can result in DSBs possibly from collapsed replication forks.

Defective BER pathways will lead to unrepaired DNA lesions or DNA repair intermediates that cause mutagenesis and genome instability when encountered by replication forks. A recent research showed that mutations in the SSB repair scaffold protein XRCC1 resulted in severe ocular motor apraxia, axonal neuropathy and progressive cerebellar ataxia [110]. Besides, hyperactivation of PARP1 was also observed in XRCC1 mutated cells, and the deletion of PARP1 rescued the loss of cerebellar neurons and ataxia in XRCC1-defective mice, suggesting a pathological relationship between the XRCC1 mutants and neurodegeneration through hyperactivation of PARP1. Mutations in OGG1, the oxoguanine glycosylase 1 responsible for removal of the 8-oxoguanine (8-oxoG) generated by ROS, are frequently found in human lung cancers [111]. And OGG1 knockout mice displayed significant lung tumorigenesis with accumulation of 8-oxoG in genome [112]. The unrepaired 8-oxoG, when encountered by DNA replication, leads to G to T and A to C

substitutions [113]. This indicates the importance for removal of endogenous base damages by BER to avoid mutagenesis.

1.1.2.2 Bulky adducts and nucleotide excision repair (NER)

UV-induced DNA damage leads to bulky DNA lesions such as cyclobutane pyrimidine dimers (CPDs). Environmental mutagens as well as some chemotherapeutic drugs like cisplatin can also result in similar helix-distorting structures [114]. When replication forks come across bulky DNA adducts, they have to bypass the lesion through translesion synthesis (TLS) pathway, in which the error free polymerases are switched into error-prone Y-family TLS polymerase such as Polη with the help of PCNA monoubiquitination. The mechanism of TLS pathway will be fully discussed in the following sections (Section 1.2.3 and Section 1.2.4). To eliminate the risks associated with TLS, these bulky adducts of DNA are usually processed prior to DNA replication by nucleotide excision repair pathways. NER can be initiated through two different pathways: global genome NER (GG-NER): initiated by recognition factor XPC-RAD23B anywhere in the genome where bulky DNA lesion is generated, and transcription-coupled NER (TC-NER): initiated when a transcribing RNA polymerase is stalled at a DNA lesion. This process requires the TC-NER specific factors including CSA, CSB and XAB2 [115]. Although initiated differently, the ultimate consequence of both GG-NER and TC-NER is recruitment of the core NER factors. The XPC-RAD23B directly interacts with

and recruits TFIIH complex which contains two helicase subunits XPB and XPD that open the DNA at bulky lesions [116]. Subsequently, XPA is recruited through interactions with TFIIH and XPC-RAD23B. XPA is considered a central component of NER complex, as it binds to TFIIH, XPC-RAD23B, RPA and ERCC1-XPF to form the pre-incision complex of NER. RPA binds and protects the undamaged DNA strand as well as helps recruit the two endonucleases, ERCC1-XPF and XPG to incise 5′ and 3′ of the DNA lesion on the damaged strand, respectively [117] [118]. Gap filling DNA synthesis will start after the 5′ incision has completed, which involves PCNA as well as Polε and Polδ and is eventually ligated to the 3′ end by LIG1 or XRCC1-LIG3 as soon as the 3′ incision is made by XPG in a FEN1-like manner [119]. PCNA was also reported to interact with XPG, which will be discussed in the following section (Section 1.2.4).

TC-NER, although initiated differently from GG-NER, shares very similar core NER complex with GG-NER, except that some GG-NER specific factors such as XPC are replaced by TC-NER specific factors including USP7 and XAB2 [120]. The TC-NER pathway prioritizes the maintenance of genomic integrity in regions of the genome undergoing the process of RNA synthesis.

Aberrant NER pathways can result in global bulky DNA lesions persisting in the genome, which subsequently have to be bypassed during DNA replication by error prone TLS pathway, increasing mutagenesis. Indeed, defective NER

pathways cause severe DNA repair disorders. Mutations in XP repair proteins which compromise the GG-NER pathway lead to the photosensitivity syndrome Xeroderma Pigmentosum (XP) [121]. The most prominent feature of the disease is extreme sensitivity to sunlight, with other symptoms including hearing loss and high risk of skin cancer. Although Polη is not an XP repair protein, its mutation can lead to similar symptoms of XP, called Xeroderma pigmentosum variant (XPV), because of defects in TLS pathways required for the bypass of bulky adducts during DNA replication [122]. On the other hand, mutations in CSA or CSB which affect the TC-NER pathway cause Cockayne syndrome (CS), with similar features of sunlight sensitivity but also other symptoms such as growth failure, eye abnormality, premature aging and neurodegeneration [123]. The relationships between many of the symptoms of CS and the DNA repair defects are still yet to be completely elucidated but they are thought to result from an inability to perform normal transcription when damage is present in active genes.

1.1.2.3 Double strand breaks (DSBs), non-homologous end joining (NHEJ) and homologous recombination (HR)

DNA double strand breaks (DSBs) are more dangerous than any of the other DNA damage in cells because they can lead to severe consequences including loss and rearrangement of chromosomes. Apart from various exogenous agents which directly cause DSBs, such as ionizing radiation (IR), all of the

unrepaired DNA damage of the other types can eventually turn into DSBs [124]. Nearly all DSBs are harmful, except for the physiological break generated during the processes of V(D)J recombination and class switch recombination in the immune system. NHEJ and HR are the two major pathways in eukaryotic cells to repair the DSBs.

NHEJ is an error-prone DSB repair pathway which can occur throughout the cell cycle. In NHEJ, DSBs are recognized and bound by the Ku70-Ku80 heterodimer (Ku) to protect the two ends from over-resection as well as to recruit other proteins for the joining of two ends [125]. Ku promotes binding of XRCC4-LIG4 complex to DSBs, which facilitates the joining of two blunt ends [126]. Processing enzymes such as DNA-PK with the endonuclease Artemis can be recruited to DSBs to initiate end processing and resection [127]. Template-independent polymerases like Polμ and Polλ also interact with Ku and function in NHEJ, and these are a major source of errors generated by this repair pathway [128].

HR, in comparison, is a more error-free DSB repair pathway which requires the presence of a homologous DNA donor, usually the sister chromatid in dividing cells [129]. During S-G2 phase, BRCA1 localizes to sites of DSBs through a signalling pathway involving the phosphorylation of H2AX Ser139 (γH2AX) and subsequent histone ubiquitination by RNF8-UBC13 and RNF168 [130] [131]. BRCA1 recruits CtIP and MRE11-RAD50-NBS1 (MRN) complex to initiate

extensive DNA end resection, generating 3′ single-stranded overhangs for recombination [132]. BRCA1 also interacts with PALB2 which brings BRCA2 to sites of DSBs, and BRCA2 recruits RAD51 which is loaded onto the single-stranded overhang to form recombinase filaments [133] [134]. The RAD51 recombinase filaments facilitates strand invasion into the homologous donor to form a D-loop intermediates and use the homologous donor as the template to synthesize the gap DNA and finally generate either crossover or non-crossover products [129]. Due to the synthesis using a homologous template, the HR is considered an error-free pathway for the repair of DSBs. There is also evidence that PCNA, recruiting Polδ to the D-loop formed by RAD51, is involved in the recombination-associated DNA synthesis [135]. The single ended DSBs coming from collapsed replication forks, usually triggered by prolonged fork stalling or replication encountering SSBs as was mentioned in Section 1.1.2.1, requires RAD51-dependent HR pathway to repair the breaks [136]. This indicates HR functions in response to replication stress.

Similar to other types of DNA repair pathways, defective in DSB repair pathways result in severe diseases and genome instability. It was reported that mutations in LIG4 or Artemis caused Radiosensitive severe combined immunodeficiency (RSSCID) due to aberrant NHEJ in the V(D)J recombination during B-cell maturation [137] [138]. Apart from disease in the immune system, mutations in XRCC4 can lead to microcephalic syndromes with facial dismorphism and short

stature but without recognizable immunological phenotypes [139], showing the importance of NHEJ pathway in development of individuals. Mutations in genes involved in HR, however, are more frequently seen in familial breast and ovarian cancers, especially BRCA1 [140]. This increases the genome instability for cancer predisposition, and on the other hand can be targeted for chemotherapy which will be discussed later (Section 1.4.3).

1.1.2.4 Interstrand crosslink (ICL) repair

Some chemical agents, including mitomycin C (MMC), nitrogen mustards, and all kinds of platinum based chemotherapeutic drugs, can covalently link two opposite DNA strands together, forming the interstrand crosslink (ICL) structure. This completely blocks DNA replication as the two linked strands are not able to be separated [141]. Therefore, ICLs can be extremely toxic if left unrepaired. Fanconi anemia (FA) is a chromosomal instability disorder with features of bone marrow failure, skeletal defects and cancer predisposition, as well as hallmarks of hypersensitivity to agents that induce ICLs [142]. Thus, the FA can be a perfect model to study ICL repair. Up till now, there are 22 FA complementation groups identified (subtypes A, B, C, D1, D2, E, F, G, I, J, L, M, N, O, P, Q, R, S, T, U, V, W) [143-152], and mutations in each of the FA genes can lead to specific FA phenotypes. These FA proteins function together in different aspects of the ICL repair and maintain chromosome stability. FANCM is responsible for recognizing DNA lesions of ICL [153], and then recruits other FA proteins

(A/B/C/E/F/G/L) to form an FA core complex [154]. The FA core complex is a large multisubunit ubiquitin ligase, with FANCL an E3 ubiquitin ligase working with UBE2T (FANCT) as the E2 to mono-ubiquitylate the downstream FANCD2 and FANCI [155]. The monoubiquitination of FANCD2-FANCI is thought to recruit and activate downstream proteins including TLS polymerase and HR proteins but its exact role still remains to be proven. FANCD2-FANCI monoubiquitination was also reported to be responsible for recruitment of XPF-ERCC1-SLX4 complex for the nucleolytic incision of the ICLs [156]. Apart from the FA signalling pathway, other FA proteins are also key proteins for various repair pathways, such as BRCA1 (FANCS), BRCA2 (FANCD1), PALB2 (FANCN) and RAD51 (FANCR) in HR pathway, REV7 (FANCV) involved in TLS, and XPF (FANCQ) in NER pathway. This indicates a collaborative mechanism of TLS, NER and HR pathways in repair of ICLs. The overall ICL repair starts from fork stalling at the ICLs and endonucleolytic incision occurs on both sides of ICLs catalysed by MUS81-EME1, XPF-ERCC1 and SLX1-SLX4 endonuclease complexes [157-159] to release the DNA lesion into a single strand. The unhooked DNA lesion is then bypassed through TLS pathway and repaired through NER pathway. Finally, the two single ended incised strands are processed by HR pathway using the replicated strand as homologous template. The involvement of multiple repair pathways for ICL repair suggests many other proteins in these pathways that are relevant in ICL repair, though they are not reported as FA proteins. PCNA is one of these important proteins

involved in ICL repair, with crucial functions in TLS polymerase transition, recruitment of XPG in NER as well as mediating all the gap filling synthesis in these repair pathways. Interestingly, PCNA was also reported to interact with FANCD2 [160], suggesting its potential function in bringing FANCD2 to the stalled replication fork at the ICL to initiate the repair, though the function of this interaction still remains elusive.

1.1.2.5 DNA-protein crosslink (DPC) repair

Apart from ICL, there are also other kinds of crosslinked DNA lesions, including intrastrand crosslinks and DNA-protein crosslinks (DPCs). Intrastrand crosslinks, such as CPDs caused by UV irradiation or cisplatin treatment, are resolved by TLS and NER pathway as was discussed previously (Section 1.1.2.2). DPCs are covalent DNA-protein interactions which can arise from the trapping of enzymes whose catalytic mechanisms include an intermediate that is covalently attached to DNA such as TOP1 or TOP2, or they can be generated by chemical crosslinking agents such as formaldehyde. Of note, DPC-like structures from stable but not covalent binding of proteins with DNA can also lead to similar consequences to DPCs [161]. DPCs are very toxic to cell viability as they completely block replication and transcription. DPCs can be repaired by direct hydrolysis of the covalent bond between DNA and proteins by Tyrosyl-DNA phosphodiesterase 1 (TDP1) or TDP2 for TOP1 or TOP2 trapping respectively [162], or by nucleolytic incision through MRN complex to induce

DSBs which are repaired by HR pathway [163], or by protease degradation of the crosslinked proteins catalysed by the metalloprotease SPRTN [164] [165]. Interestingly, SPRTN is also a PCNA binding protein with affinity to ubiquitylated PCNA [166], so PCNA is also involved in recruiting SPRTN to stalled replication forks for DPC processing. It was also reported that Y117C mutation of SPRTN causes the Ruijs-Aalfs syndrome characterized by progeroid phenotypes, genomic instability and susceptibility toward early onset hepatocellular carcinoma [167], supporting the importance of SPRTN in prevention of replication stress during DNA replication and maintenance of genome stability.

1.1.2.6 DNA damage checkpoints

DNA damage checkpoints are biochemical processes that delay or arrest the cell cycle progression as a result of detecting DNA damage [168]. ATM and ATR are two well-known sensors in the DNA damage checkpoint pathways. Mutation of ATM will result in severe DNA repair disorder Ataxia Telangiectasia (AT) [169]. AT is characterized by cerebellar degeneration, genome instability, immunodeficiency, clinical radiosensitivity and cancer predisposition. ATR is an essential gene, but hypomorphic mutation of ATR leads to Seckel syndrome characterized by intrauterine growth retardation, microcephaly, dwarfism and mental retardation [170]. ATM was found binding preferentially to DNA termini by atomic force microscopy [171], and its protein kinase activity is stimulated by agents that induce DSBs [172], indicating that ATM functions in response to

DSBs. The substrates of ATM include Chk2, p53, BRCA1 and itself. The autophosphorylation of ATM increases its kinase activity through conversion from oligomers to monomers [173]. In contrast, ATR was observed to have higher affinity for UV-induced DNA than undamaged DNA using assays for electrophoretic mobility shift [174], and its protein kinase activity was reported to be activated after UV irradiation [175], showing that ATR participates in signalling of UV-induced DNA damage. It is however reported that this activation is also due to the generation of RPA-coated ssDNA after this type of damage as ATR is activated by its activating partner ATRIP which is recruited to SSBs by interaction with RPA [176]. ATR is particularly important in signalling DNA damage arising from DNA replication forks, which regulates S phase progression and origin firing in this context. ATR shares many of the substrates with ATM, except that it phosphorylates Chk1 instead of Chk2 as a downstream effector [177]. Both Chk1 and Chk2 are protein kinases activated by phosphorylation, and they both phosphorylate the substrate Cdc25A, inactivating it by nuclear exclusion and ubiquitin-mediated proteasomal degradation [178]. Cdc25A is a phosphatase that drives the cell cycle by dephosphorylating downstream CDKs to induce their activation, regulating both the G1/S transition by CDK2 and CDK4 dephosphorylation and the G2/M transition by CDK1 dephosphorylation. Therefore, the ATM-Chk2-Cdc25A or the ATR-Chk1-Cdc25A signalling pathways lead to accumulations of phosphorylated inactivated form of CDKs and arrest the cell cycle. p53 is also

a substrate of both ATM and ATR. When p53 phosphorylation occurs as a result of the DNA damage signalling, p53 is stabilized by repressing MDM2-mediated degradation [179]. Thus, the accumulation of p53 by increasing levels of DNA damage signalling triggers the expression of p53 regulated genes such as p21, leading to cell cycle arrest (via CDK inhibition [180] and the inhibition of PCNA-dependent DNA synthesis [181]) or apoptosis. Of note, ATM phosphorylates H2AX at Ser139 (to generate γH2AX) to initiate the signalling of DSBs for their repair [182]. Therefore, γH2AX is often used as a marker for the presence of DNA breaks.

1.2 PCNA and its functions in DNA replication and repair

First discovered as being enriched in actively proliferating cells by an antibody from patients with systemic lupus erythematosus (SLE) [183] and identified as an auxiliary protein for Polδ [57] [184], the sliding clamp protein proliferating cell nuclear antigen (PCNA) is now widely known for its essential roles in the process of DNA replication and repair [185]. The human *PCNA* gene is located on Chromosome 20p12.3 (UCSC Genome Browser). It contains 7 exons and is abundantly expressed in proliferating cells. PCNA is very conserved throughout species, with 96.9% of sequence identity between human and mouse, 70.5% between human and drosophila, and even PCNA in human and *S. cerevisiae* has 35.2% of sequence identity with another 120 similar amino acid positions (Uniprot).

1.2.1 PCNA and its protein structure

PCNA is a member of DNA sliding clamp family, which are proteins of structural and functional similarity. The sliding clamp protein of prokaryotes is the β-subunit of DNA Polymerase III Holoenzyme, the structure of which was elucidated in 1992 [186]. From the crystal structure of the β subunit, it can be seen to form a head-to-tail dimer, with three topologically identical domains in each monomer, to form a ring-shaped pseudo-hexameric structure. The hole in the middle of the ring has a diameter of about 35Å which is large enough to accommodate DNA with diameter of about 25Å. Such a toroidal structure enables the β subunit to bind with αε polymerase in prokaryotes, sliding freely on replicating DNA so as to increase the processivity of DNA Polymerase III Holoenzyme as a common function of DNA sliding clamp family protein, which has been reported in 1991 [187].

Although eukaryotic PCNA and prokaryotic β subunit only share about 10% homology in sequence, their structures are strikingly similar. The crystal structure of *S. cerevisiae* PCNA was first determined in 1994 [188]. Similar to the β subunit, the overall structure of PCNA shows pseudo-hexameric symmetry (Fig. 1.2.1A). However, compared to the homodimer that forms β subunit, the sliding clamp PCNA is a homotrimer with each monomer containing two structurally identical domains which were termed Domain I (residues 1-117) and Domain II (residues 135-258). Each domain consists of 9 antiparallel

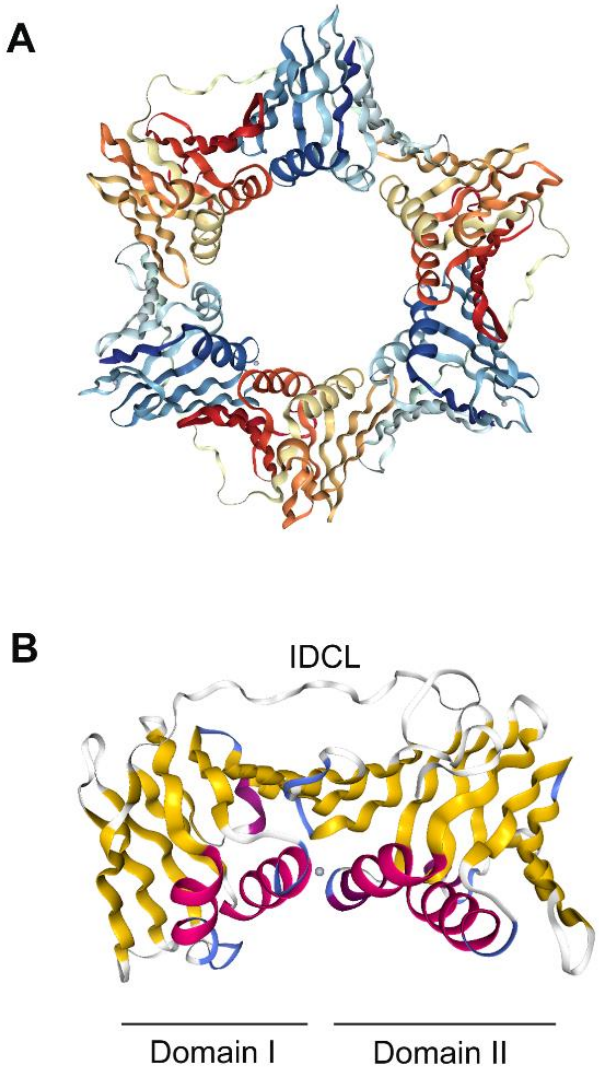


Figure 1.2.1 Crystal structure of PCNA in *S. cerevisiae* (PDB ID 1PLR). (**A**) Structure of PCNA sliding clamp homotrimer. (**B**) Structure of PCNA monomer. Domains are as indicated. Red colour stands for α helices and yellow colour stands for β sheets. Grey colour represents the connecting loop.

strands of β sheets connecting with two α helices in the inner surface of the ring, with nine lysine and arginine residues in or adjacent to the α helices to provide the electrostatic positive potential of the inner surface (Fig. 1.2.1B). This enables the PCNA sliding clamp to move stably on the DNA and prevents electrostatic hindrance with negatively charged phosphate backbones of DNA molecules. The crystal structure of human PCNA-DNA complex revealed that

side chains of PCNA interfacial residues (K20, K77, R149, H153, K217 and K80) form a right-hand spiral that closely matches the pitch of B-DNA and contact with five consecutive phosphates on DNA strands [189]. PCNA tilts at an angle of ~ 20° relative to the DNA fibre and rotates to contact with adjacent phosphates on DNA strands in one direction to keep the sliding orientation of PCNA. An interdomain β sheet in each monomer connects the last strand β sheet of Domain I and the first strand of Domain II (Fig. 1.2.1B). This is termed Interdomain connecting loop (IDCL) (residues 118-134). The IDCL of PCNA plays very important roles in PCNA-client interaction, which will be further discussed in the following section (Section 1.2.2). Similar to the β subunit, monomers of PCNA also interact head-to-tail to form the sliding clamp complex. The interaction is between two β sheets of the main domains, with 8 hydrogen bonds across the intermolecular surface. $PCNA^{S115P}$ is a yeast mutant that disrupts the intermolecular hydrogen bond and led to cold sensitivity for growth and DNA replication defects in *S. cerevisiae*, indicating the importance of the trimeric structure [190]. As was mentioned in previous sections, the loading of PCNA onto the replicating DNA needs to open and close the ring, which requires energy for the formation of the intermolecular hydrogen bonds (Section 1.1.2.2.2). The eukaryotic clamp loader RFC complex was reported to interact with amino acids 36-55 (Domain I) and 196-215 (Domain II) of closed human PCNA when bound with ATP [54]. The interaction of RFC with primed DNA stimulates its ATPase activity and the ATP hydrolysis causes conformational

changes that provide the energy for closing the sliding clamp and releases RFC from PCNA [191]. PCNA sliding clamp is then loaded and encircles the DNA to enable processive DNA replication. It was also proposed that PCNA may form a back to back double homotrimer complex in mammalian cells to explain for PCNA interactions with multiple clients simultaneously [192]. But I think this is unlikely to be true because the PCNA homotrimer doublets reported in this paper were never repeated in other researches. And the double trimer model explaining the PCNA multi-interactions has very little biological significance since transient and dynamic PCNA-client interactions was proposed, which will be discussed later (Section 1.2.2).

1.2.2 PCNA-client interaction model

As a sliding clamp protein, the main function of PCNA is to efficiently recruit its clients to sites of DNA synthesis during the processes of DNA replication and repair. PCNA was first discovered as an auxiliary protein for the processivity of Polδ [184]. Later, the cell cycle checkpoint regulator p21 was found to counteract PCNA-dependent DNA synthesis through direct interaction with PCNA in SV40 in the in vitro DNA replication system [181]. Further yeast two-hybrid screen revealed a C-terminal region of p21 interacting with PCNA IDCL, and peptide mapping by assays of ELISA and pull-down experiments found an 8 amino acid sequence QTSMTDFY (residues 144-151 of p21) to be critical for PCNA binding [193]. The structure of the C-terminal region of p21 interacting

with PCNA IDCL was determined in 1996 [194]. According to the crystal structure (Fig. 1.2.2), the Q144 of p21 binds in a small pocket of PCNA outer surface, and the residues 146-151 (SMTDFY) form a 3_{10} helical conformation in which T145 and S146 form hydrogen bonds with T148 and D149. This configuration puts M147, F150 and Y151 into a hydrophobic pocket of PCNA IDCL. The Y151 of p21 forms hydrogen bonds with Q131 and Y133 of PCNA IDCL.

Apart from p21, the interactions of PCNA with other clients were investigated in the following years, including FEN1 [195], LIG1 [196] and XPG [197]. The sequence alignment of the binding motif of these PCNA interacting proteins revealed a consensus sequence termed PCNA-interacting protein box (PIP box), with the protein sequence of Q-x-x-[ILM]-x-x-[FY]-[FY] [198]. The consensus sequence of the PIP box structurally indicates the common PCNA-client interaction pattern. The first glutamine binds in a small pocket of PCNA, while the fourth medium hydrophobic amino acid, usually I, L, or M, as well as the last two highly hydrophobic aromatic amino acid, usually F or Y, position in the hydrophobic pocket of PCNA IDCL. It has also been reported that some PCNA clients carry a PIP box with non-consensus sequence, such as Polη [199] and Srs2 [200]. The PIP boxes of these proteins, though non-consensus, structurally show canonical PIP box-IDCL interacting structure, with hydrophobic amino acids inserting into hydrophobic pockets of PCNA. An N-

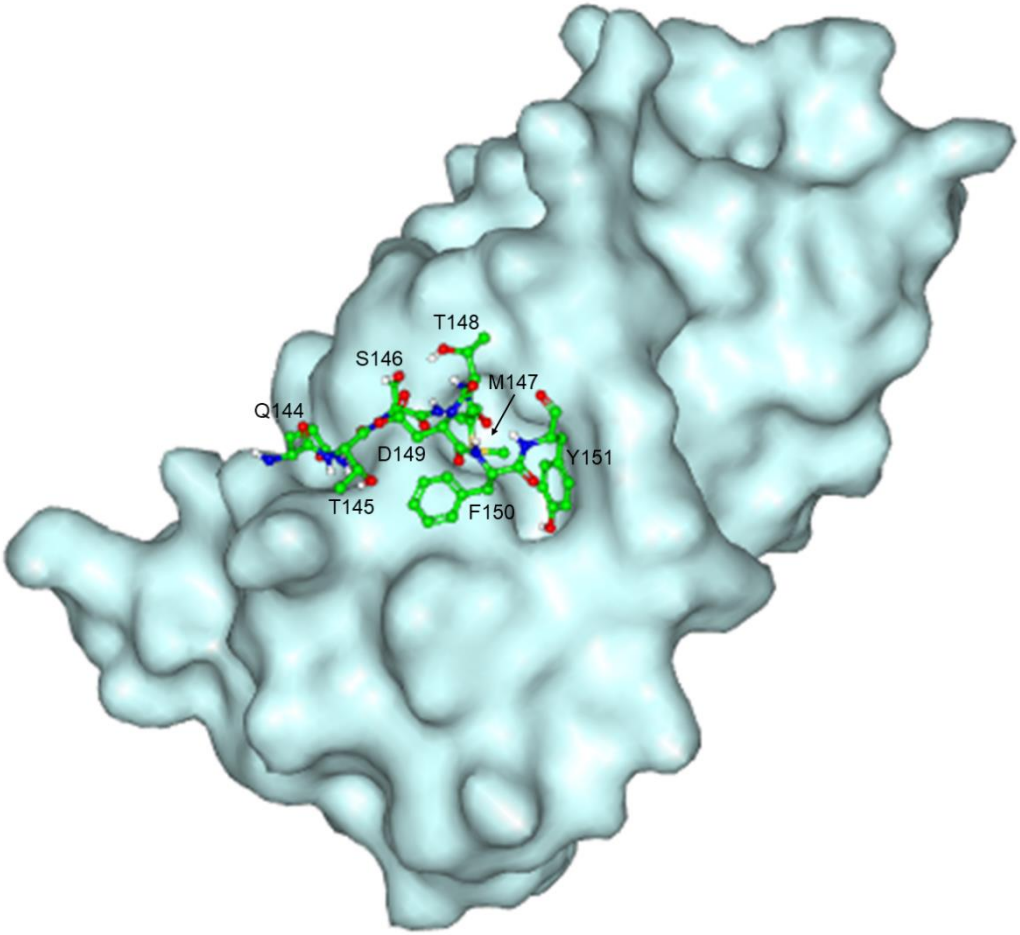


Figure 1.2.2 Structure of human PCNA bound to PIP-box of p21 (PDB ID 1AXC). The PCNA monomer is depicted in the surface representation (light blue), and the PIP-box of p21 is depicted in the stick representation (with carbon, oxygen, nitrogen, hydrogen and sulfur atoms coloured green, red, blue, white and yellow, respectively). The side chains of the p21 PIP-box are as indicated.

terminal KA box was also found flanking the PIP box of PCNA binding proteins in some cases, by screening a random peptide library for binding to PCNA [201]. Also, another PCNA binding motif, termed AlkB homolog 2 PCNA interacting motif (APIM), has been idendified in some PCNA partners. It was first discovered in the oxidative demethylase human AlkB homolog 2 (hABH2) with a sequence of [KR]-[FYW]-[LIVA]-[LIVA]-[KR] [202]. Interestingly, PIP boxes are often found in the N- or C-terminal unstructured regions of the PCNA clients, for

example, the N-terminal natively disordered domain of MSH6 forming a flexible tether to PCNA [203]. Therefore, the interaction between PCNA and clients is unlikely to affect the activity of clients, enabling PCNA to bring proteins to site in a sterically open way for activity.

Since PCNA interacts with its protein partners via its IDCL, it was previously assumed that in eukaryotic cells the three IDCLs in a PCNA trimer can interact with three protein partners simultaneously in a ‘toolbelt’-like manner as occurs on the archeal PCNA [204]. However, this model has been recently challenged by the demonstration that PCNA trimers with a single interaction domain can function, at least in vitro [205]. It was also reported that an increase in PCNA-client interaction strength can lead to even more severe defects than deletion of the respective partner [206]. Therefore, PCNA has likely evolved to interact with its partners in a transient and dynamic way.

Given that hundreds of proteins containing PIP boxes potentially interact with PCNA in a dynamic fashion, there must be a hierarchy for the PCNA binding affinity. Structural biology researches have revealed that the affinity of PIP box with the IDCL is determined by the ability of PIP box to pack into the hydrophobic surface of PCNA, with the highest affinity being of the p21 PIP box [207]. Also, the relevant abundance as well as cellular localization of clients will influence which proteins can bind with PCNA at any particular moment.

1.2.3 PCNA modifications

PCNA, in a similar way to other proteins, is regulated by post translational modifications which influence its protein stability and client interactions.

The protein stability of PCNA is regulated by phosphorylation and acetylation. PCNA can be phosphorylated on Tyrosine 211 by the tyrosine kinase EGFR [208]. The unphosphorylatable mutant $PCNA^{Y211F}$ had lower protein stability, and stability was restored by the proteasome inhibitor MG132, suggesting that phosphorylation of PCNA on Y211 could stabilise PCNA by inhibiting its proteasomal degradation. However, a biological function for PCNA regulation in this manner has not been determined. Apart from phosphorylation to stabilize the protein, the acetylation of PCNA was also reported to trigger its degradation during nucleotide excision repair [209]. The acetyltransferase CBP and p300 acetylated PCNA at Lys13, 14, 77 and 80 upon UV irradiation to remove PCNA from chromatin after NER. Cells expressing PCNA with the lysine mutated to arginine showed sensitivity to UV irradiation, suggesting that there may be a role for acetylation-induced PCNA removal and degradation during NER. However, given that PCNA is likely needed for NER, the exact role for this pathway is unclear.

PCNA mono-ubiquitination is the major pathway regulating DNA damage tolerance and translesion synthesis in eukaryotic cells. The Rad6-Rad18 dependent PCNA mono-ubiquitination at K164 was first discovered in 2002 in *S. cerevisiae* in response to UV or MMS treatment [210]. The $PCNA^{K164R}$ as

well as Rad6 or Rad18 deletion yeast strains showed no growth defect but sensitivity to UV irradiation and MMS treatment, suggesting a role for this modification in DNA repair pathways. DNA damage-dependent PCNA mono-ubiquitination at K164 was also found in a variety of human cells in 2004, along with a specific binding to the translesion polymerase Polη which was known for bypass of UV-induced DNA lesions [211]. Further structural analysis identified a ubiquitin-binding motif UBZ in Polη in addition to the PIP box, serving to increase the affinity of Polη for mono-ubiquitylated PCNA specifically [212]. It has been reported that RAD18 is recruited to RPA-coated ssDNA generated at sites of stalled replication through direct interaction with RPA, so as to trigger PCNA mono-ubiquitination [213]. Therefore, when PCNA is mono-ubiquitylated at sites of DNA lesions, Polη can outcompete Polδ at the lesion, so that a DNA polymerase switch can occur to a translesion polymerase to bypass the lesion. On the contrary, during unperturbed cell proliferation, the PCNA mono-ubiquitination must be erased and the USP1-UAF1 complex has been reported to mediate PCNA deubiquitination in human cells [214].

In addition to PCNA mono-ubiquitination, Rad5-Mms2-Ubc13 -dependent PCNA poly-ubiquitination at K164 was also discovered in yeast in 2002 [210]. This activates a lesion bypass mechanism using template-switching to restore DNA synthesis past the blocking lesion. HLTF and SHPRH are both human homologs of Rad5, and HLTF/SHPRH-MMS2-UBC13 complex was also

reported to mediate PCNA poly-ubiquitination in human [215] [216]. Knock-down of either HLTF or SHRPH increased spontaneous mutagenesis and HLTF-deficient mouse embryonic fibroblasts showed more chromosome breaks and fusions after MMS treatment, suggesting the importance of this protein in maintaining genome stability. The ZRANB3 translocase contains a PIP box as well as a ubiquitin-binding NZF motif, and it was reported to bind to poly-ubiquitylated PCNA and remodel the stalled replication fork to facilitate fork restart [217]. Given that both mono- and poly-ubiquitination of PCNA share the same amino acid K164, the regulation between mono- and polyubiquitination of PCNA still remains to be elucidated.

1.2.4 PCNA functions in DNA replication and repair

As was mentioned above, the ability of PCNA to encircle and slide on DNA as well as the PIP box-IDCL binding affinity makes PCNA a scaffold to recruit proteins for replication fork-related processes [204]. Therefore, PCNA can regulate a variety of pathways in DNA replication and repair.

The main function of PCNA in DNA replication is to work as a sliding clamp to increase the processivity of DNA polymerases. As was discussed in previous sections, PCNA binds to four subunits of human Polδ and greatly enhances its processivity on lagging strands [57]. The leading strand polymerase Polε was also reported to carry a PIP box and interact with PCNA [218], although a small domain of the Polε catalytic subunit itself also encircles double stranded DNA

giving this enzyme intrinsic processivity [219]. Therefore, the function of PCNA to enhancing the processivity of Polε on leading strands is actually non-essential, and the presence of PCNA was proven only necessary to maintain the same processivity of Polδ and Polε [220]. The translesion polymerases Polη, Polι and Polκ interact with mono-ubiquitylated PCNA through a non-consensus PIP box and ubiquitin-binding motifs as was described in the previous section (Section 1.2.3). This interaction is critical in the polymerase switch of the translesion synthesis pathway: the UBZ domain of Polη is critical in the restoration of UV-irradiation response in Polη-null xeroderma pigmentosum variant (XPV) fibroblasts [212]. Apart from DNA polymerases, PCNA also recruits FEN1 and LIG1 to replication forks for Okazaki fragment processing, and perturbation of these interactions leads to defects in joining Okazaki fragments [73] [74]. The overall function of PCNA in enhancing DNA synthesis is regulated by p21, which is a cell cycle regulator usually stimulated by p53-dependent checkpoint activation [221]. The p21 protein was first found to inhibit PCNA-dependent DNA synthesis by blocking the PCNA enhancement of Polδ processivity [181]. As was mentioned above, the p21 PIP box has the highest affinity for the PCNA IDCL compared to all other reported PIP box-IDCL interactions, suggesting a competition model for how p21 can prevent other replication proteins from interacting with PCNA [207]. Therefore, p21 protein or its C-terminal peptide is often utilized as a replication inhibitor in studies of PCNA interactions.

Apart from proteins involved in DNA synthesis, yeast two-hybrid screening also identified PCNA as a binding partner of yeast MLH1 and MSH2, which are proteins with function in DNA mismatch repair [222]. Further researches distinguished PIP boxes in the N-terminal of MSH3 and MSH6, in which an alanine substitution abrogates their PCNA binding and dramatically increases the mutation rate in yeast [223]. The induction of p21 dramatically decreased the in vitro mismatch repair activity, and this was rescued by adding excessive PCNA, indicating important role of PCNA interactions in mismatch repair pathway. PCNA was also reported to be involved in epigenetic inheritance during DNA replication. As was discussed previously (Section 1.1.1.4), it recruits the maintenance DNA methyltransferase DNMT1 [84], the chromatin assembly factor CAF1 [101] and SWI/SNF-like chromatin remodeler SMARCAD1 [224] to regulate DNA methylation as well as nucleosome assembly at replication forks. The PCNA-binding deficient DNMT1 was still able to restore methylation in DNMT1 knockout mouse ES cells as was mentioned above [96], and a catalytically active truncated DNMT1 lacking the PCNA-binding domain displayed only twofold reduced post-replicative DNA methylation activity [225]. Thus, PCNA facilitates DNMT1 recruitment for its activity at the replication fork but evidence to date suggests this is dispensable for the maintenance of DNA methylation.

PCNA is also required for DNA repair not only for gap filling steps but also

through interaction with a wide range of repair factors. The first study of PCNA in DNA repair was in 1992, when PCNA was reported to be required for DNA synthesis to convert nick intermediates into continuously repaired products in nucleotide excision repair [226]. An in vitro DNA repair synthesis assay was carried out in 1995 with UV-damaged DNA in human cell extracts [227]. This experiment revealed that Polδ or Polε could perform DNA synthesis with the presence of PCNA, RFC and RPA, and that LIG1 was required for generation of ligated circles, which suggested the role of PCNA in gap filling DNA synthesis during NER. Later, the endonuclease XPG which functions in excision of DNA lesions during NER was discovered to interact with PCNA [197]. The XPG^{R992A} or XPG^{R992E} mutants disrupted its PCNA interaction and failed to fully complement NER in an NER-deficient cell line. Therefore, PCNA interaction with XPG is important in NER pathway. Apart from being involved in NER pathway, PCNA was also found to interact with the short-patch BER scaffold protein XRCC1 [228] and the glycosylase UNG2 [229]. The PCNA interaction with FEN1 and LIG1 was also reported critical in long-patch BER pathway [74]. The interaction of PCNA with FANCD2 and SPRTN which was mentioned above (Section 1.1.2.5) indicates its role in helping with ICL and DPC processing.

In addition to these roles in DNA synthesis and repair, PCNA also functions in cell cycle regulation. The replication licensing factor Cdt1 functions in the

initiation of DNA replication. It interacts with PCNA and undergoes ubiquitin-dependent proteasomal degradation initiated by DNA-associated PCNA interaction during S phase [230]. This process prevents DNA re-replication which can be induced if Cdt1 is active in S phase, as mutation of the Cdt1 PIP box led to stabilized Cdt1 protein and DNA re-replication. Similarly, the cell cycle inhibitor p21 also undergoes PCNA-dependent degradation in S phase as well as after UV irradiation. Presumably this is to release PCNA to other interacting proteins to enable DNA replication in S phase or polymerase switching for translesion synthesis, as a 6Myc-tagged p21 that blocked the ubiquitination sites on p21 led to increase in DNA replication stress in S phase or after UV irradiation [231]. A further important substrate for PCNA-dependent degradation is the histone H4 methyltransferase SET8. The activity of this enzyme must be restricted to G2, so that newly synthesized strands only contain histone H4 unmethylated at K20 to endure proper use of templates for HR [232] [233]. The interaction between SET8 and PCNA removes this protein from acting on replicated DNA in S phase [234]. These, and other PIP-degron substrates are targeted by a pathway involving the E3 ubiquitin ligase $CRL4^{Cdt2}$ which mediates DNA-associated PCNA dependent ubiquitination. The PIP-degron motif is a subset of PIP boxes, with a TD motif at position 5 and 6 and a basic residue 4 amino acids downstream [235].

Common PCNA interacting proteins involved in various cellular processes are

listed in Table 1.2.4.

Pathway	Function	Protein	Organism	PIP box
DNA replication	DNA polymerase	Polδ POLD1p125 POLD3p66 POLD4p12	 *H. sapiens* *H. sapiens* *H. sapiens*	 KATQCQL QVSITGFF KRLITDSY
		Polε Pol2 Dpb2	 *S. cerevisiae* *S. cerevisiae*	 QTSLTKFF QMFLTKYY
	Flap endonuclease	FEN1	*H. sapiens*	QGRLDDFF
	DNA ligase	LIG1	*H. sapiens*	QRSIMSFF
	Licensing factor	Cdt1	*X. laevis*	QMRVTDFF
	Helicase activator	Mcm10	*S. cerevisiae*	QHTLDVYI
Bypass lesions	TLS polymerase	Polη	*H. sapiens*	QTLESFF
		Polκ	*H. sapiens*	KHTLDIFF
Nucleotide excision repair (NER)	Endonuclease	XPG	*H. sapiens*	QLRIDSFF
Base excision repair (BER)	Glycosylase	UNG2	*H. sapiens*	QKTLYSFF
	Endonuclease	APE2	*H. sapiens*	QKNLKSYF
	BER scaffold	XRCC1	*H. sapiens*	Not found
	Poly (ADP-ribose) polymease	PARP1	*H. sapiens*	QDLIKMIF
Mismatch repair	MMR initiation complex	MSH3	*H. sapiens*	QAVLSRFF
		MSH6	*H. sapiens*	QSTLYSFF
DPC repair	Metalloprotease	SPRTN	*H. sapiens*	QNVLSNYF
Epigenetic inheritance	DNA methyltransferase	DNMT1	*H. sapiens*	QTTITSHF
	Chromatin remodeler	SMARCAD1	*H. sapiens*	Not found
	Chromatin assembly factor	CAF1	*H. sapiens*	QARLPF KAEITRFF
Cell cycle regulator	CDK inhibitor	p21	*H. sapiens*	QTSMTDFY

Table 1.2.4 Common PCNA-binding proteins in various cellular pathways. The determined PIP boxes are included, with conserved PIP box residues underlined.

1.3 PCNA-associated DNA repair disorder (PARD) caused by a point mutation of PCNA p.Ser228Ile

1.3.1 PCNA variations among species

Because of its essential role in DNA replication and repair, PCNA is highly conserved among eukaryotes [236]. In the Exome Aggregation Consortium (ExAC) dataset, the *PCNA* gene has a constraint metric z = 2.84 for missense variation, and pLI (probability of loss-of-function intolerance) = 0.94, which indicates that the PCNA variation in human population is highly constrained and that loss-of-function of PCNA is not tolerated [237]. However, this does not seem to affect PCNA mutagenesis in tumours. There are 60 unique single-nucleotide variations (SNVs) that have been reported in all the human cancer database so far (BioMuta).

Complete knockout of PCNA in yeast, flies or mice is lethal due to its critical role in DNA replication [238-240]. However, many PCNA mutants have been generated in yeast for structure-function studies, which are summarized in Table 1.3.1. The $PCNA^{K164R/K164R}$ homozygous knock-in mouse is the only PCNA mutation previously constructed in mammalian system. Mice with this mutation grew normally but were infertile with a dramatically altered mutation spectrum of hypermutated immunoglobulin genes [241]. This suggested the importance of PCNA mono-ubiquitination at K164 in meiotic progression as well as in somatic hypermutation. In human the first and only naturally occuring

PCNA mutants	Protein region	Phenotypes
S115P	Trimer interface	Cold sensitivity for growth [190], synthetic lethality with *rad*52Δ [250]
A251V	C-terminus	Cold sensitivity for growth and synthetic lethality with *rad*52Δ [250]
C81R	Trimer interface	Defective MMR [250]
C22Y	Interface α helix	Defective MMR [250]
E143K	Trimer interface	Defective MMR [251]
L68S	IDCL-adjacent	Defective MMR [251]
K164R	Ubiquitination site	UV/MMS sensitivity [210]
K127R, K164R	Ubiquitination site	Less UV/MMS sensitivity [210]
DD41,42AA	Domain I beneath IDCL	UV/HU/MMS sensitivity [190], reduced growth in FOA [248]
RD61,63AA	IDCL-adjacent	Reduced growth in FOA [248]
LI126,128AA	IDCL	Reduced growth in FOA [248], growth defect [249]
PK252,253AA	C-terminus	Growth defect and MMS sensitivity [249]

Table 1.3.1 PCNA mutants in *S. cerevisiae* and their phenotypes. FOA, 5-fluoro-orotic acid, kills cells expressing the URA3 gene at the telomere which is normally repressed.

pathogenic mutation of PCNA was reported in 2014, p.Ser228Ile [242], which will be fully discussed in the next section (Section 1.3.2).

1.3.2 PCNA-associated DNA repair disorder

In 2014, the Crosby and Green laboratories reported a novel DNA repair disorder identified in the Ohio Amish community [242]. The affected individuals had symptoms of short stature, premature aging, neurodegeneration and photosensitivity, which are common features of DNA repair disorders such as Ataxia Telangiectasia (AT) and Xeroderma Pigmentosum (XP) [243] [244]. Autozygosity mapping and linkage analysis revealed a homozygous single

nucleotide substitution of c.683G>T in exon 6 of PCNA which is likely the causal pathogenic variant. This mutation results in a change of amino acid position of 228 from serine into isoleucine (p.Ser228Ile, or S228I). Both primary fibroblasts and lymphoblastoid cells derived from affected individuals showed sensitivity to UV irradiation, and a decrease in unscheduled DNA synthesis (UDS) as well as in RNA synthesis recovery (RRS) after UV irradiation, indicating that the S228I alteration compromises both GG-NER and TC-NER [242]. However, the replication fork localization of PCNA as well as DNA replication speed were not found to be affected in $PCNA^{S228I}$ primary fibroblasts or derived lymphoblastoid cells. Thus, the disease caused by $PCNA^{S228I}$ was named PCNA-associated DNA repair disorder (PARD).

Ser228 is in Domain II of PCNA, spatially close to the IDCL, and the crystal structure of $PCNA^{S228I}$ protein showed a dramatic conformational change of the IDCL [245]. We confirmed this conformational change with a crystal structure of $PCNA^{S228I}$ at 2.5Å resolution. This structure shows that the larger side chain of isoleucine causes a steric clash with Tyr133 in the IDCL, resulting in a 90° repositioning of the Tyr133 side chain and further significant changes which propagate along the IDCL [246]. Apart from these IDCL specific changes, the overall structure and intermolecular surface between monomers were unchanged in $PCNA^{S228I}$ structure (Fig. 1.3.2). A series of PCNA interacting proteins have been found to have impaired interaction with the $PCNA^{S228I}$

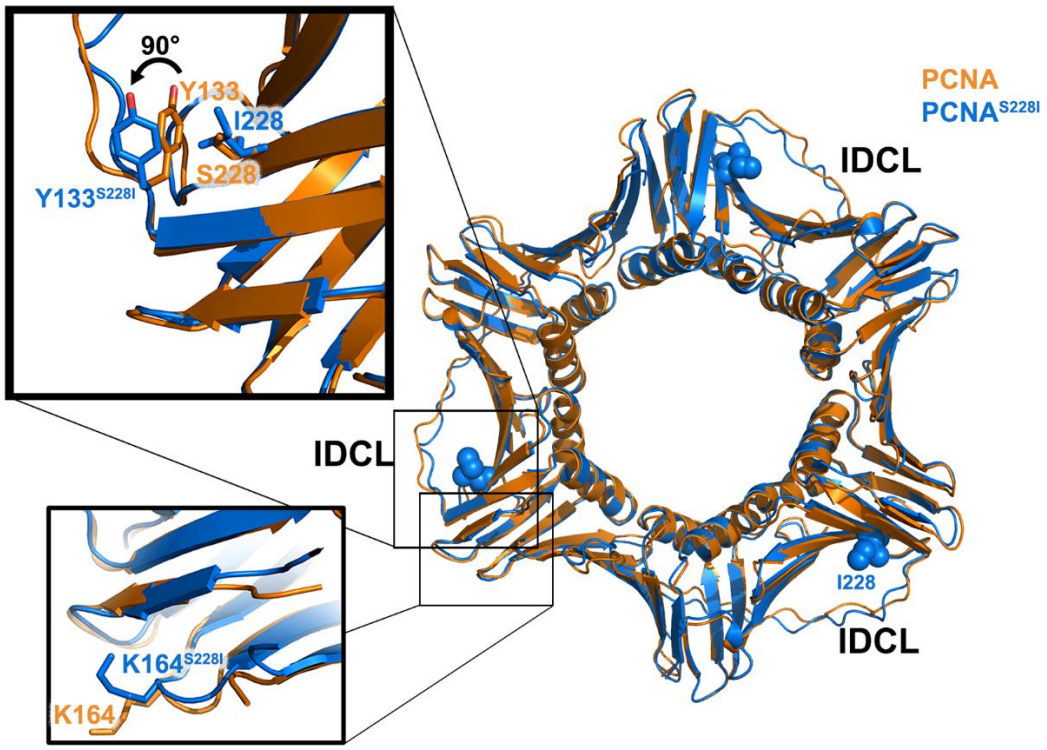


Figure 1.3.2 PCNA^{S228I} results in structural changes at the IDCL. Apo PCNA^{S228I} structure (blue, PDB ID 5MOM) is overlayed on Apo structure of PCNA^{WT} (orange, PDB ID 1VYM). The mutated I228 residues are shown as spheres. The top left inset zoom shows the rotation of Y133 and changes propagating along the IDCL caused by S228I alteration. The bottom left inset zoom shows no changes in K164 and its surrounding structural environment. Figure from Wilson, *et al.* [234]

mutant by techniques of Surface Plasmon Resonance (SPR) and GST-pull down, including the important PCNA partners: FEN1, LIG1, XPG, Cdt1 and DNMT1 [242] [246]. The reduced interaction between FEN1 and PCNA^{S228I} was further confirmed by immunoprecipitation in lymphoblastoid cell extracts from affected individuals [242]. The binding of p21, however, was only affected by S228I alteration in a limited way. The influence of the S228I alteration on PCNA interactions apparently affects PCNA functions as this mutation significantly

sensitizes cells to treatment with T2AA or T3: chemicals that competitively bind near the IDCL to block PCNA interactions with PIP box proteins [247]. Consistent with no structural change detected at K164 and its surrounding structural environment (Fig. 1.3.2), no alterations were detected in mono-ubiquitination at K164 after UV irradiation in cells from affected individuals, suggesting that the TLS pathways are unlikely to be affected by this mutation. The main aim of the work in this thesis has been to determine which cellular pathways are affected by the S228I mutation, and the mechanisms by which any such effects occur.

1.4 Functions of poly(ADP)ribosylation in DNA replication and repair

First described as a DNA-dependent nuclear enzymatic activity of polyadenylic acid synthesis in 1963 [252], poly(ADP)ribosylation was found to be catalysed by the PARP1 and PARP2 enzymes [253] [254], which are of great importance to the DNA damage response (DDR) and contribute to many DNA repair and replication fork processing pathways [255]. PARP1/2 catalyse PARylation through polymerizing ADP-ribose units on themselves, histones and other target proteins [256]. The substrate for PARylation is NAD^+ and catabolism of PAR chains is necessary to maintain NAD^+ homeostasis. The most well characterised enzyme for PAR chain degradation is the PAR glycohydrolase

PARG [257], deletion of which sensitizes cells to genotoxic stress [258].

1.4.1 Poly(ADP)ribosylation in DNA repair

PARP1 has long been regarded as a surveillance factor for DNA breaks in DDR. The PARP1 protein structure was identified in 1984, and it contains three main domains: an N-terminal DNA binding domain, a BRCT auto-modification domain and a C-terminal catalytic domain (Fig. 1.4.1) [259]. In 1979, PAR synthesis was first observed in human lymphocytes after UV irradiation or treatment with DNA damage agents like MNNG, giving the first evidence of PARylation function in DNA repair [260]. One year later, it was reported that PAR synthesis occurred after dimethyl sulphate (DMS) treatment which induced DNA excision repair, and that NAD^+ starvation inhibited the rejoining of DNA breaks, suggesting the importance of PARylation in DNA repair [261]. In 1990 after the structure of PARP1 was determined, the second zinc finger domain of the PARP1 DNA binding domain was proven to be responsible for the recognition of DNA strand breaks [262]. Further experiments in human cell extract confirmed the PARP1 function in repair of strand breaks induced by γ irradiation as well as PARP1 auto-PARylation which acts to reduce its binding affinity to DNA breaks [263]. Thus, these early research studies indicated PARP1 functions in detection and repair of both single and double strand breaks.

XRCC1, which has been mentioned in previous sections (Section 1.1.2.1), is a key factor for single strand break repair (SSBR) pathways. XRCC1 was

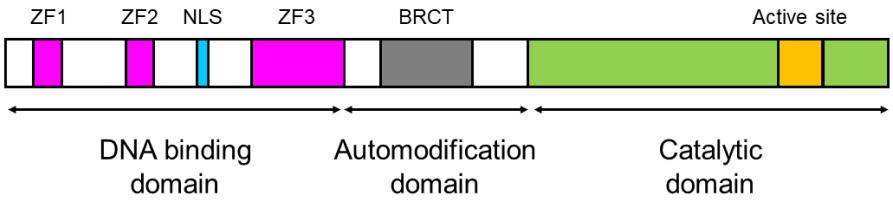


Figure 1.4.1 The schematic representation of PARP1 and its domains. PARP1 protein contains an N-terminal DNA binding domain with three zinc finger (ZF) motifs and one nuclear localization signal (NLS), an automodification domain containing a BRCT domain, and a C-terminal catalytic domain with a conserved PARP1 active site.

reported to specifically interact with PARP1 using the yeast two-hybrid system [264] and further found to carry a PAR-binding sequence motif for its recruitment to actively PARylated sites [265]. It was confirmed by using PARP1-deficient human cell extracts that deletion of PARP1 dramatically inhibits the in vitro DNA repair of uracil or 8-oxoguanine, showing the great importance of PARP1 in process of base excision repair [266]. XRCC1 foci can be detected immediately after the formation of PAR foci upon H_2O_2 treatment, but these could not be detected in PARP1-depleted cells, indicating the crucial role that PARP1 was playing in XRCC1 recruitment to resolve oxidative stress [267]. Thus, PARP1 recognizes and binds to SSBs, recruiting XRCC1 by catalysing PARylation to initiate DNA single strand break repair pathways.

Apart from SSB repair, early researches also implicated PARP1 function in DSB repair [263]. PARP1 was reported to be phosphorylated by and to catalyse PARylation of DNA-PK in vitro. This PARylation stimulated the activity of DNA-PK towards substrates such as RPA and p53, and suggested a potential role of

PARP1 in NHEJ [268]. The DDR kinase ataxia telangiectasia mutated (ATM) interacts with PARP1 and PAR polymers, and PARP1 depletion dramatically reduced the phosphorylation of ATM substrates including H2AX after ionizing radiation (IR) [269]. However, it was also reported that PARP inhibition induced DSBs which were still processed by ATM signalling even though the ATM activity was reduced [270]. This led to a hypersensitivity of ATM-deficient cells to PARP inhibitors. Therefore, PARP1 facilitates ATM signalling in response to DSBs but is not essential for this process. As will be discussed later (Section 1.4.2), PARP1 and PAR polymers interact with MRE11 and NBS1 [277], the main functions of which are mediation of DNA resection during HR or initiation of fork restart. More importantly, PARP1 was reported to be involved in the recruitment of BRCA1 to DNA lesions through the PAR-binding domain on BARD1, and PARP inhibitors suppressed the fast recruitment of BRCA1 to DSBs but did not abrogate it [271], indicating that PARP1 helps with the recruitment of HR factors to break sites but is actually not crucial for the HR pathway.

1.4.2 PARP1 at replication forks

Early research provided evidence that PARP1 activity was related to the growth rates of cells [272], and that PARP1 was hyperactivated on newly replicated chromatin compared to unreplicated regions [273], giving the first hint of PARP1 function in DNA replication. Later experiments showed that PARP1 co-

precipitated with the multiprotein replication complex including Polα, Polδ, RFC, etc. [274]. Interestingly, PARP1 was also reported to bind to PCNA, with a PIP box inside the catalytic domain such that PCNA binding would inhibit its enzymatic activity [275]. Deletion of PARP1 in mouse embryonic fibroblasts (MEF) resulted in hypersensitivity to hydroxyurea (HU) treatment and in a delay in re-entry to G2/M phase after HU release, suggesting a crucial role of PARP1 at replication forks stalled by nucleotide depletion [276]. This was confirmed by further experiments that discovered PAR polymers colocalized with RPA after HU treatment, indicating they are formed at stalled replication forks [277]. While the PARP1 protein level was not reported to increase at stalled forks, the protein level of PARG that degrades the PAR polymer was observed to decrease at stalling forks, resulting in hyper-PARylation of unknown substrates at stalled replication forks [278].

Stalled replication fork processing includes several pathways: fork protection, fork reversal and fork restart. PARP1, as well as PAR polymer, was found to co-precipitate and colocalize with the DNA resection endonuclease MRE11 after HU treatment [277] [279], and inhibition of PARP1 significantly decreased the percentage of fork restart by DNA fibre assay [277], suggesting that PARP1 functions in recruiting MRE11 to stalled replication forks to initiate HR-dependent fork restart. However, PARP1 inhibition in BRCA2-deficient cells showed increased degradation of stalled replication forks mediated by MRE11,

indicating that PARP1 also participates in inhibition of over-resection during fork protection [280]. These apparently contradictory findings presumably highlight variable PARP1 functions in different cellular contexts, acting to keep balanced fork restart pathways to maintain genome stability. In other studies, PARP1 inhibition was reported to reduce the four-way junction structure of fork reversal in U2OS and MEF cells under camptothecin (CPT) treatment that traps Top1 at nicked DNA intermediates during replication to induce fork stalling [281]. Further researches distinguished RECQ1 helicase to be involved in resolving fork reversal, the function of which could be inhibited by interaction with PARylated PARP1 or PAR polymers [282]. Thus PARP1 inhibition increased the genome instability of U2OS cells under CPT treatment, which could be rescued by RECQ1 knock-down, indicating that PARP1 functions at reversed replication forks to prevent RECQ1-mediated untimely restart of the reversed forks upon replication stress and maintain the genome stability. Taken together these studies make it clear that PARP1 plays important roles in processing stalled replication forks to enhance genome stability under replication stress.

Apart from stalled replication forks, recently PARP1 signalled SSB repair pathway was also reported to be active at normal DNA replication forks, especially in cells with compromised FEN1 or LIG1 function. The inhibition of rapid degradation of PAR by using PARG inhibitor enabled the detection of PAR chains at replication forks under these conditions [283]. This gave a new insight

into how PARP1 surveillance operates on unligated Okazaki fragments to maintain genome stability, and suggested a crosstalk between SSB repair pathway and DNA replication.

1.4.3 PARP inhibitors and cancer chemotherapy

BRCA1 and BRCA2 are key regulators of homologous recombination, and mutations of BRCA1/2 are found in most familial breast and ovarian cancers. In 2005, BRCA1 or BRCA2-deficient cells were first observed to be exquisitely sensitive to PARP inhibitors, with treatment of BRCA-defective cells resulting in severe G2/M arrest in cell cycle and increased chromosome rearrangements [284]. This result led to the concept of synthetic lethality in cancer chemotherapy. PARP inhibitors (PARPi), including olaparib, niraparib, veliparib, rucaparib, etc., were designed to compete with NAD^+ at the active site of PARP1 so as to inhibit its catalytic activity [285]. The mechanism of PARPi sensitivity in BRCA1/2-deficient cells has been widely studied. Active HR was observed after PARPi treatment in BRCA1/2-proficient cells by labelling RAD51 foci, which implied that PARPi generated DSBs in BRCA1/2-proficient cells which are then repaired by HR [284]. BRCA1/2-deficient cells are defective in HR so that have to rely on error prone NHEJ for the repair of breaks and thus PARPi increases genome instability in this genetic background. The mechanism by which PARPi induces DSBs has long been considered to be a result of persistent unrepaired endogenously generated SSBs eventually being converted into DSBs. However,

this cannot explain the results that WT cells were more sensitive to a combined treatment of PARPi and MMS than PARP1 depleted cells [286]. Chromatin immunoprecipitation (ChIP) assays using anti-PARP1 antibody showed that more DNA was pulled down in cells treated with both MMS and PARPi than those treated with MMS alone [286], suggesting that PARP trapping contributes to the cellular effects of PARPi treatment. Further research showed that the amount of PARP1 found on chromatin after triton extraction was correlated with PARPi concentration when combined with identical doses of MMS, and that the sensitivity of WT DT40 cells to different PARP inhibitors was also correlated with the trapping capacity of each PARPi [287]. This supported the hypothesis that the PARP1 trapped at DNA lesions by PARPi can generate structures equivalent to DNA-protein crosslinks, blocking the DNA replication machinery and leading to fork collapse, which generates the DSBs induced by PARPi treatment. The result that PARPi treatment drastically increased the degradation of stalled replication forks in BRCA2-deficient cells implied that loss of protection from over-resection by MRE11 at stalled forks after PARP1 inhibition can also contribute to the PARPi sensitivity in BRCA2-deficient cells [280]. In summary, the sensitivity to PARPi in BRCA1/2-deficient cells is likely an integrative consequence of unrepaired SSB accumulation, PARP trapping leading to fork collapse as well as hyper-unstable replication forks.

Recent studies on PARP inhibitors mainly focus on the mechanisms that lead

to chemoresistance towards PARPi in BRCA-deficient cells and searching for new synthetic lethal proteins with PARPi for new potential applications in cancer clinic. One of the most famous PARPi chemoresistance factors is 53BP1, a BRCA1 antagonizer, the dysfunction of which was reported to restore resistance to PARPi in BRCA-deficient cells by re-enabling HR [288]. CRISPR screens have been carried out to identify both other synthetic lethalities and resistance factors. Screens for resistance factors lead to the recent identification of new components of the NHEJ pathway, such as REV7 and Shieldin complex [288] [289]. Proteins related to HR are always shown to be synthetic lethal with PARPi, leading to the concept of 'BRCAness', which is now being utilised as a screening tool to stratify patients for treatment with PARPi in the cancer clinic [290]. Other pathways have also been found to be synthetic lethal with PARPi, including the RNaseH2 ribonucleotide removal pathway. Loss of this pathway induces aberrant ribonucleotide processing resulting in DNA nicks that cause PARP trapping by PARPi and thus increased sensitivity to this treatment [291]. This research gives new insights on PARPi sensitivity and broadens the application of PARPi in cancer chemotherapy.

1.5 Outline of Thesis

As was described above, the p.Ser228Ile alteration of PCNA dramatically disrupts the conformation of IDCL, which perturbs the interaction of PCNA with

many of its protein clients, including FEN1, LIG1, XPG, DNMT1, Cdt1, etc. [234]. However, cells with S228I alteration seem to tolerate such dramatic perturbations in PCNA client interaction. The aims of this work were to determine which cellular pathways are affected by the S228I mutation and the mechanism by which the defective pathway leads to PARD, as well as to reveal mechanisms of cell tolerance to the compromised PCNA client interactions. I managed to answer these questions by:

- Generating and phenotypically analysing an isogenic PCNA^{S228I} knock-in cell line in hTERT RPE-1 cells as well as a WT control using the CRISPR-Cas9 technique. With the cell line I recapitulated several phenotypes observed in the cell lines derived from affected individuals (Chapter 3).

- Investigating pathways which are likely to be affected by the S228I alteration using the isogenic cell line. I sought to investigate post translational modifications of PCNA as well as cellular sensitivity to different damaging agents and olaparib sensitivity was discovered in PCNA^{S228I} cells (Chapter 4).

- Searching for the mechanism for olaparib sensitivity in PCNA^{S228I} cells by investigating the role of PARP1 in olaparib sensitivity, response of cells to oxidative stress as well as activity of PARP1 at replication forks. Through the investigation I proposed a model explaining the olaparib sensitivity in PCNA^{S228I} cells (Chapter 5).

Chapter 2: Materials and Methods

2.1 Cell culture

2.1.1 Cell lines

Human hTERT RPE-1 cells were from ATCC (Ref. CRL-4000), and cultured in DMEM-F12 (Lonza) with 10% FBS (Sigma) and 1% penicillin and streptomycin (PAA). EBV-transformed lymphoblastoid cell lines were maintained in RPMI-1640 Medium (Sigma) with 10% FBS (Sigma), 2 mM L-Glutamine (Sigma) and 1% penicillin and streptomycin (PAA).

2.1.2 Cell maintenance

Frozen cells were thawed at 37°C and resuspended in desired growth medium. Cells were cultured in a T75 tissue culture flask at 37°C with 5% CO_2.

RPE-1 cells were passaged at 70-90% confluency. To passage, cells cultured in T75 flasks were washed with 6 ml of PBS (Gibco) and incubated in 1 ml of 0.05% Trypsin (Lonza) at 37°C for 5-10 minutes. To quench the trypsinisation, cells were resuspended in 5 ml of growth medium and seeded in desired cell numbers. Lymphoblastoid cells were passaged every three days, and cells for continued culture were placed at 200,000 cells/ml of medium in a T75 flask.

For long-term storage of the RPE-1 cells, cells were harvested by trypsinisation and centrifuged at 300 g for 5 min. After washing with PBS, cells were

resuspended in 1 ml freezing medium of 10% DMSO (Sigma) in FBS, and then transferred to a sterile cryovial (Greiner) and cooled to -80°C at 1°C per minute. The cryovials were then kept in liquid nitrogen for long-term storage.

For long-term storage of the lymphoblastoid cells, cells were harvested by centrifugation at 300 g for 5 min and washed with PBS. Then cells were resuspended in 1 ml freezing medium (complete RPMI medium with 5% DMSO) and transferred to a sterile cryovial and cooled to -80°C at 1°C per minute. The cryovials were stored in liquid nitrogen at the temperature of -140°C to -180°C.

2.1.2.1 Cell counting

Cells were stained with the same volume of trypan blue (Sigma) and counted automatically in a counting slide (BioRad) with the BioRad cell counter.

2.1.3 Cell transfection

Transient transfection of RPE-1 cells was performed using FuGENE®6 (Promega) according to manufacturer's protocol. A certain number of cells were seeded according to the size of the plate one day before transfection. On the day of transfection, FuGENE®6 was mixed completely with antibiotic- and serum-free DMEM-F12 medium and incubated for 5min at room temperature to equilibrate. Plasmids were then added to the mixture and mixed thoroughly by vortexing. The solution was incubated at room temperature for further 15 min to allow the formation of plasmids/FuGENE®6 complex and added drop-wise to

the RPE-1 cells with the culture medium changed to antibiotic-free medium (DMEM-F12 with 10%FBS). The amount of cells, FuGENE®6, serum-free DMEM-12, plasmids and antibiotic-free medium are indicated in Table 2.1.3 according to sizes of plates.

Plate size	Cell number (10^6 cells)	Serum-free DMEM-F12 (µl)	FuGENE®6 (µl)	Plasmids (µg)	Culture medium (ml)
6 cm (T25)	0.3	155	9.9	3.6	4
10 cm (T75)	1.0	403	25.7	8.58	9.5
15 cm (T175)	4.0	990	63.2	21.1	24

Table 2.1.3 Amount of cells and reagents for RPE-1 transfection using FuGENE®6 according to the plate size.

2.1.4 siRNA knock-down

Gene knock-down in RPE-1 cells was carried out by transfection of siRNA synthesized by Life Technologies with reagent of Lipofectamine® RNAiMAX (Invitrogen) according to manufacturer's protocol. One million RPE-1 cells were seeded in a T25 flask one day before siRNA transfection. On the day of transfection, 17 µl RNAiMAX was diluted in 250 µl Opti-MEM® Medium (Gibco) in a 1.5 ml Eppendorf tube. In a separate tube, 52 pmol of siRNA was diluted in 250 µl Opti-MEM® Medium. The RNAiMAX and siRNA solution were combined, mixed thoroughly by pipetting up and down, and incubated for 5 min at room temperature to form siRNA-lipid complexes. 500 µl of solution was added drop-wise to the RPE-1 cells with the culture medium changed to 3.5 ml of antibiotic-

free medium, so that the final concentration of siRNA in cell culture was 12.5 nM. Culture medium was replaced with normal growth medium 24 hr after transfection. Cells were harvested 48 hr after transfection with the best knock-down efficiency.

SiRNA sequence:

Luciferase: 5′-CGUACGCGGAAUACUUCGA-3′

PARP1: 5′-AAGAUAGAGCGUGAAGGCGAA-3′

2.1.5 Cell survival assay

In lymphoblastoid cells, the cell survival assay was carried out by treating cells at $2x10^5$ cells/ml with indicated doses or the appropriate vehicle. Cell numbers were counted after 3 days, and the survival rate was calculated as cell numbers relative to that with the vehicle treatment.

In RPE-1 cells, $1.25x10^4$ cells were seeded in 6-well plates 24 hr before drug treatment. Cells were treated with indicated doses of drugs for 6 days, and washed twice with PBS before being stained with 0.5% crystal violet (VWR) in 20% methanol (Sigma) for 30 min. Then the plates were rinsed completely in distilled water and left for dry at room temperature overnight. The crystal violet staining was resolubilized in 10% acetic acid (VWR) for 1 hr and the relative cell number was determined by measuring the light absorbance with the excitation of 595 nm using the CLARIOstar plate reader (BMG Labtech).

2.1.6 FACS analysis

In order to distinguish different phases of the cell cycle, the fluorescence activated cell sorting (FACS) was applied by labelling Bromodeoxy-uridine (BrdU) as nucleotide incorporation and propidium iodide staining for DNA content. Exponentially growing lymphoblastoid cells or RPE-1 cells were incubated with 10 µM BrdU at 37°C for 30 min and then harvested for fixation in 4% PFA at room temperature for 20 min. After fixation, cells were washed in 1 ml PBS and penetrated with 0.2 mg/ml pepsin in 2M HCl at room temperature for 20 min. Cells were washed twice with 1 ml PBS, blocked using the Fc block solution (BD) when necessary, and then probed with anti-BrdU (1:50, 347580, BD), or sometimes anti-PAR (1:100, 4336-BPC-100, AMS Biotech) diluted in BSA-T (0.5% BSA, 0.5% Tween20) at room temperature for 1 hr. After being washed in 1 ml BSA-T twice, cells were probed with Alexa Flour anti-mouse 633 or anti-rabbit 488 (both 1:200, Invitrogen) diluted in BSA-T at room temperature protected from light for 1hr. Washed in BSA-T as before, cells were incubated with 0.5 mg/ml RNase A in PBS at 4°C overnight and stained with 10 µg/ml propidium iodide about 30 min before analysis on a SONY Cell Sorter SH800Z.

2.2 DNA analysis

2.2.1 DNA extraction

2.2.1.1 Bacteria

The plasmids in transformed bacteria were extracted using the method depending on the number of bacteria in culture.

For screening of positively transformed clones, plasmids were purified from 5 ml of bacteria culture using the NucleoSpin® Plasmid Kit (MACHEREY-NAGEL). Bacteria were pelleted at 1,700 g for 10 minutes. The supernatant was discarded, and cells were resuspended in 250 µl Buffer A1 with RNase A. Then 250 µl Buffer A2 was added and mixed gently by inverting the tube 6-8 times. The solution was incubated at room temperature for 5 min to lyse the bacteria completely. The solution was neutralised with 300 µl Buffer A3, inverted 6-8 times to precipitate all proteins and chromosomal DNA. The plasmid DNA was separated from the supernatant of the centrifugation for 5 min at 11,000 g at room temperature. Then the plasmid DNA was bound to a silica membrane in a NucleoSpin® Plasmid Column and washed with Buffer AW as well as A4, and finally eluted in 50 µl Buffer AE (10 mM Tris.Cl, pH 8.5).

For purification of plasmids from more than 100 ml bacterial culture, the NucleoBond® Xtra Midi Kit (MACHEREY-NAGEL) was used according to manufacturer's protocol. Bacteria were pelleted by centrifugation at 6,000 g for

10 min at 4°C and supernatant aspirated. Cells were resuspended in 8 ml Buffer RES with RNase A and lysed by adding 8 ml Buffer LYS and inverting the tube 5 times gently. The solution was incubated at room temperature for 5 min, and neutralized with 8 ml Buffer NEU to precipitate all the proteins and chromosomal DNA. The lysate was then applied to a NucleoBond® Xtra Column with the column filter pre-equilibrated by Buffer EQU, so that the cell debris as well as precipitated proteins and chromosomal DNA were separated by the filter and plasmid DNA was bound to the silica resin of the column. The filter was washed with 5 ml Buffer EQU and removed, then the column was washed with 8 ml Buffer WASH before the plasmid DNA being eluted by 5 ml Buffer ELU. The plasmid DNA in the eluted solution was concentrated and desalted by isopropanol precipitation. After being washed with 2 ml 70% ethanol, the plasmid DNA was dissolved in Buffer AE (10 mM Tris.Cl, pH 8.5) for further experiments.

2.2.1.2 Cultured cells

Genomic DNA from RPE-1 or lymphoblastoid cells was extracted using the GenElute™ Mammalian Genomic DNA Miniprep Kit (Sigma) according to manufacturer's protocol. Up to $5x10^6$ cells were harvested by trypsinisation, and cells were pelleted at 300 g for 5 min. The supernatant was aspirated and cells were resuspended thoroughly using 200 µl Resuspension Solution. 20 µl of RNase A Solution was added to remove RNA in the solution. Then the solution

was added with 20 µl Proteinase K solution and 200 µl Lysis Solution C sequentially, mixed thoroughly by vortexing and incubated at 70°C for 10 min to lyse the cells and degrade all the proteins in the solution. Then the lysate was mixed thoroughly with 200 µl ethanol and transferred to the GenElute Miniprep Binding Column pre-treated with 500 µl of Column Preparation Solution. The genomic DNA was bound to the silica membrane of the column by centrifugation at 6,500 g for 1 min, and washed twice with 500 µl of Wash Solution. The genomic DNA was finally eluted using 200 µl Elution Solution.

2.2.2 Polymerase Chain Reaction (PCR)

PCR amplifies a specific sequence from the template DNA. Primers for PCR were purchased from either Eurofins Genomics or Life Technologies. Sequences of the primers used in this thesis are summarized below. The lyophilized primers were dissolved in nuclease-free H_2O (Severn Biotech Ltd.) to get a 100 µM stock, and further diluted to 10 µM working stock. The Phusion High Fidelity DNA Polymerase (NEB) was used for PCR reaction, and the general 50 µl PCR master mix as well as amplification conditions were indicated in Table 2.2.2A and Table 2.2.2B, respectively.

Component	Final concentration
Nuclease-free H_2O	- (Up to 50 µl)
5X Phusion HF Buffer	1X
10 mM dNTPs	200 µM
10 µM Forward Primer	0.5 µM
10 µM Reverse Primer	0.5 µM
Template DNA	<250 ng*
Phusion DNA Polymerase	1U/50 µl PCR

Table 2.2.2A Standard master mix for PCR using the Phusion High Fidelity DNA Polymerase. * Varies under different circumstances. For genomic DNA template an amount of 250 ng was used for 50 µl PCR reaction, while 10 ng was used for plasmid DNA template.

Step	Cycle	Temperature (°C)	Time
Initial denaturation	1	98	30 sec
Denaturation	30-40	98	10 sec
Annealing		45-72*	20 sec
Elongation		72	30 sec/kb product
Final extension	1	72	10 min

Table 2.2.2B Standard thermocycling conditions for a routine PCR. * Optimized according to Tm of the primers. Typically primers were annealed at 3°C above the Tm of the lower Tm primer for PCR using Phusion DNA Polymerase.

Primer sequences for PCR amplification used in this thesis:

For HDR template construction:

PCNA NestedTOP: ACTTCTAGGTTAACTAGACCAG

PCNA NestedBOT: TTCCATTACAATCTATTTGTTG

HDR1 EcoRTOP: GATCA gaattc AGAGGTACAAATTTGGTGAC

HDR1 BglBOT: GATC agatct CCAATACAAGTGTTTGTGGG

HDR2 MfeTOP: GATC caattg TCACTTTGGAGGGAGCTATG

HDR2 BamHBOT: GATC ggatcc GCTGATTGCATTCCTGTGTATAC

For clone genotyping (See Chapter 3):

p1 (same as PCNA NestedTOP): ACTTCTAGGTTAACTAGACCAG

p2: ggaacccttaatataacttcg

p3 (same as PCNA NestedBOT): TTCCATTACAATCTATTTGTTG

p4: ggtagaatttcgacgacctg

For cDNA sequencing:

PCNA ORF TOP: CACCATGTTCGAGGCGCGCC

PCNA ORF BOT: AGATCCTTCTTCATCCTCG

2.2.3 Site-directed mutagenesis

Mutations were induced into plasmids using the technique of site-directed mutagenesis with the QuickChange II XL site-directed mutagenesis kit (Agilent Technologies) according to manufacturer's protocol. Two complimentary oligonucleotides containing the desired mutation were synthesized as primers for the reaction. The site-directed mutagenesis was carried out with 25 µl reactions and the thermocycling conditions indicated in Table 2.2.3A and Table 2.2.3B. After the thermocycling, the parental plasmid was degraded with 1 µl

10 U/µl DpnI resctriction enzyme at 37°C for 1 hr. And the amplified mutated plasmid was transformed into XL10-Gold® Ultracompetent Cells (Section 2.3.3).

Reagent	Quantity
Nuclease-free H_2O	Up to 25 µl
10X reaction buffer	2.5 µl
QuickSolution	1.5 µl
dNTP mix	0.5 µl
Forward primer	63 ng
Reverse primer	63 ng
Template plasmid	25 ng
PfuUltra HF DNA polymerase (2.5 U/µl)	0.5 µl

Table 2.2.3A 25µl master mix for QuickChange II XL site-directed mutagenesis.

Step	Cycle	Temperature (°C)	Time
Initial denaturation	1	95	1 min
Denaturation	18	95	50 sec
Annealing		60	50 sec
Elongation		68	1 min/kb plasmid
Final extension	1	68	7 min

Table 2.2.3B Standard thermocycling conditions for QuickChange II XL site-directed mutagenesis.

Primers used for site-directed mutagenesis in this thesis:

PAMremove primers:

Forward: GGTTAATTACTGACCAGTATGTATCACATATGAC

Reverse: GTCATATGTGATACATACTGGTCAGTAATTAACC

S228IBspHI primers:

Forward: GGGTACATCTGC ACT CAT GAT GAGTGTCACcg

Reverse: cgGTGACACTC ATC ATG AGT GCAGATGTACCC

2.2.4 DNA gel electrophoresis

The sizes of DNA were determined by gel electrophoresis. The agarose gel was made with Tris-Acetate EDTA (TAE) or Tris-Borate EDTA (TBE) buffer, and the DNA was electrophoresed alongside with DNA ladders (ThermoFisher) on an agarose gel containing 1X RedSafe (iNtRON Biotech) for about 2 hr at 80 V. The bands were visualized using the ChemiDoc Imager (BioRad).

2.2.5 DNA purification

2.2.5.1 DNA precipitation

DNA was precipitated for salt removal and generation of more concentrated DNA. The ion concentrations were equalized by adding 1/10 of the DNA volume of 3 M Sodium Acetate buffer, pH 5.2 at 4°C. DNA was then precipitated by adding 2-3 volumes of cold 100% ethanol and being incubated at -20°C for 1 hr. The precipitated DNA was pelleted by centrifugation at 13,000 rpm at 4°C for 15 min and supernatant carefully aspirated. The pellet was washed in 250

µl cold 70% ethanol and dissolved in desired volume of Buffer AE (10 mM Tris.Cl, pH 8.5).

2.2.5.2 DNA purification from agarose gels/PCR clean-up

The purification of DNA from agarose gels or PCR reactions was carried out using the NucleoSpin® Gel and PCR Clean-up Kit (MACHEREY-NAGEL). For DNA extraction from agarose gels, DNA fragments of desired size on the gel were excised using a scalpel (Swann-Moston) and the gel slice was dissolved in Buffer NTI for 10 min at 50°C. For PCR clean-up, samples were also mixed with Buffer NTI of 2X volumes. The NTI mixture was applied to a NucleoSpin® Gel and PCR Clean-up Column and DNA was bound to the silica membrane by centrifugation at 11,000 g for 30 sec. The silica membrane was washed with Buffer NT3 twice and the DNA was eluted with 15-30 µl Buffer NE.

2.2.6 DNA quantity determination and sequencing

The nucleic acid quality and concentration was measured by Nanodrop spectrophotometer (Nanodrop Technologies). The Nanodrop was first calibrated with the blank control, and 1.5 µl of DNA or RNA was loaded onto the Nanodrop. The nucleic acid concentration was then determined by the Nanodrop, and the A260/A280 ratio of 1.8 to 2.1 was accepted as good quality of DNA samples.

The Sanger Sequencing of DNA samples was carried out by GATC Services of

Eurofins Genomics.

2.2.7 Single-cell DNA gel electrophoresis (Comet assay)

Alkaline comet assay was utilized to detect DNA breaks in cells after certain treatment. Briefly, lymphoblastoid cells after certain treatment were harvested and resuspended in ice-cold PBS. The ice-cold cell suspension was mixed with 42°C 1.2% low melting point agarose (Invitrogen) in PBS for a final concentration of 0.6%, and quickly spread on the pre-coated superfrost slides (VWR) with 0.6% normal agarose (Sigma) in H_2O. After the agarose solidified, the slides were placed in alkaline lysis buffer (2.5 M NaCl, 0.1 M EDTA, 10 mM Tris.Cl pH 10.0, 1% DMSO, 1% Triton X-100, pH adjusted to 10) at 4°C for 1 hr. After being washed three times with cold MilliQ H_2O, the slides were then subjected to electrophoresis in the electrophoresis buffer (1 mM EDTA, 0.36 M NaOH, 1% DMSO) at 25 V for 25 min at 4°C. After the electrophoresis, the slides were neutralised with 0.4 M Tris.Cl pH 7.0 three times for 5 min at 4°C. The slides were washed in MilliQ H_2O at room temperature for 30 min before drying overnight. Cells were stained with 1:10,000 SYBR Gold (Invitrogen) diluted in MilliQ H_2O at pH 8.0 for 30 min, and the slides were dried at 60°C for 2 hr before analysing. For analysis of comet tails, pictures were taken with a Nikon Eclipse Ni-E microscope (Nikon Instruments Europe B.V.) and analysed using the Komet 5.5 image analysis software (Andor Technology, Belfast, Northern Ireland) by Dr Arnaud Legrand.

2.3 DNA cloning

2.3.1 Restriction digestion

The specific restriction enzymes (NEB) were used to generate DNA fragments with desired DNA ends for cloning. The restriction digestion was set up according to the NEB cloner (https://nebcloner.neb.com/#!/redigest). A 50 µl reaction usually consisted of 1X restriction digest buffer (NEB), 1 µg DNA, 1 µl restriction enzyme and ddH_2O to 50 µl. The DNA was digested at 37°C for 1 hr, and analysed by agarose gel electrophoresis at 80 V for 2 hr and visualized by the ChemiDoc Imager (BioRad).

2.3.2 DNA ligation

The DNA fragments with complimented cohesive ends were ligated using T4 DNA ligase (NEB). The reaction was set up as follows: 1X T4 DNA ligase buffer (NEB), same moles of DNA fragments, 1 µl T4 DNA ligase and ddH_2O to 20 µl. The reaction was incubated at room temperature for 10 min, and inactivated at 65°C for 10 min for further cloning, or kept on ice for bacterial transformation.

2.3.3 Bacterial transformation

For transformation of DH5α, 25 µl cells together with plasmids were incubated on ice for 30 min. The DH5α cells were then heat-pulsed at 42°C for 30 sec and immediately incubated on ice for another 3 min. The transformed cells were incubated in 100 µl LB broth at 37°C for 1hr and spread on LB agar plates with

the specific antibiotic for the transformed plasmids.

For transformation of XL10-Gold® Ultracompetent Cells for site-directed mutagenesis (Section 2.2.3), 45 µl of cells were aliquoted to a prechilled 14 ml BD Falcon polypropylene round-bottom tube and mixed with 2 µl β-ME on ice for 10 min with gentle swirling every 2 minutes. 2 µl of DpnI-treated DNA was transferred to each tube and mixed by gentle swirling. Cells with the plasmids were incubated on ice for 30 min and heat-pulsed at 42°C for 30 sec before incubation on ice for another 2 min. The transformed competent cells were recovered in 0.5 ml preheated S.O.C broth (Invitrogen) at 37°C for 1 hr before being spread on LB agar plates with the specific antibiotic for the transformed plasmids.

Plates were incubated at 37°C for 16 hr to allow single colonies to grow. Single colonies were picked into 5 ml LB broth with the specific antibiotic and incubated at 37°C with shaking overnight to amplify the colonies. Cells were either pelleted for Miniprep of plasmids or expanded in 100-200 ml LB broth for another overnight incubation for Midiprep of plasmids depending on the amount of plasmids desired (Section 2.2.1.1).

2.4 RNA analysis

2.4.1 RNA extraction

RNA was extracted from cultured RPE-1 cells in 6-well plates using TRIZOL

extraction protocol. Cells were harvested by trypsinisation and washed with PBS. Cells were lysed with 1 ml of TRIZOL® Reagent (Invitrogen) by pipetting until homogenate solution was generated. The homogenized samples were incubated at room temperature for 5 min to permit the complete dissociation of nucleoprotein complexes. 200 µl chloroform (Sigma) was added, mixed vigorously and incubated at room temperature for 3 min before centrifugation at 12,000 g for 15 min at 4°C to separate the RNA exclusively in the colourless upper aqueous phase. The aqueous phase was then separated and mixed with 500 µl isopropanol (Sigma) and incubated at room temperature for 10 min to precipitate the RNA. The RNA was pelleted by centrifugation at 12,000 g for 10 min at 4°C. The RNA pellet was washed with 1 ml 75% ethanol, and finally dissolved in 30 µl nuclease-free H_2O with an incubation at 55-60°C for 10 min. The concentration and purity of the extracted RNA was determined by Nanodrop spectrophotometer (Section 2.2.6).

2.4.2 Reverse transcription of RNA into complimentary DNA (cDNA)

The SuperScript™ II Reverse Transcriptase Kit (Invitrogen) was used to synthesize first-strand cDNA from the purified RNA. A 20 µl reaction was applied for the reverse transcription of 1 ng to 5 µg total RNA. The master mix was made according to Table 2.4.2. The concentration of the product cDNA was determined by Nanodrop spectrophotometer (Section 2.2.6).

Reagent	Quantity
500 µg/ml Oligo $(dT)_{18}$ primers	0.5 µl
500 µg/ml Random primers	0.5 µl
Total RNA	1 µl (1 ng to 5 µg)
10 mM dNTP mix	1 µl
Nuclease free H_2O	9 µl
The mixture was heated to 65°C for 5 min and quick chilled on ice. After that, the following component was added to the mixture:	
5X First-Strand Buffer	4 µl
0.1 M DTT	2 µl
40 units/ul RNaseOUT™	1 µl
The mixture was incubated at 25°C for 2 min, and the following amount of enzyme was added to the mixture:	
SuperScript™ II Reverse Transcriptase	1 µl (200 units)
The mixture was incubated at 42°C for 50 min for reverse transcription to occur, and inactivated by heating at 70°C for 15 min.	

Table 2.4.2 Master mix and reaction conditions for reverse transcription of RNA into cDNA.

2.5 Protein analysis

2.5.1 Whole cell extraction

The extraction buffer containing Benzonase nuclease (Novagen) that digests all forms of DNA and RNA to release proteins from chromatins was used to extract the whole cell lysis. The extraction buffer consists of 0.5% NP40, 40 mM NaCl, 50 mM Tris.Cl pH 7.5, 2 mM $MgCl_2$, 2X protease inhibitor cocktail (Roche) and 25 U/ml Benzonase. Harvested cells were washed once in PBS and then resuspended in the extraction buffer, the amount of which was dependent on the number of cells to lyse. The lysate mixture was transferred to ice and incubated for 10 min for Benzonase to work. An aliquot can be taken for the

whole cell extraction. NaCl was increased to 150 mM with 20 min incubation at 4°C. The lysate was centrifuged at 21,000 g for 20 min at 4°C and the supernatant was collected as the cell lysate for further applications. The protein concentration was determined by Bradford assay when necessary. Bradford reagent (Sigma) was mixed with different dilutions of BSA (Sigma) in PBS and standard curve was determined by measuring the absorbance of light 595 nm (A_{595}) using the Novaspec Plus Spectrometer (Amersham Biosciences). The absorbance of lysates was also measured and the protein concentration was determined by the standard curve.

2.5.2 Western blotting

Protein lysate was mixed with 5X Laemmli sample buffer (0.25 M Tris.Cl pH 6.8, 50% Glycerol, 10% SDS, 0.5 M DTT, 0.25% Bromophenol blue) and boiled at 95°C for 10 min to denature the protein. Denatured samples were loaded onto 8-15% poly-acrylamide gels, and the electrophoresis was carried on at 80 V for about 30 min until the proteins started to separate and changed to 160 V. The samples were run alongside the Blue Prestained Protein Standard ladder (NEB). After that, proteins were blotted onto an Amersham™ Protran™ 0.2 µm nitrocellulose membrane using semi-dry transfer at 13 V for 35 min. Following the transfer, the membrane was blocked for 30-60 min with gentle shaking in the blocking buffer which is usually 3% milk (Sigma) in 1X PBS-T (0.1% Tween20 in PBS) depending on properties of the primary antibody. After

blocking, the membrane was incubated with appropriate primary antibody solution diluted in the blocking buffer for 2 hr at room temperature or overnight at 4°C. Membranes were washed in 1X PBS-T three times for 5 min and incubated with HRP-conjugated goat anti-mouse or anti-rabbit IgG secondary antibody (Thermo) at a dilution of both 1:50,000 in the blocking buffer at room temperature for 1 hr. Membranes were washed in 1X PBS-T three times for 5 min and illuminated with ECL reagent (BioRad) for visualization on the ChemiDoc Imager (BioRad). Alternatively, the membrane after being washed from the primary antibody incubation can be incubated with the IRDye® 800CW or 680RD fluorescence secondary antibody (LICOR) at a dilution of 1:25,000 in the blocking buffer protected from light at room temperature for 1 hr. Membranes were washed in 1X PBS-T three times for 5 min and visualized on the Odyssey® CLx Imaging System (LICOR). Table 2.5.2 summarizes the sources and conditions of primary antibodies used for Western blotting in this thesis.

Primary antibodies	Species	Source	Dilution
Anti-PCNA	Mouse	PC10, Millipore	1:10,000
Anti-actin	Mouse	AC40, Sigma	1:1,000
Anti-Ub PCNA^{K164}	Rabbit	D5C7P, CST	1:1,000
Anti-PARP1	Rabbit	9542, CST	1:500
Anti-p21	Rabbit	EPR362, Abcam	1:1,000

Table 2.5.2 Primary antibodies used for Western blotting in this thesis.

2.5.3 Visualizing protein localization using immunofluorescence microscopy

In the cases when triton pre-extraction is required, cells growing on 22x22 mm glass coverslips were first rinsed in PBSS (PBS with 0.5 mM $MgCl_2$ and 0.5 mM $CaCl_2$, Gibco) and then CSK buffer (10 mM PIPES pH 7.0, 100 mM NaCl, 300 mM Sucrose and 3 mM $MgCl_2$). The soluble proteins were removed by 0.2% Triton X-100 (BDH) in CSK buffer on ice for 90 sec, and the cells were carefully washed with CSK buffer one more time. After the extraction, cells were fixed with 2% PFA in PBS at room temperature for 20 min and then 100% methanol at -20°C for 20 min. Then cells were washed with PBS once and continued with regular permeabilisation process. For experiments that do not require pre-extraction, cells were simply fixed with 2% PFA in PBS at room temperature for 20 min and washed in PBS once. Then the cells were permeabilised with 0.5% Triton X-100 in PBS for 5 min and immediately washed with PBS once. Coverslips were blocked with the blocking buffer (3% BSA in PBS) for 30 min and washed twice with PBS-T. EdU labelling was performed before primary antibody incubation using Click-iT EdU Alexa Flour 647 Imaging Kit (Invitrogen) according to the manufacturer's protocol. Then the cells were probed with appropriate primary antibody solution diluted in the blocking buffer at room temperature for 1 hr or at 4°C overnight. The coverslips were rinsed in PBS-T three times, and probed with Alexa Flour secondary antibodies (1:500, Invitrogen) diluted in the blocking buffer at room temperature for 45 min protected from light. After being washed with PBS-T for another three times, cells were labelled with 0.2 µg/ml DAPI to stain the DNA at room temperature

for 5 min protected from light. After that, coverslips were mounted with Prolong™ Gold antifade reagent (Invitrogen) and the slides were stored at 4°C. Slides were imaged and pictures were taken with a Zeiss 510 Metahead Confocal Microscope (Zeiss) or a Leica SP8 X-SMD FLIM Confocal Microscope (Leica). Table 2.5.3 summarizes the sources and conditions of primary antibodies used for immunofluorescence microscopy in this thesis.

Primary antibodies	Species	Source	Dilution
Anti-PCNA	Mouse	PC10, Millipore	1:1,000
Anti-PCNA	Rabbit	Ab18197, Abcam	1:1,000
Anti-phospho H2AX^{S139}	Mouse	JBW301, Millipore	1:1,000
Anti-Cdt1	Rabbit	3386, CST	1:100
Anti-p21	Rabbit	EPR362, Abcam	1:500
Anti-PAR	Rabbit	4336-BPC-100, AMS Biotech	1:200

Table 2.5.3 Primary antibodies used for immunofluorescence microscopy in this thesis.

The automated quantification for the microscopy images was carried out using Cell Profiler software (https://cellprofiler.org/). Briefly, the total cell count was determined by DAPI and the foci numbers or intensity were measured according to a certain threshold. The threshold was set according to the diameter and intensity of the foci. All the settings remained unchanged throughout the analysis to ensure the results are unbiased.

2.5.4 Strep-tagged protein purification and mass spectrometry

The whole cell extract of cells expressing strep-tagged proteins were generated according to the processes above (Section 2.5.1). The cell lysates were then incubated with Strep-Tactin Superflow Plus (Qiagen) for 1 hr at 4°C in binding buffer (0.5% NP40, 150 mM NaCl, 50 mM Tris.Cl pH 7.5, 2 mM EDTA, 1X Protease Inhibitor Cocktail (Roche)). Beads were washed in binding buffer and eluted with NuPAGE LDS sample buffer and NuPAGE reducing agent (both Thermo). Bound proteins were separated through electrophoresis in NuPAGE Midi 4–12% SDS-PAGE gel (Thermo) and stained with Safe Stain (Invitrogen). Bands corresponding to endogenous and strep-tagged proteins were excised and analysed by mass spectrometry. The entire analysis was carried out by Dr Roman Fischer in Target Discovery Institute (TDI), University of Oxford. Briefly, gelbands were destained with 50% methanol in 5% acetic acid before reduction (10 mM DTT), alkylation (50 mM iodoacetamide) and digest with Trypsin. Extracted peptides were analysed with a nAcquity (Waters) coupled Orbitrap Elite (Thermo) LC–MS/MS system. The peptide mixture was separated using a gradient of 2–40% Acetonitrile in 0.1% formic acid. Precursors between 300 and 1500 m/z were isolated with a mass window of 1.8 m/z and analysed after CID fragmentation in the ion trap with a normalized collision energy of 35%. RAW data was analysed with PEAKS (Bioinformatics Solutions) version 7 using 10 ppm precursor and 0.5 Da fragment mass accuracy.

Chapter 3: Construction of PCNA^{S228I} knock-in cell lines

3.1 Overview

The major symptoms of PARD are growth retardation, neurodegeneration and photosensitivity. Similar clinical manifestations are often associated with genetic disorders resulting from mutations in other DNA replication and repair genes. Specifically, mutations of DNA replication proteins such as ORC and Cdc6 can lead to Meier Gorlin Syndrome which is characterized by severe growth retardation [27], and mutations of NER proteins (the XP complementation groups) result in DNA repair disorders including Xeroderma Pigmentosum (XP), which has symptoms including neurodegeneration and photosensitivity [121]. Therefore, it seems likely that the specific combination of symptoms found in PARD results from failures in multiple DNA metabolic pathways. The aim of my project was to identify the specific cellular processes that are affected by the S228I mutation, and to determine the cellular circumstances in which different pathways have different requirements for PCNA activity.

Although I had access to cell lines derived from affected individuals, the following considerations led me to decide to generate a novel isogenic knock-in cell line to underpin the proposed work:

1. Given that the affected individuals are all from one family, it remains a possibility that the cellular phenotypes observed in these cell lines result from, or are confounded by, other unidentified polymorphisms co-segregating in this family. Recapitulation of our original observations in an independent system will show definitively that the reported cellular phenotypes are caused by the $PCNA^{S228I}$ alteration.

2. Additionally, unknown adaptive genetic or epigenetic modifications might be acquired during development in order to compensate for the most severe phenotypes caused by the mutation (especially those related to cell proliferation and cell cycle progression), and these would mask any underlying defects caused by $PCNA^{S228I}$. By generating the $PCNA^{S228I}$ mutation *de novo* I can monitor cellular phenotypes very rapidly after derivation, eliminating this possibility.

3. Our original work used control cell lines derived from related but unaffected individuals. These are, of course, genetically heterogeneous, and this generates challenges in distinguishing any normal cell-cell variability in cellular activities from mutation specific effects. The knock-in cell line will provide an isogenic control, allowing identification of even subtle consequences of $PCNA^{S228I}$ alteration.

4. The major limitations associated with the use of lymphblastoid cell lines derived from affected individuals would also significantly limit the experimental

work that could be performed to investigate pathways of DNA repair affected by PCNA^{S228I}. The lymphoblast derived cell lines were immortalised using EBV transformation, a relatively uncharacterised process that certainly overrides cellular checkpoint responses and alters the cell cycle. Many repair assays are microscopy based and require adherent cell lines, as does the gold standard test for DNA repair activity – the clonogenic survival assay. Ethical considerations mean that we cannot obtain new skin biopsies from affected individuals and hence clonogenic survival assays using primary fibroblasts are no longer possible due to limited availability of material. The knock-in cell lines will provide an unlimited source of material for both cellular and biochemical assays.

Therefore, I chose hTERT RPE-1 cells (ATCC Ref. CRL4000) to construct the PCNA^{S228I} knock-in cell lines to provide a more physiological model with intact cell cycle and DNA damage checkpoint responses. The RPE-1 cells were first analysed by MFISH to verify that they had the expected karyotype and the copy number of the *PCNA* gene was determined to be 2 as expected by FISH using BAC probes against the PCNA locus (Appendix Fig. A). In this chapter, I will describe the procedures I used to generate PCNA^{S228I} knock-in RPE-1 cell line through CRISPR-Cas9 technique, and validate the knock-in cell line by several phenotypic studies.

3.2 Generation of PCNA^{S228I} knock-in cell lines through CRISPR-Cas9 technique

Clustered Regularly Interspaced Short Palindromic Repeat (CRISPR)-Cas9 endonuclease was first discovered as part of a bacterial defence mechanism against the DNA of invading phage [292]. Cas9 endonuclease is guided to the target DNA region with the help of a single stranded guide RNA (sgRNA) matching a 20-nucleotide sequence (protospacer) within genomic loci and excises DNA immediately upstream of a required 5′-NGG protospacer adjacent motif (PAM) [293]. The excision of Cas9 generates DSBs activating NHEJ or HR pathway, which enables this mechanism to be a widely used genome editing tool.

The overall strategy for constructing the PCNA^{S228I} knock-in RPE-1 cell line was to induce a DSB in intron 6 of *PCNA* using Cas9 and allow homology-directed repair (HDR) to occur using a template encoding the S228I alteration in exon 6 as well as containing a PGK-Neo selection cassette in intron 5 (Fig. 3.2). Thus, screening by resistance to G418 selected for cells that had been targeted in at least one locus of *PCNA*, or in which random integration of the HDR template had occurred. Successful clones resulting from the former were identified by PCR screening of G418 resistant clones.

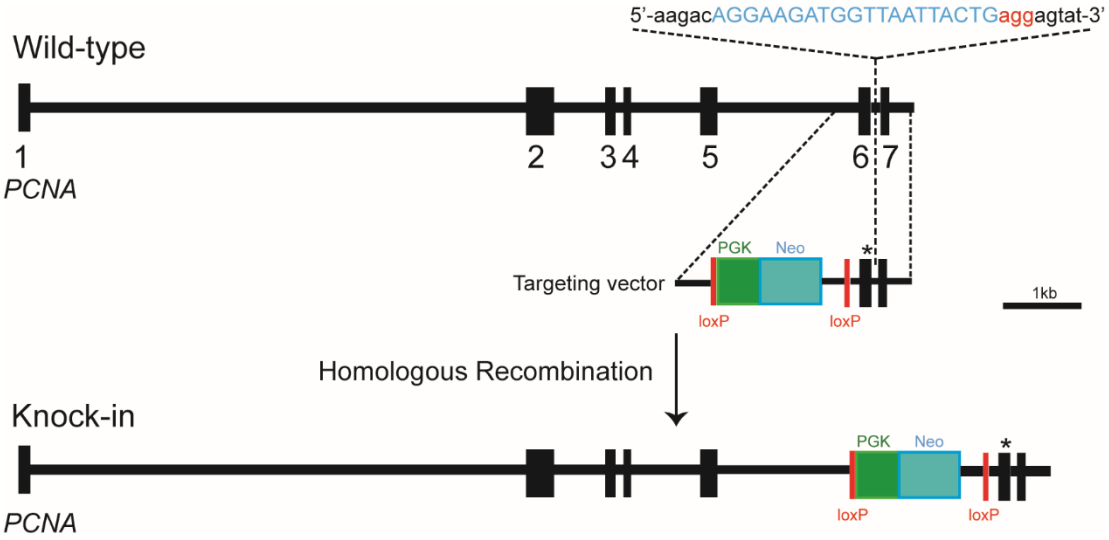


Figure 3.2 The overall strategy of constructing PCNA^{S228I} knock-in cell lines using CRISPR-Cas9 technique. The guide RNA was designed in intron 6, and the targeting vector containing a PGK-Neo cassette in intron 5 with the S228I alteration in exon 6 (asterisk) was applied as an HDR template for the purpose of knocking in the mutation and providing a selection marker simultaneously.

3.2.1 Constructing the targeting vector

First of all, I designed the sequence of sgRNA using an online CRISPR Design Tool (http://tools.genome-engineering.org). The sgRNA is in intron 6, with the PAM 77bp away from the sequence coding for S228I mutation. The sgRNA has an off-target score of 37.6 and an on-target score of 60.1, which is estimated to be suitable for genome editing. The sgRNA was cloned into the pSpCas9(BB)-2A-GFP vector for co-expression with Cas9 according to the protocol from Zhang lab [294]. The pSpCas9(BB)-2A-GFP plasmid, also called PX458, was kindly provided by Dr Ben Davis, Transgenics Core facility, WCHG [294]. Briefly, the sgRNA oligos (sequence with guide RNA underlined: sgRNA TOP: CACC GAGGAAGATGGTTAATTACTG, sgRNA BOT: AAAC CAGTAATTAACCATC TTCCTC) were annealed and cloned into the PX458 plasmid using BbsI

restriction site. The transformed competent cells were selected against ampicillin and the sequence was verified by Sanger sequencing using the U6-Fwd primer (Appendix Fig. B1).

In order to construct an HDR template with a PGK-Neo cassette in intron 5 of the *PCNA* gene, I amplified two PCR products of approximately 500bp from genomic DNA purified from RPE-1 cells. These corresponded to regions of the *PCNA* gene 5′ and 3′ of the predicted cutting site of the Cas9 with the PCNA guide RNA (reference coordinates from GRCh38/hg38 assembly). The primers for the PCR amplification each included restriction enzyme cleavage sites for ease of cloning into the target vector (see Chapter 2 for primer sequences). The source of the PGK-Neo cassette was plasmid PL452, also provided by Dr Ben Davis (Appendix Fig. B2) [295]. PL452 was digested with EcoRI and BamHI to release the PGK-Neo cassette, which was then ligated to the two PCR products (Fig. 3.2.1A).

The assembled HDR template was cloned into pBluescript SKII(+) through double antibiotic selection (ampicillin and kanamycin), the sequence of the resulting plasmid verified by Sanger sequencing (data not shown). In order to protect the HDR template from cutting by Cas9, I mutated the PAM sequence using site-directed mutagenesis (SDM) and confirmed the presence of the mutation by Sanger sequencing (Fig. 3.2.1B). This HDR template was used as the WT control for the isogenic knock-in cell lines. I next introduced the S228I

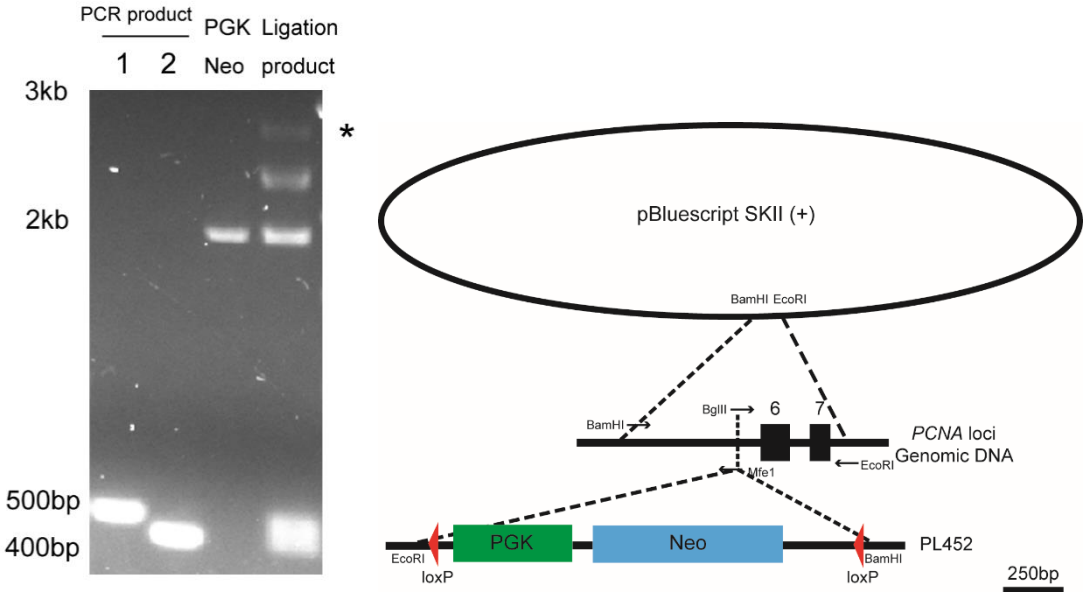


Figure 3.2.1A Assembly of the homology arm. The two PCR products were from genomic PCR of PCNA using the primers with restriction enzyme cleavage sites shown in the strategy. The PGK-Neo cassette was digested and purified from the PL452 plasmid. And the asterisk showed the desired product for the assembly and was ligated to pBluescript SKII(+) backbone.

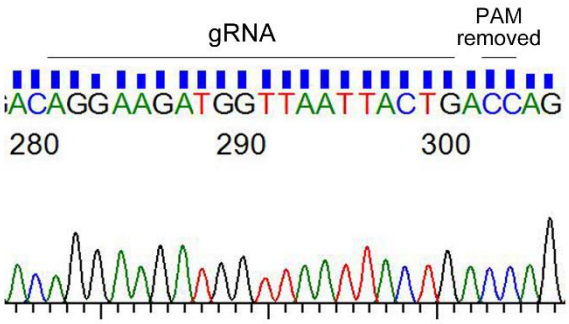


Figure 3.2.1B Sequencing result of PAM removal site-directed mutagenesis. AGG was mutated to ACC.

mutation into the HDR template plasmid by SDM. To increase the efficiency of downstream genotyping, I designed SDM primers that created the S228I mutation with additional synonymous mutations generating a BspHI restriction site (Fig. 3.2.1C). Therefore, the final HDR template vector for the CRISPR-

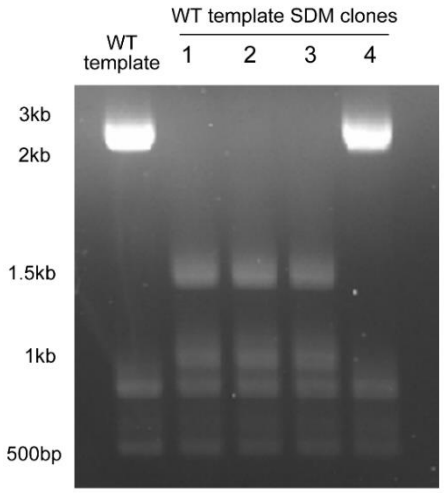


Figure 3.2.1C BspHI-NheI double digestion after site-directed mutagenesis to introduce the S228I mutation in the plasmid of HDR template. Here clones 1-3 have the desired mutation and we used clone 1 for plasmid.

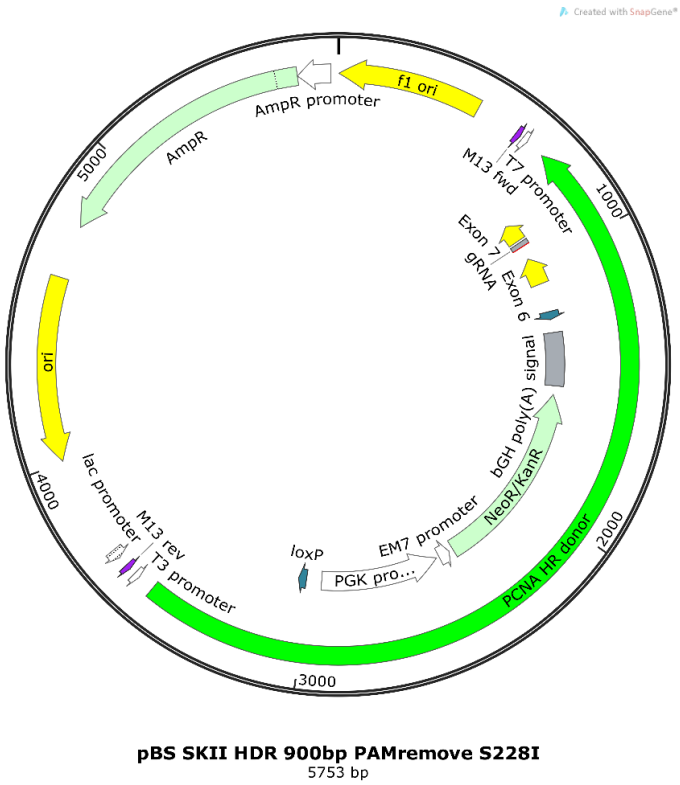
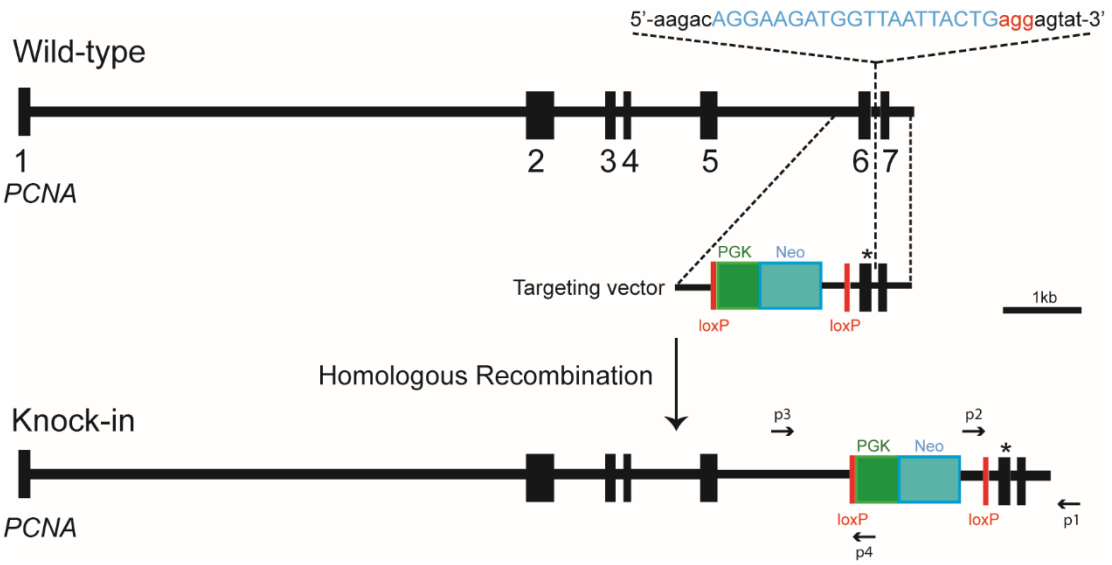


Figure 3.2.1D The map of the HDR template vector. The S228I alteration is in exon 6, which is not shown in the map.

Cas9 knock-in of PCNA^{S228I} mutation was created, containing a PGK-Neo cassette in intron 5 with about 500bp of 5′ and 3′ of *PCNA* homologous sequence (Fig. 3.2.1D).

3.2.2 Screening and clone genotyping

After successful cloning of the HDR template, 4x10^6 RPE-1 cells were cotransfected with the plasmid that expresses GFP-Cas9 and the guide RNA (pSpCas9(BB)-2A-GFP with sgRNA) as well as the HDR template (either WT or S228I mutated version). A control transfection of HDR template and pSpCas9(BB)-2A-GFP without guide RNA was performed. After 24 hours selection was applied (1 mg/ml G418, Gibco) and this was maintained with a change of medium every two days. After the majority of control cells were killed (ascertained by microscopic inspection of plates), the targeted cell populations were serially diluted to generate individual colonies derived from single cells. Colonies were then isolated independently, expanded and genotyped to identify edited clones. For genotyping by PCR, primers were designed to anneal 3′ to the target site outside the homology arm (p1) and in the PGK-Neo cassette (p2) to identify clones with the PGK-Neo cassette inserted at the correct genomic position. Additionally, primer p1 together with a primer that anneals 5′ to the target site outside the homology arm (p3) were used to obtain the sequence of any alleles without the PGK-Neo cassette, which I defined as ‘non-loxP allele’ (Fig. 3.2.2A). The expected long PCR product which could be amplified by



Primer names	Product sizes (bp)
p1, p2	666
p1, p3	1087
p3, p4	629

Figure 3.2.2A Primers designed for genotyping PCR of the knock-in clones. Primers p1, p2, p3 and p4 are shown in the map. The desired PCR product sizes from different pairs of primers are as indicated in the table.

these primers from the allele containing with a PGK-Neo cassette is over 3 kb and is therefore not amplified by the conditions used for this PCR. I genotyped 80 WT clones and 130 S228I clones, and identified 8 (10%) and 11 (8.46%) clones with the PGK-Neo cassette inserted into the correct genomic location, respectively (Table 3.2.2). Serendipitously, WT clone 50-11 (transfected with HDR template without the S228I mutation) has both the PGK-Neo cassette insertion in one allele as expected, and the non-loxP allele also shows PAM removal with conversion to a sequence identical to the PAM mutation sequence of HDR template (Fig. 3.2.2B), demonstrating that this editing strategy has the potential to target both alleles in a single round. In the same manner, S228I

	Number of clones (%)	
Cell line	WT	S228I
PGK-Neo (recombinant cells)	8 (10%)	11 (8.46)
Negative (random integration or senescent cells)	72 (90%)	119 (91.54%)
Total clones screened	80	130

Table 3.2.2 Targeting efficiency of CRISPR-Cas9 knock-in RPE-1 WT controls and S228I mutation cell lines.

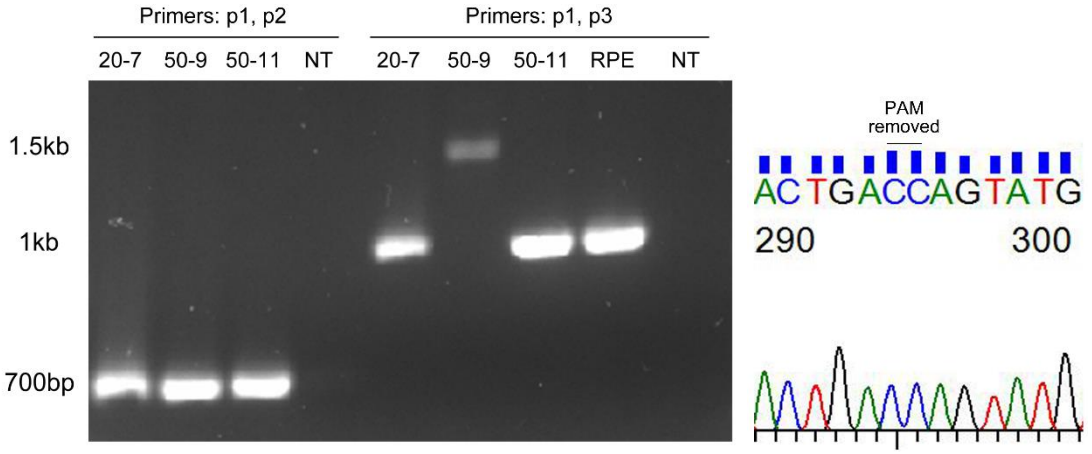


Figure 3.2.2B Genotyping results of some of the clones of WT and the sequencing result of clone $WT_{50\text{-}11}$ amplified by primers p1 and p3. RPE: RPE-1 parental cells genome as template; NT: no PCR template (same as following).

clone 50-18 (transfected with HDR template containing S228I mutation and concomitant BspHI site) was found to have one allele carrying the PGK-Neo cassette as well as the S228I-BspHI site (Fig. 3.2.2C), and the other allele with PAM removal by conversion to a sequence identical to HDR template encoding S228I with the BspHI site. Inspection of the sequence of this allele confirms that it contains the S228I mutation (Fig. 3.2.2D). There is a 274 bp homologous region between the PAM site and the beginning of the PGK-Neo cassette, and

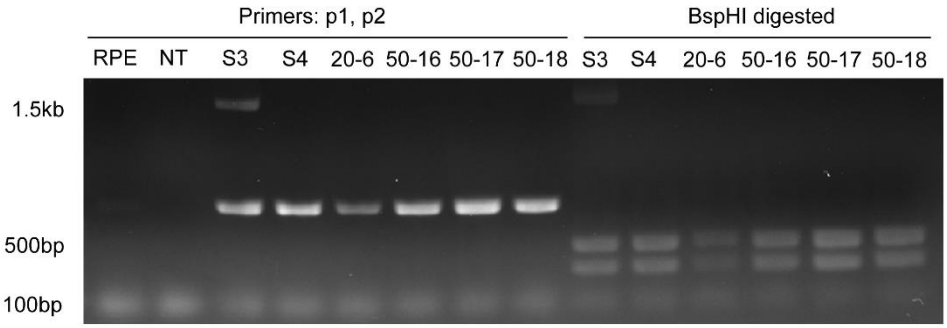


Figure 3.2.2C Genotyping results of some of the clones of S228I. The PCR products of p1 and p2 indicated alleles having PGK-Neo cassette recombination, with the BspHI digestion showing the induction of S228I alteration.

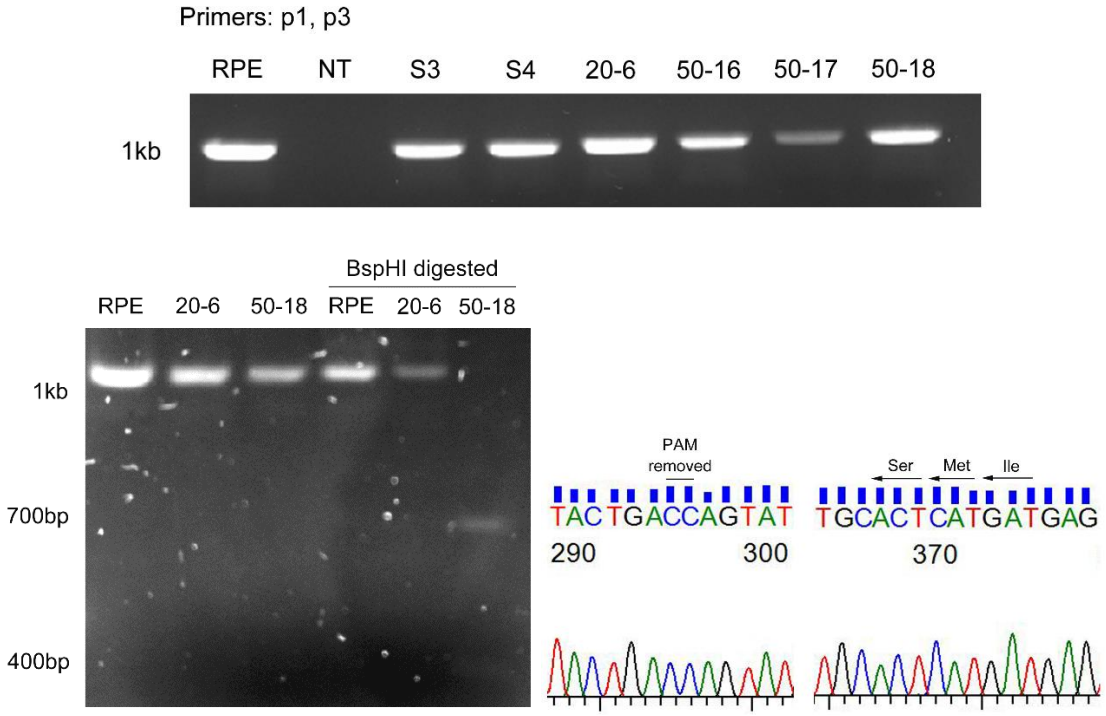


Figure 3.2.2D Genotyping results of some of the clones of S228I. The PCR products of p1 and p3 indicated alleles without PGK-Neo cassette recombination. The BspHI digestion showed induction of S228I alteration, with the sequencing result of clone S228I$_{50\text{-}18}$ amplified by primers p1 and p3.

the S228I mutation site is 77 bp from the PAM, therefore it is likely that in this clone homologous recombination initiated at the PAM on both alleles and

resolved on one allele after the S228I mutation site but before the PGK-Neo cassette (Fig. 3.2.2E). To confirm that the clone $S228I_{50\text{-}18}$ is homozygous for $PCNA^{S228I}$, I generated and sequenced cDNA from this clone. Only $PCNA^{S228I}$ was expressed, with no detectable WT signal observed in this clone (Fig. 3.2.2F).

I expressed Cre recombinase in both WT control clone $WT_{50\text{-}11}$ and S228I mutation clone $S228I_{50\text{-}18}$ with the intention of eliminating the PGK-Neo cassette. Single colonies were cloned and expanded for genotyping as above. However, after PCR screening 37 WT clones and 22 S228I clones, none were identified in which the PGK-Neo cassette had been removed. Further PCR using primers annealing 5′ to the target site outside the homology arm (p3) and in the 5′ of the PGK-Neo cassette (p4) (Fig. 3.2.2A) generated no product for either the $WT_{50\text{-}11}$ or $S228I_{50\text{-}18}$ clones (data not shown). This suggests that there have been some unexpected rearrangements in the 5′ region of the PGK-Neo knock-in locus. It is possible that there have been multiple insertions of the HDR template, or some other rearrangements that prevent the expected PCR products being formed, possibly because of the long non-homologous PGK-Neo sequence. We also noticed that the hTERT of the RPE-1 is right at the *PCNA* locus (see Appendix A), and if it was inserted right in the intron 5 of *PCNA* gene, the existence of over 3 kb hTERT insertion and 1.8 kb PGK-Neo cassette in the intron is likely to affect the splicing of PCNA mRNA. Were this

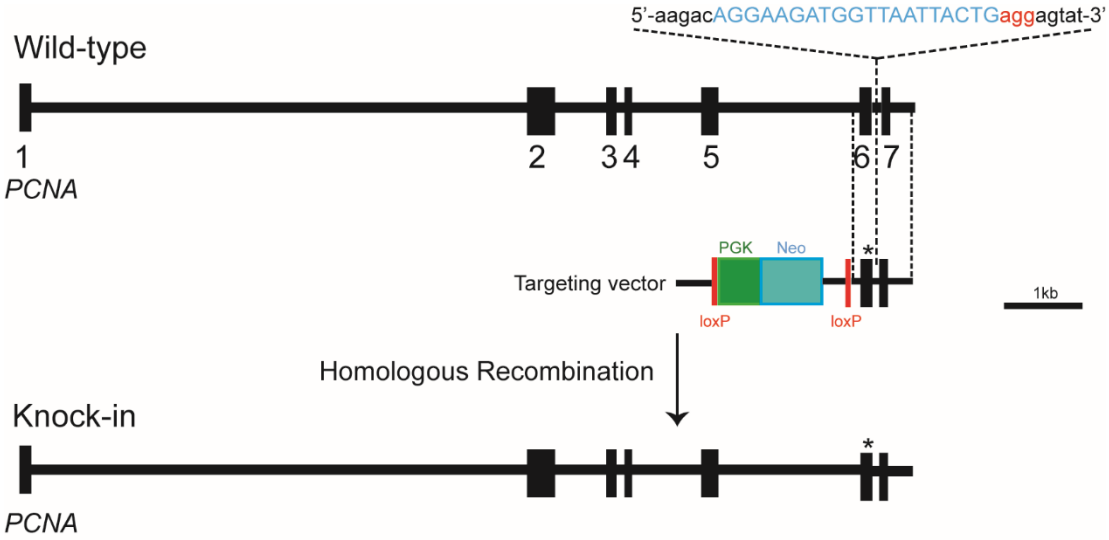


Figure 3.2.2E A proposed mechanism for the allele without PGK-Neo cassette recombination but containing S228I alteration.

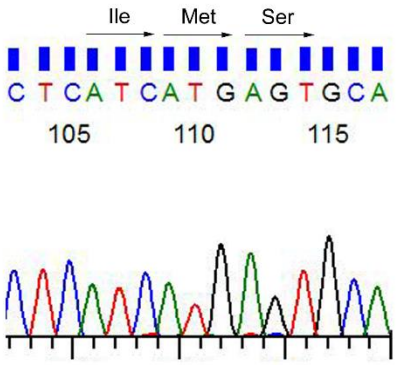


Figure 3.2.2F Sequencing result of the cDNA of the clone S228I$_{50\text{-}18}$. The amino acid residues for the protein translation are indicated and the Ser228 is mutated to isoleucine.

the case, it seems likely that this would affect expression of the *PCNA* gene from this allele, resulting in the two clones being effectively hemizygous, PCNA$^{WT/Neo}$ and PCNA$^{S228I/Neo}$. However, as there is no clue about the exact sequence around 5′ region of the PGK-Neo knock-in locus, we can hardly investigate the sequence of this region by Sanger Sequencing. We performed MFISH on the two cell lines to ensure that no gross chromosomal

rearrangements had occurred, and both clones show a normal karyotype (Appendix Fig. C). Given that the two cell lines have been generated by similar procedures, are indistinguishable by genotyping PCR and karyotype, and the cDNA sequence of the $S228I_{50\text{-}18}$ clone showed exclusive $PCNA^{S228I}$ expression, we decided that this pair of isogenic cell lines are suitable for further research.

3.2.3 Phenotypic validation of $PCNA^{S228I}$ knock-in cell lines

Previous research has shown that there are no differences in the amount of PCNA protein expressed when comparing extracts from EBV-transformed lymphoblastoid cells derived from affected individuals or controls [246]. Western blots were performed in order to determine the PCNA protein expression level in the $PCNA^{S228I}$ knock in cell line. A decrease of about 50% in the amount of PCNA protein was detected in the S228I knock-in cell line (Fig. 3.2.3A). Previous studies in the Green laboratory have demonstrated that knocking down PCNA expression to less than 20% of normal has no apparent effect on cellular proliferation (C. Green personal communication). The $PCNA^{S228I}$ knock-in cells survive about 50% decrease in PCNA protein level, suggesting that there might be some other pathways activated to compensate for the loss of PCNA protein, or that the endogenous PCNA is so abundant that cells can tolerate 50% of decrease in PCNA protein level. Therefore, the possibility that the reduction in PCNA amount can cause significant phenotypes

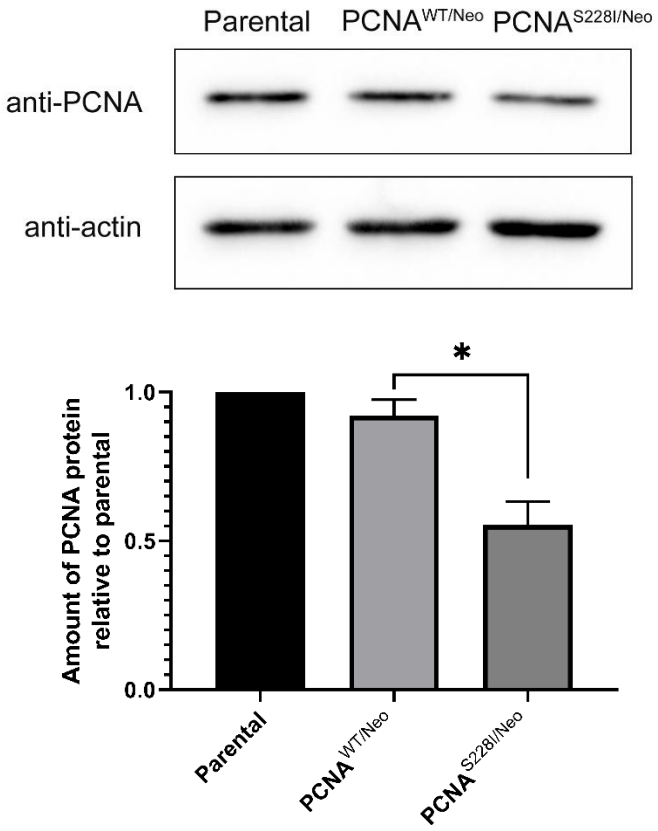


Figure 3.2.3A Anti-PCNA Western blot of the whole cell lysate of the knock-in cell lines. Parental: RPE-1 parental cells as control. Anti-actin is loading control. The quantification was carried out from three independent Western blots. Histogram shows amount of PCNA protein relative to RPE-1 parental cells. Error bars represent SEM. * $p<0.05$, two-tail student's t-test.

should still be considered when interpreting data from this cell line. Immunofluorescence microscopy using an anti-PCNA antibody and pulsed EdU incorporation to mark sites of active DNA synthesis, showed PCNA localized at replication forks as expected in both WT and S228I knock-in cells (Fig. 3.2.3B), which is consistent with the result in primary fibroblasts derived from affected individuals [242], confirming that PCNA localization was not affected by the S228I mutation.

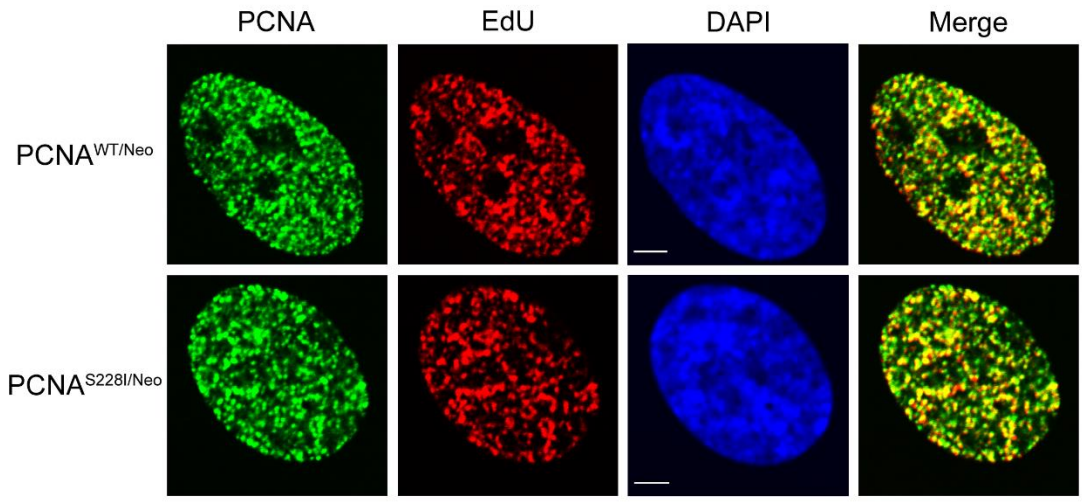


Figure 3.2.3B Immunofluorescence of knock-in cell lines against PCNA. The active replication sites can be observed by EdU labelling, which colocalize with PCNA in both WT and S228I knock-in cells. Scale bar = 3 μm.

The cell cycle profile of the newly generated isogenic cell lines was investigated by Fluorescence Activated Cell Sorting (FACS) using propidium iodide to measure DNA content and BrdU incorporation to mark actively replicating cells. A slight increase in S phase cell percentage was found in PCNA^{S228I} knock-in RPE-1 cells compared to the WT cell line (Fig. 3.2.3C). Similar results were obtained when I analysed the cell cycle profile of lymphoblastoid cell lines derived from affected individuals and controls (Fig. 3.2.3D) [246]. Additionally, quantitative fluorescence microscopy after EdU pulse incorporation showed that there is a slight increase in the %EdU positive cells in the PCNA^{S228I} line (Fig. 3.2.3E). These data suggest that the S228I mutation has subtle influences, if any, on the cell cycle, with cells carrying this mutation spending slightly more time in S phase than their WT counterparts.

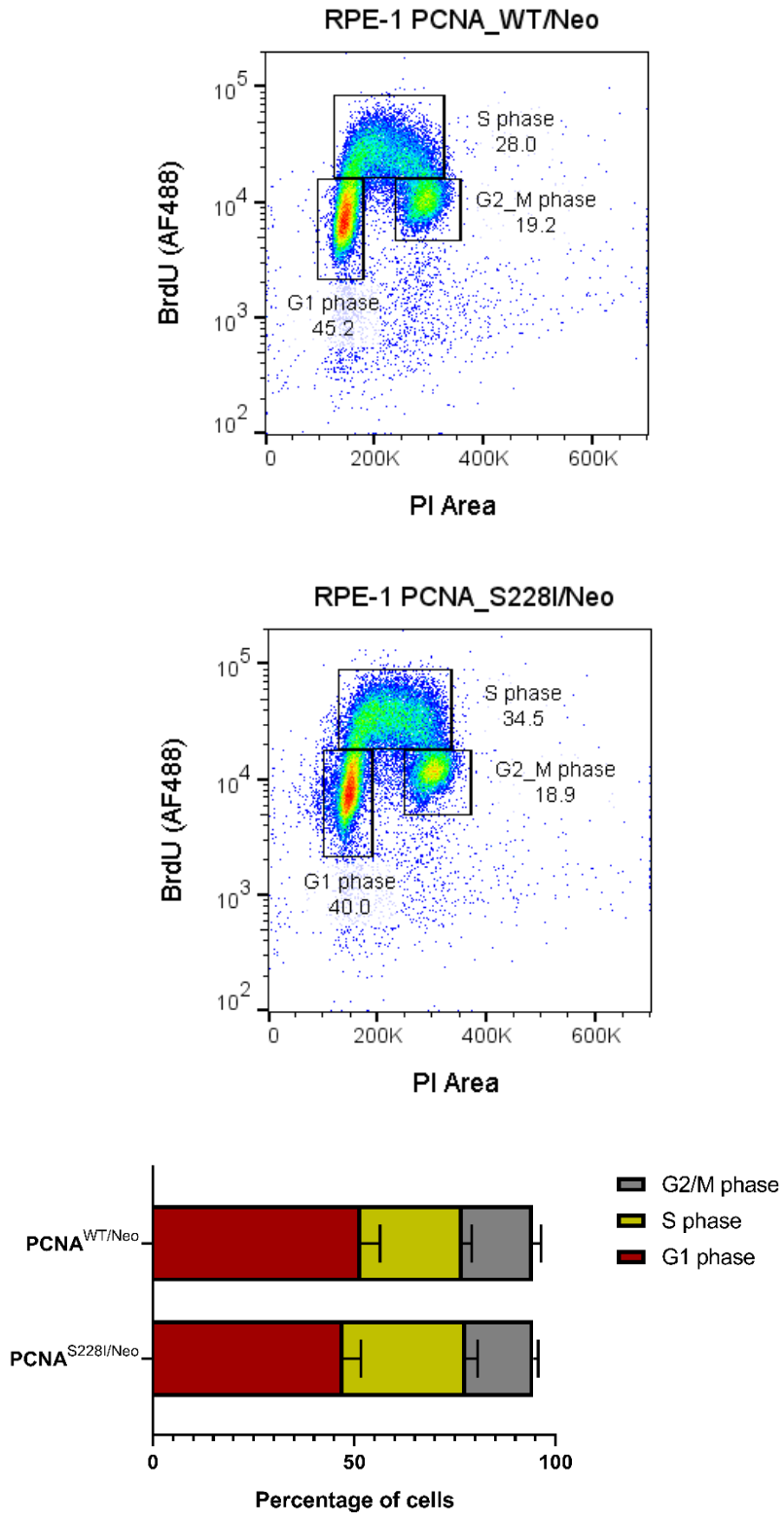


Figure 3.2.3C FACS cell cycle analysis of PCNA^{S228I} knock-in RPE-1 cells. The dot plots are representatives from three independent FACS analysis plotting DNA content (PI) against BrdU (AF488) to determine percentages in G1, S, G2/M cell cycle phases. The graph shows the average cell cycle proportions for each cell line, with the error bars indicating SEM.

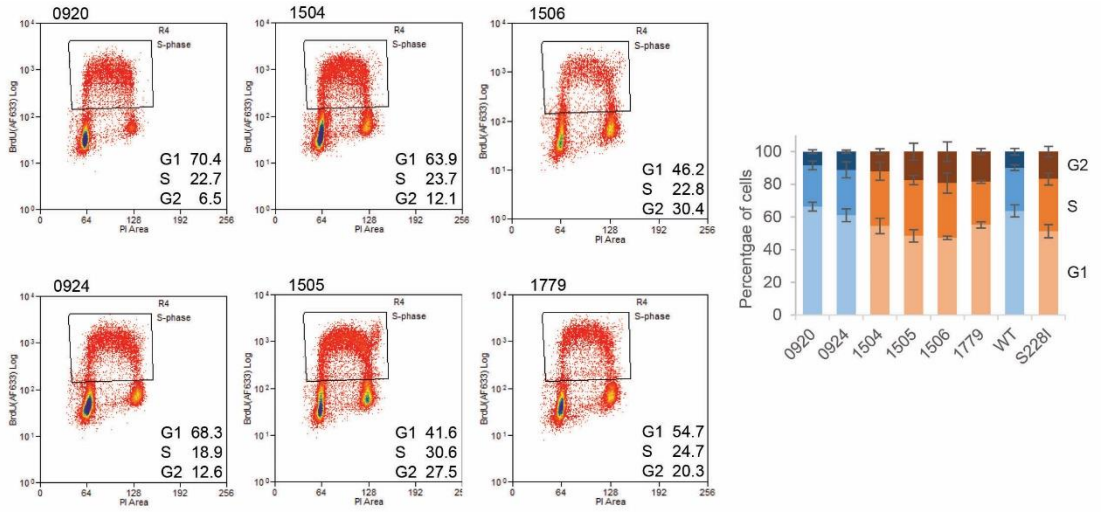


Figure 3.2.3D FACS cell cycle analysis of EBV-transformed lymphoblastoid cells derived from affected individuals. The dot plots are representatives from three independent FACS analysis plotting DNA content (PI) against BrdU (AF488) to determine percentages in G1, S, G2/M cell cycle phases. The graph shows the average cell cycle proportions for each cell line and each genotype (WT and S228I), with the error bars indicating SEM. We can see a slightly larger S and G2 phase percentage in cells from affected individuals (1504, 1505, 1506, 1779) than those from control individuals (0920, 0924). The result has been published by Wilson, *et al.* [246].

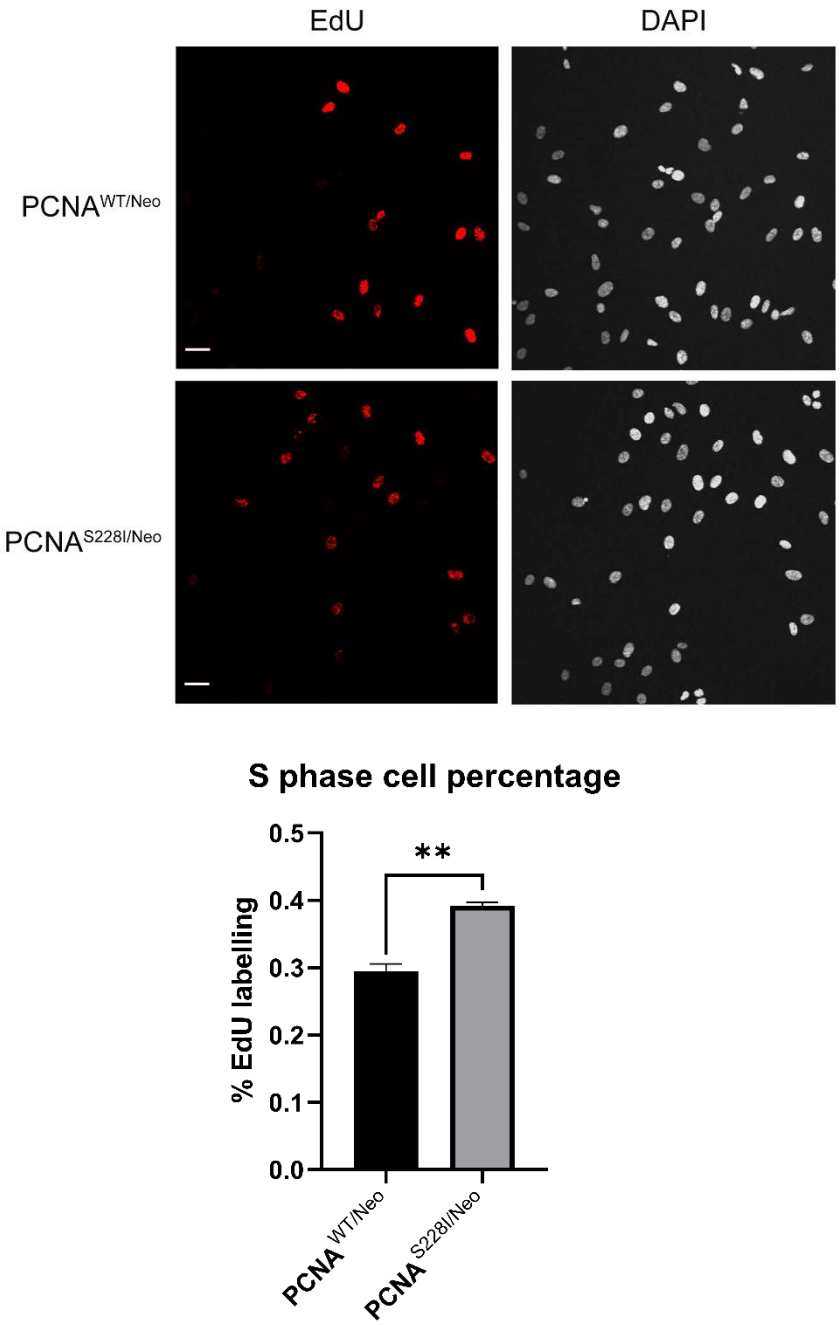


Figure 3.2.3E Quantitative fluorescence microscopy of knock-in cells after EdU pulse incorporation. S phase cell number was determined by EdU positive labelling, and total cell number was determined by DAPI labelling. The imaging picture is a representative from three independent fluorescence microscopy experiments. The percentage was calculated in each single repeat. N=3. Scale bar = 35 μm. Error bars represent SEM. ** $p<0.01$, two-tail student's t-test.

Given that PCNA regulates degradation of Cdt1 and p21 [230] [231], and that the interaction of PCNA with Cdt1 is drastically impaired in the S228I mutant [246], we hypothesised that Cdt1 might be more stable during S phase in PCNA^{S228I} cells, which could lead to re-replication and might extend the length of S phase. However, using immunofluorescence microscopy I did not detect any cells in S phase (as determined by EdU incorporation) with detectable Cdt1 or p21 expression, in either WT or S228I lines (Fig. 3.2.3F). Therefore, by immunostaining I cannot draw any conclusions that there are defects in S phase degradation of Cdt1 or p21 in PCNA^{S228I} cells.

We have previously shown that the S228I alteration of PCNA leads to a dramatic conformation change of the IDCL and thus impairs but does not completely abolish the interaction of PCNA with many of its protein partners [246]. We hypothesised that a partially perturbed interaction surface might be particularly sensitive to additional competition for PCNA interaction. We tested this using PCNA^{S228I} lymphoblastoid cells derived from affected individuals and showed that these cells were significantly sensitive to T3 (3,3′,5-triiodothyronine) treatment [246]: T3 is a PCNA inhibitor that competitively binds near to the IDCL and blocks binding of other clients [247]. To determine whether this cellular phenotype was recapitulated in the PCNA^{S228I} RPE-1 line I used a cell survival assay. Briefly, known numbers of S228I or WT cells were plated sparsely in wells of 6 well dishes, treated with increasing concentrations of T3 or vehicle

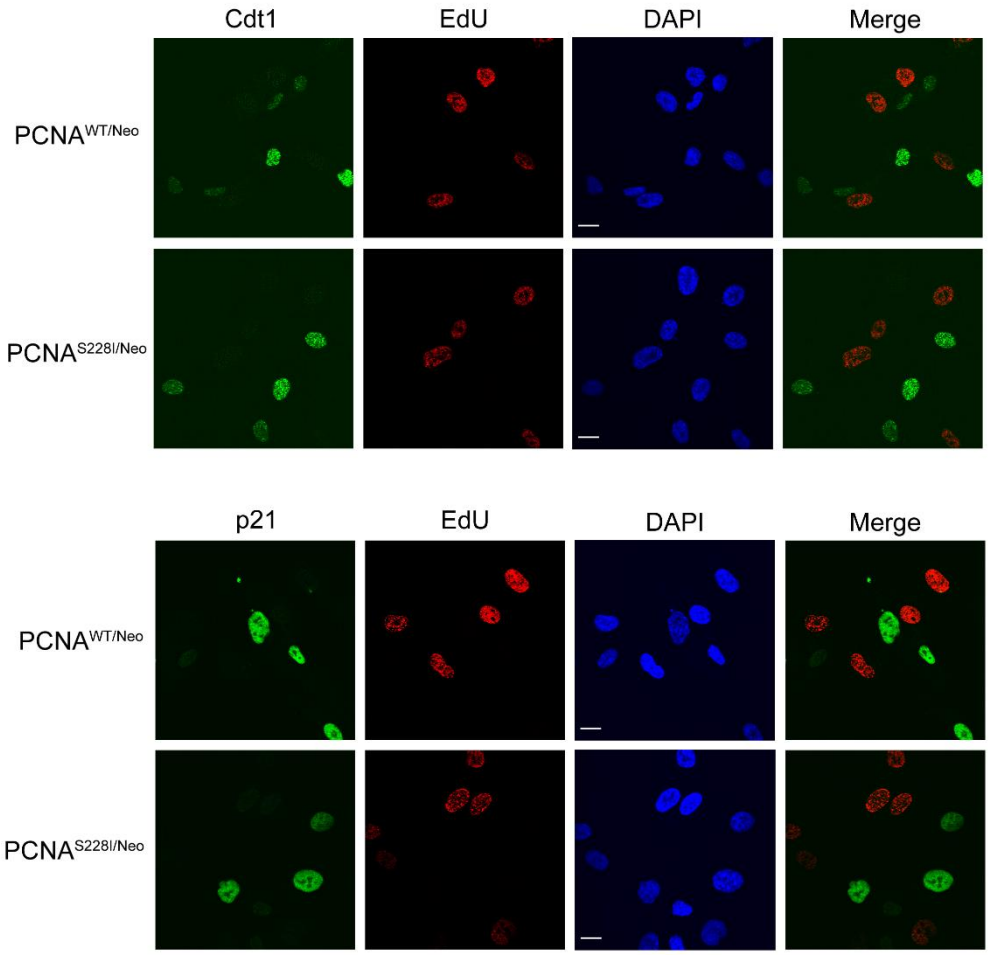


Figure 3.2.3F Immunofluorescence microscopy of knock-in cells against Cdt1 or p21. The imaging pictures are representatives from three independent immunofluorescence microscopy experiments. The S phase cells are determined by EdU incorporation. Cdt1 and p21 were labelled by antibodies. Neither Cdt1 nor p21 expression can be found in EdU labelled cells in both WT and S228I knock-in cells. Scale bar = 15 μm.

and allowed to grow for 6 days prior to staining cellular material with crystal violet. The stain was resolubilized using 10% acetic acid and the absorbance of the resulting solution was measured with the excitation of 595nm to determine the relative cell numbers. PCNA^{S228I} knock-in cells were significantly more sensitive to T3 treatment compared with the WT control or parental cell

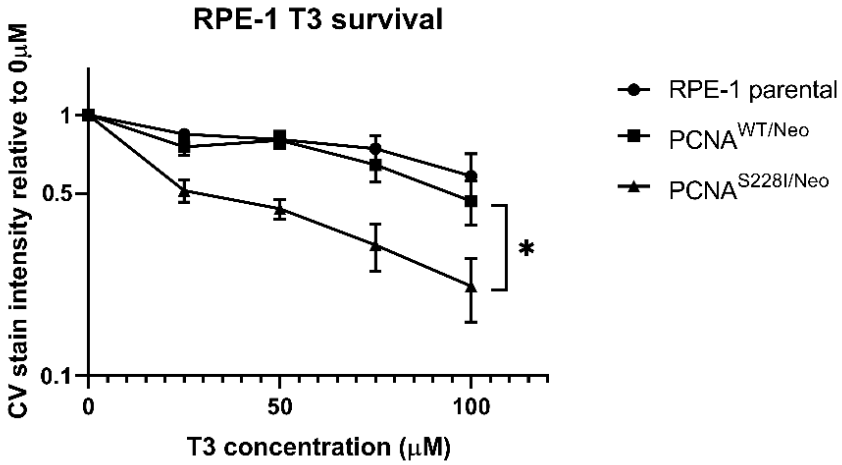


Figure 3.2.3G T3 cytotoxicity to PCNA^{S228I} knock-in RPE-1 cells. Cells were treated with T3 24 hours after seeding and stained by crystal violet (CV) 6 days after drug treatment. N=3. Error bars represent SEM. * $p<0.05$, single-tail student's t-test.

lines (Fig. 3.2.3G), consistent with what we have observed in lymphoblastoid cells. Together, this data demonstrated that increased sensitivity to PCNA competition is likely to be a direct result of the S228I change. The consequences of this for normal cellular activities remain to be determined, but this phenotype might represent one outcome of perturbation to the dynamics of the PCNA-interactome which likely underpins PARD.

3.3 Discussion

In this chapter, I have described a successful strategy for the CRISPR-Cas9 knock-in of a point mutation in a highly conserved and highly expressed gene, *PCNA*. And since *PCNA* is such an essential gene, induction of point mutations

in endogenous *PCNA* locus is very difficult and the knock-in efficiency can be extremely low, which is possibly the reason why attempts to generate knock-in cell lines by CRISPR-Cas9 technique using traditional single stranded oligo-deoxynucleotide (ssODN) as HDR templates were never successful (C. Green personal communication, data not shown). The inclusion of a selection cassette (PGK-Neo) dramatically increased the selection efficiency, but the use of such a long non-homologous sequence in the HDR template also caused complications during the process of homology-directed repair. As was described, I have generated one $PCNA^{S228I}$ knock-in cell line and one WT control knock-in cell line by similar procedures, both with one allele containing the S228I mutation only (WT control unchanged) and the other allele inserted with a PGK-Neo cassette in intron 5 apart from changes in the S228I locus. Failures in removal of the PGK-Neo cassette by Cre recombinase and PCR amplification around the 5′ loxP of the cassette indicated unexpected rearrangements occurring in this region. These can include multiple insertions of HDR templates in the process of homologous recombination with a long non-homologous region, or complicated rearrangements with the hTERT gene, if the hTERT in RPE-1 cells is unluckily inserted in this region as discussed above (Section 3.2.2). Under either circumstance, this is very likely to affect the expression of PCNA on this allele, so we suggest these cell lines to be effectively hemizygous. Nevertheless, the cDNA sequence of the S228I clone showed exclusive $PCNA^{S228I}$ expression, which at least confirms its genetic

background for mutant protein expression. Numerous attempts to derive a cleaner model system were unsuccessful, therefore the hemizygous $PCNA^{S228I/Neo}$ knock-in, and equivalent WT, cell lines described above are the best research model currently available to study the precise effect of the S228I alteration in PCNA.

Noticeably, the Western blot results showed a 50% decrease in PCNA protein level in the S228I knock-in RPE-1 cells, which was never detected in lymphoblastoid cells derived from affected individuals. This is possibly due to silence in one of the alleles with rearrangements in the 5′ of PGK-Neo cassette, and we are still unsure whether this will eventually affect the cellular phenotypes discovered in the following researches. Therefore, in the following experiments, I will investigate the cellular consequences of S228I mutation in both the RPE-1 knock-in cells and lymphoblastoid cells derived from affected individuals, so that the phenotypes are less likely to result from decrease of PCNA protein as cells from patients have normal PCNA expression [246]. Actually, the best way to eliminate the influence of PCNA amount is to stably express $PCNA^{S228I}$ in S228I knock-in cells to compensate for the reduction of PCNA protein level.

Moreover, I am also aware that my $PCNA^{WT/Neo}$ and $PCNA^{S228I/Neo}$ are both the only clone of the knock-in cell line. This leads to the situation that I cannot rule out the influence of off-target effect which possibly happened in the CRISPR-Cas9 knock-in procedure. The rescue experiments by stably expressing

$PCNA^{WT}$ protein in these cell lines can be a good attempt to eliminate the off-target effect. However, failures in rescuing the phenotypes still don't imply the existence off-target effect, as the exogenous PCNA is possibly inactive and the PCNA trimeric structure for its activity makes it difficult to anticipate the influence of S228I mutation in a heterozygous trimer. Thus, as was described above, in the following researches I will look into the phenotypes of $PCNA^{S228I}$ knock-in RPE-1 cells in parallel with lymphoblastoid cells derived from affected individuals, so that the same phenotypes discovered in different cell types are much more likely to result from the S228I mutation.

Taken together, the $PCNA^{S228I}$ mutant line shows exclusive expression of the altered variant in cDNA and has parameters of cellular PCNA localization, cell cycle profiles and T3 sensitivity consistent with those determined in cell lines from individuals affected with PARD. Thus, I proceeded to further use these cell lines to investigate other cellular consequences of the S228I mutation.

Chapter 4: Cellular consequences of the PCNA^{S228I} mutation

4.1 Overview

Because different cellular insults (such as replication stress or DNA damage) activate different cellular pathways, the discovery that a particular genetic alteration results in specific sensitivity to a particular drug or treatment can often be very informative in understanding the functional role of a gene of interest. Thus, in order to investigate the effects of the PCNA S228I mutation, a comprehensive analysis of cellular sensitivity to different agents was undertaken, in both RPE-1 PCNA^{S228I} cells and in lymphoblastoid cells derived from affected individuals. In this chapter, I present my discovery of olaparib sensitivity in PCNA^{S228I} cells at high concentrations, and my initial investigation of this phenotype.

4.2 S228I of PCNA is not a target of post translational modification

Upon our first identification of the S228I mutation as being causative for PARD, one question was often asked: are the consequences of the S228I alteration a result of the loss of a phosphorylation event on Serine 228 of PCNA? To answer this question, I isolated PCNA trimers from a stably expressing Strep-tagged PCNA^{WT} cell line in unchallenged conditions. Due to the formation of PCNA

trimers, the proteins pulled down contained both tagged $PCNA^{WT}$ and untagged endogenous WT monomers (Fig. 4.2A&B). Mass spectrometry analysis (LC-MS/MS) was carried out using the purified PCNA by Dr Roman Fischer in Target Discovery Institute, University of Oxford. We detected a number of modifications including phosphorylation of T185 (Appendix Fig. D), but no peptide containing phosphorylation of S228 was observed (Fig. 4.2D). Besides, PCNA S228 is not reported to be modified in the published literatures or databases such as Uniprot or PhophoSitePlus, either in normal or challenged conditions such as UV irradiation. We therefore conclude that there is no evidence that PCNA is normally modified on Serine 228 and thus it is unlikely that the phenotypes caused by S228I are a result of the loss of a phosphorylation on this site. Our later determination of the crystal structure of $PCNA^{S228I}$ gave a more attractive explanation for the consequences of this mutation: it indirectly alters the structure of the IDCL and prevents normal PCNA-client interactions as described in the introduction [246].

4.3 The $PCNA^{S228I}$ mutation does not significantly affect the majority of cellular DNA repair pathways

In collaboration with Dr Rose Wilson, I undertook a comprehensive survey of the sensitivity of $PCNA^{S228I}$ cells to a variety of chemical agents. Dr Wilson used the lymphoblastoid cell lines derived from affected individuals and I followed up any interesting results in my $PCNA^{S228I}$ RPE-1 line and isogenic WT. For the

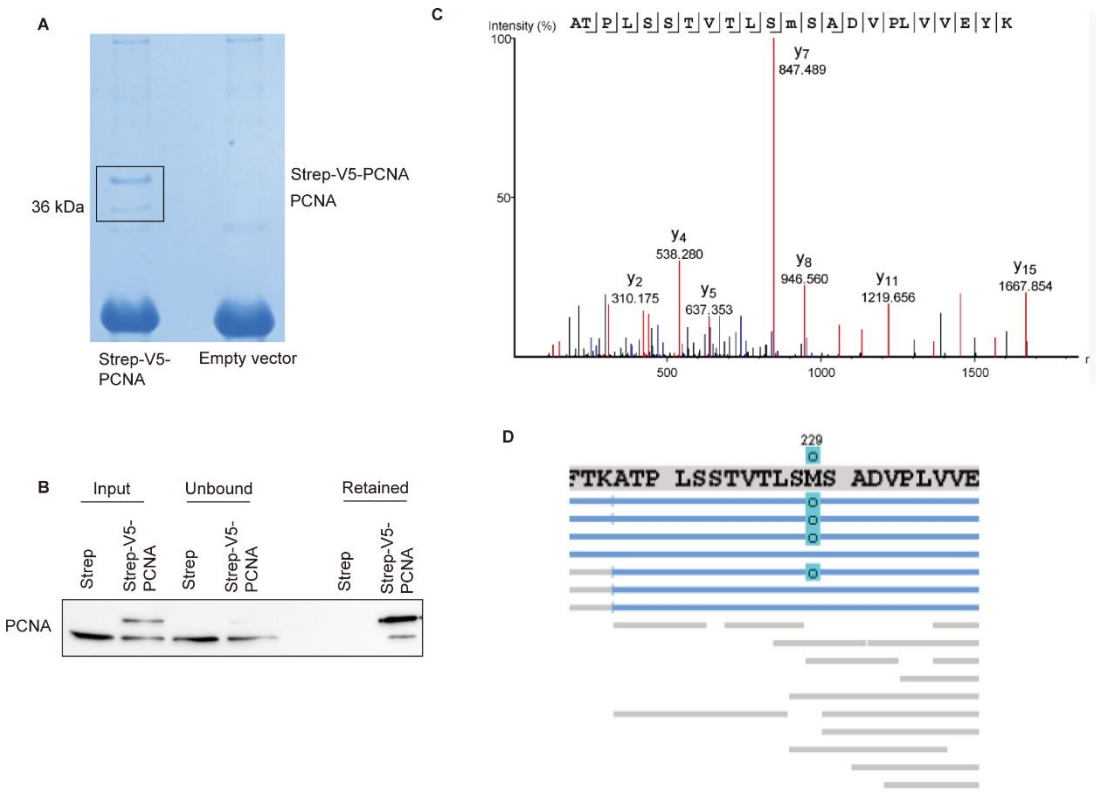


Figure 4.2 Mass spectrometry analysis of PCNA^{WT} shows no detectable PCNA phosphorylation at Ser228 in the unchallenged condition. **(A)** Coomassie stained gel of Strep-pulldown of Streptag-V5 PCNA and endogenous PCNA – bands indicated by box. Both bands were excised and sent for Mass Spectrometry analysis. **(B)** Anti-PCNA western blot shows pulldown of Strep-V5-PCNA and endogenous PCNA specifically from Strep-tagged PCNA expressing cells. **(C)** MS/MS spectrum of a peptide covering S228 demonstrating good detectability and fragmentation of tryptic peptide. The y11 fragment containing S228 generates a well detected fragment ion. **(D)** Multiple peptides covering S228 were detected. However, we did not observe potential baseline phosphorylation of S228. The work was completed in collaboration with Dr Roman Fischer in TDI, University of Oxford. Protein purification was carried out by me and Mass Spec analysis was completed by Dr Fischer. The result has been published by Wilson, *et al.* [246].

majority of treatments, the results of the survival assay showed variations between different affected individuals, but there is no evidence that these DNA damage agents are causing any sensitivity to PCNA^{S228I} lymphoblastoid cells.

These included mitomycin C (MMC), MMS, H_2O_2, etoposide, camptothecin (CPT) and ionizing radiation (IR) treatments (R. Wilson personal communication, Appendix Fig. E1 & 2). This means that any effect of the S228I alteration on the pathways that repair these specific DNA damage types is not sufficient to cause cellular sensitivity to the corresponding damaging agents.

However, lymphoblastoid cells from affected individuals did show some sensitivity to hydroxyurea (HU) at high doses (R. Wilson personal communication, Appendix Fig. E1). Given the crucial role for PCNA at the replication fork, we hypothesised that the hypomorphic PCNA mutation S228I would alter the cellular responses to replication stress. However, in my RPE-1 knock-in cells, a survival assay showed a statistically significant increase in survival rate at very high concentration of HU in $PCNA^{S228I/Neo}$ cells (Fig. 4.3). The differences in these two results presumably arises from differences in cell type and experimental procedures, and thus it is difficult to draw any conclusions from these data regarding an effect of S228I on the cellular response to nucleotide depletion. Nevertheless, because any sensitivity or resistance was only seen at high doses of HU it seems unlikely that perturbations of the cellular response to replication fork stalling underpin any major cellular phenotypes pertaining to the S228I mutation under physiological conditions.

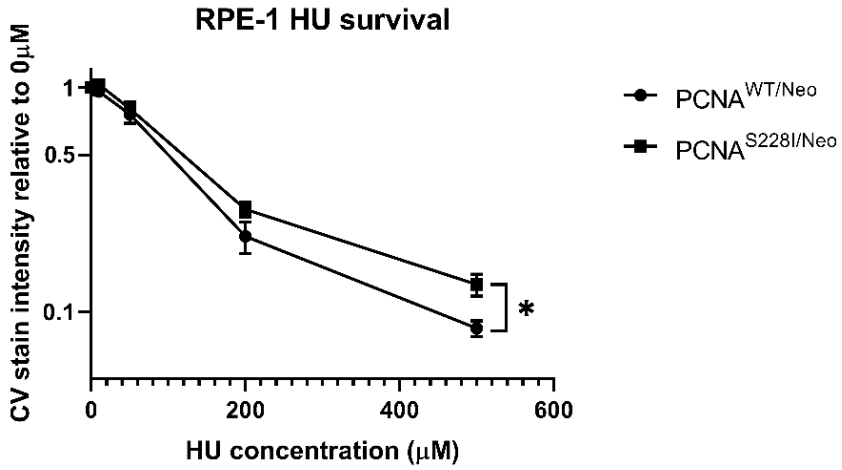


Figure 4.3 HU cytotoxicity to PCNA^{S228I} knock-in RPE-1 cells. Cells were treated with HU 24hr after seeding and stained by crystal violet (CV) 6 days after drug treatment. N=3. Error bars represent SEM. * $p<0.05$, two-tail student's t-test.

4.4 PCNA^{S228I} cells are sensitive to Olaparib

In contrast to the majority of chemical treatments tested, both lymphoblastoid and RPE-1 PCNA^{S228I} lines were sensitive to treatment with the PARP inhibitor olaparib (Fig. 4.4A & B). We note that the concentrations of olaparib used in these experiments are much higher than are needed to observe sensitivity to olaparib in HR-defective cells lines. To ascertain whether this sensitivity to olaparib is a direct consequence of perturbation to PCNA, we asked whether perturbation of PCNA activity by another method can also generate this effect. To do this I utilized the PCNA inhibitor T3 in combination with olaparib in cell survival assays. The combined treatment of WT cells with T3 and olaparib resulted in synergistic effects on cell proliferation, indicating that compromised

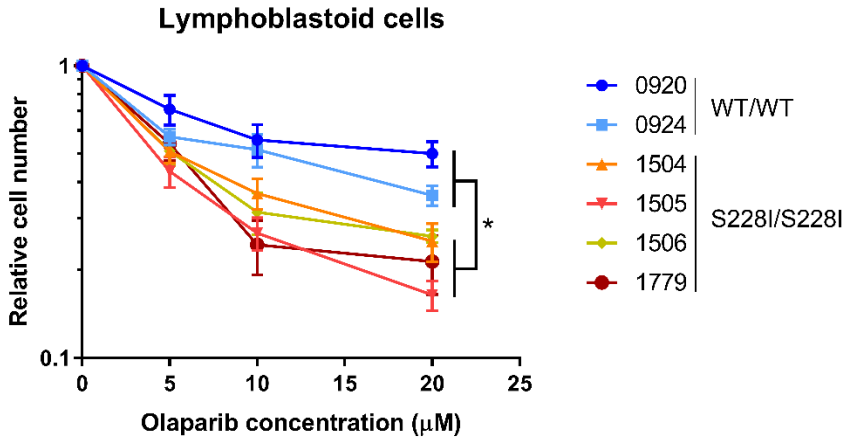


Figure 4.4A Olaparib cytotoxicity to lymphoblastoid cells derived from unaffected (WT/WT) and affected (S228I/S228I) individuals. Cells were counted before and after 72 hr treatment with olaparib and cell numbers were relative to vehicle treatment. N=3. Error bars represent SEM. * p<0.05, ANOVA. (R. Wilson personal communication)

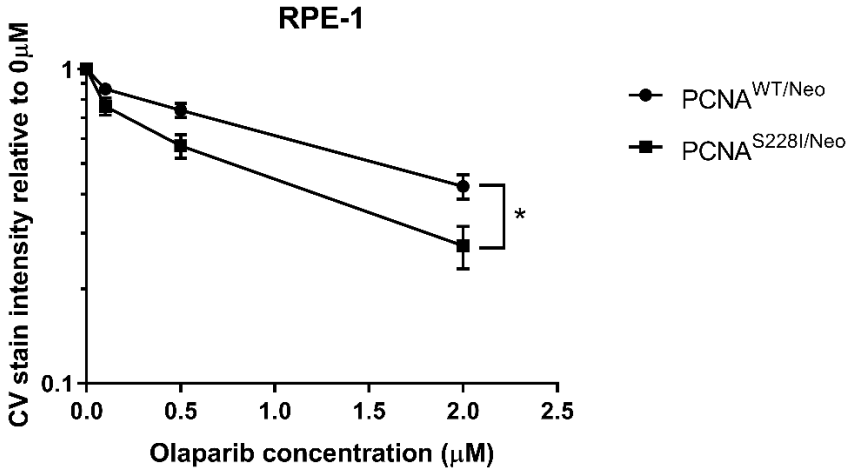


Figure 4.4B Olaparib cytotoxicity to PCNA^{S228I} knock-in RPE-1 cells. Cells were treated with olaparib 24 hr after seeding and stained by crystal violet (CV) 6 days after drug treatment. N=3. Error bars represent SEM. * p<0.05, single-tail student's t-test.

PCNA interaction can indeed lead to olaparib sensitivity (Fig. 4.4C). Given that the S228I mutation does not appear to cause defects in the repair pathways for SSBs or DSBs (no sensitivity to IR, NCS or MMS, or H_2O_2 was detected), which

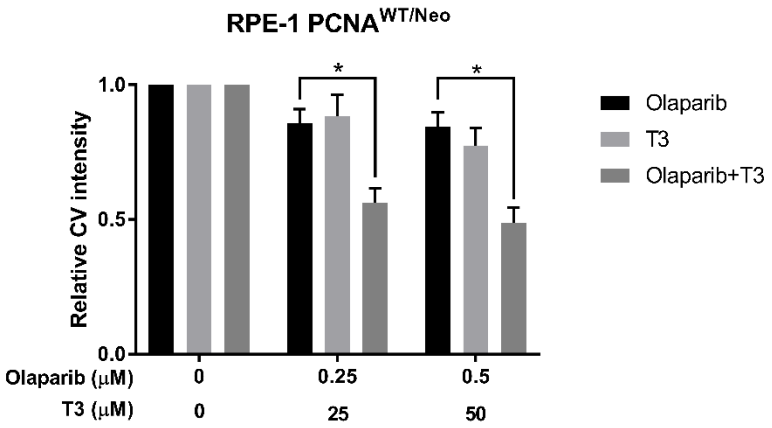


Figure 4.4C PCNA inhibitor T3 and olaparib led to cell death synergistically. The survivals were relative to 0 μM of drug concentration respectively. N=3. Error bars represent SEM. * p<0.05, two-tail student's t-test.

would explain a sensitivity to PARP inhibition, we hypothesised that there must be some other reason accounting for the olaparib sensitivity in PCNA^{S228I} cells.

4.5 Olaparib treatment generates DNA breaks in PCNA^{S228I} cells

In order to uncover the reason for olaparib sensitivity, I decided to investigate what causes cell death in S228I cells in response to the treatment. Olaparib does not cause DNA damage directly, but its action can lead to the persistence of unrepaired SSBs as well as the generation of DSBs. In lymphoblastoid cells derived from affected individuals, I applied alkaline comet assay to detect DNA breaks after olaparib treatment. S228I cells derived from affected individuals had longer comet tails compared to WT control cells after treatment with olaparib for 24 hours. No significant differences were observed between cell lines without olaparib treatment (Fig. 4.5A). This means that olaparib leads to

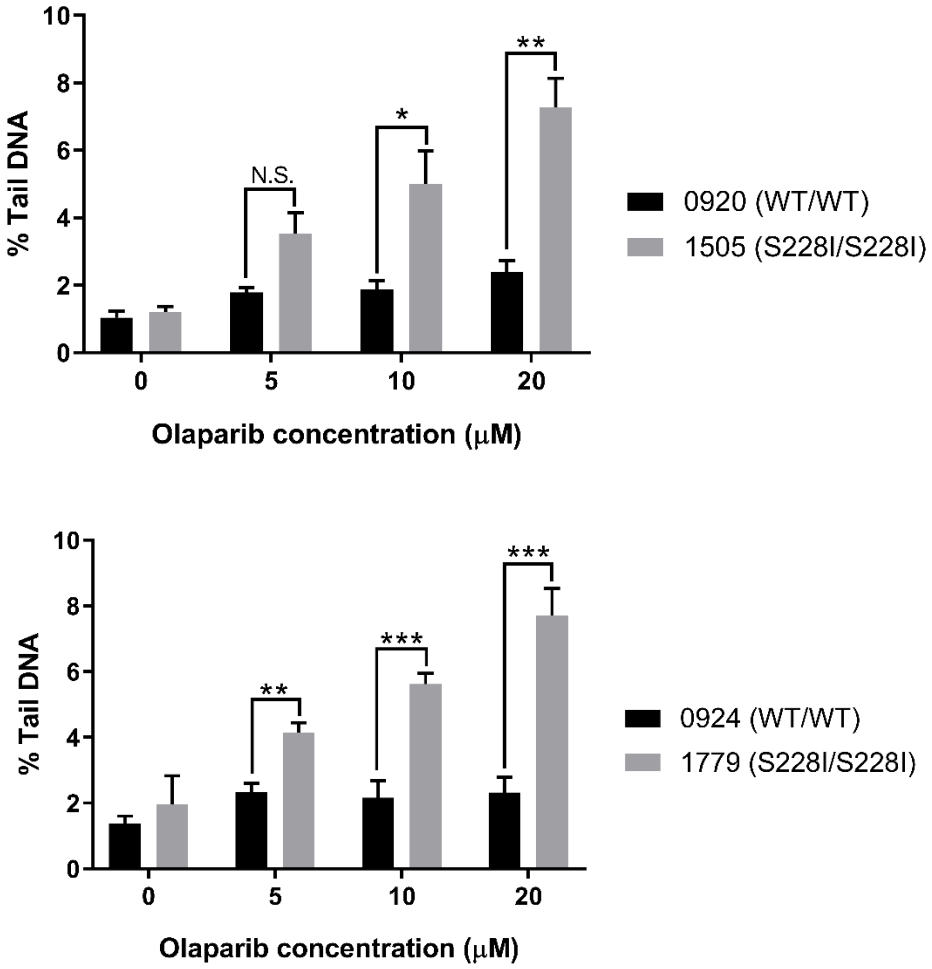


Figure 4.5A Alkaline COMET assay was performed after 24 hr treatment of olaparib in lymphoblastoid cells derived from unaffected (WT/WT) and affected (S228I/S228I) individuals. The work was completed in collaboration with Dr Arnaud Legrand in Prof Grigory Dianov's group in Department of Oncology, University of Oxford. The comet assay and data analysis were completed by me and the data was acquired by Dr Arnaud Legrand. The average % Tail DNA was calculated in each single repeat. N=3. Error bars represent SEM. N.S. no significance, * $p<0.05$, ** $p<0.01$, *** $p<0.001$, two-tail student's t-test.

more DNA breaks in lymphoblastoid cells in which PCNA is mutated to p.Ser228Ile. I confirmed this result in my RPE-1 knock-in cell lines using immunofluorescence and automated quantification: I measured γH2AX production to indicate the activation of DNA damage signalling as a readout for

the presence of DNA breaks. PCNA^{S228I} knock-in cells generated more γH2AX foci after olaparib treatment for 24 hours when compared to WT controls (Fig. 4.5B). Foci counting was automated using Cell Profiler software (see methods and materials, Section 2.5.3), to ensure the results are unbiased. Taken together, these data lead me to conclude that olaparib causes DNA damage specifically in PCNA^{S228I} cells.

4.6 Olaparib disrupts cell cycle progression in PCNA^{S228I} cells

As was described in the introduction, DNA damage sensing usually leads to checkpoint activation and cell cycle arrest. I thus investigated whether S228I cells have a perturbed cell cycle after olaparib treatment. I initially treated lymphoblastoid cells derived from affected individuals with a high dose of olaparib for 6 hours and found no significant changes in cell cycle profiles as determined by FACS (Fig. 4.6A). However, given that 6 hours is shorter than a complete cell cycle, I thought this duration of treatment may not have been long enough to detect a difference by this method. After treating the same cells with olaparib for 24 hours, I indeed found a clear disruption in the cell cycle of cells with the S228I mutation (Fig. 4.6B & C). There are 2 dramatic differences in the FACS profiles of S228I and WT cells after this treatment: firstly, there are more cells with a sub-G1 DNA content in PCNA^{S228I} cells after treatment; and secondly there is a new population of cells with the DNA content between G1

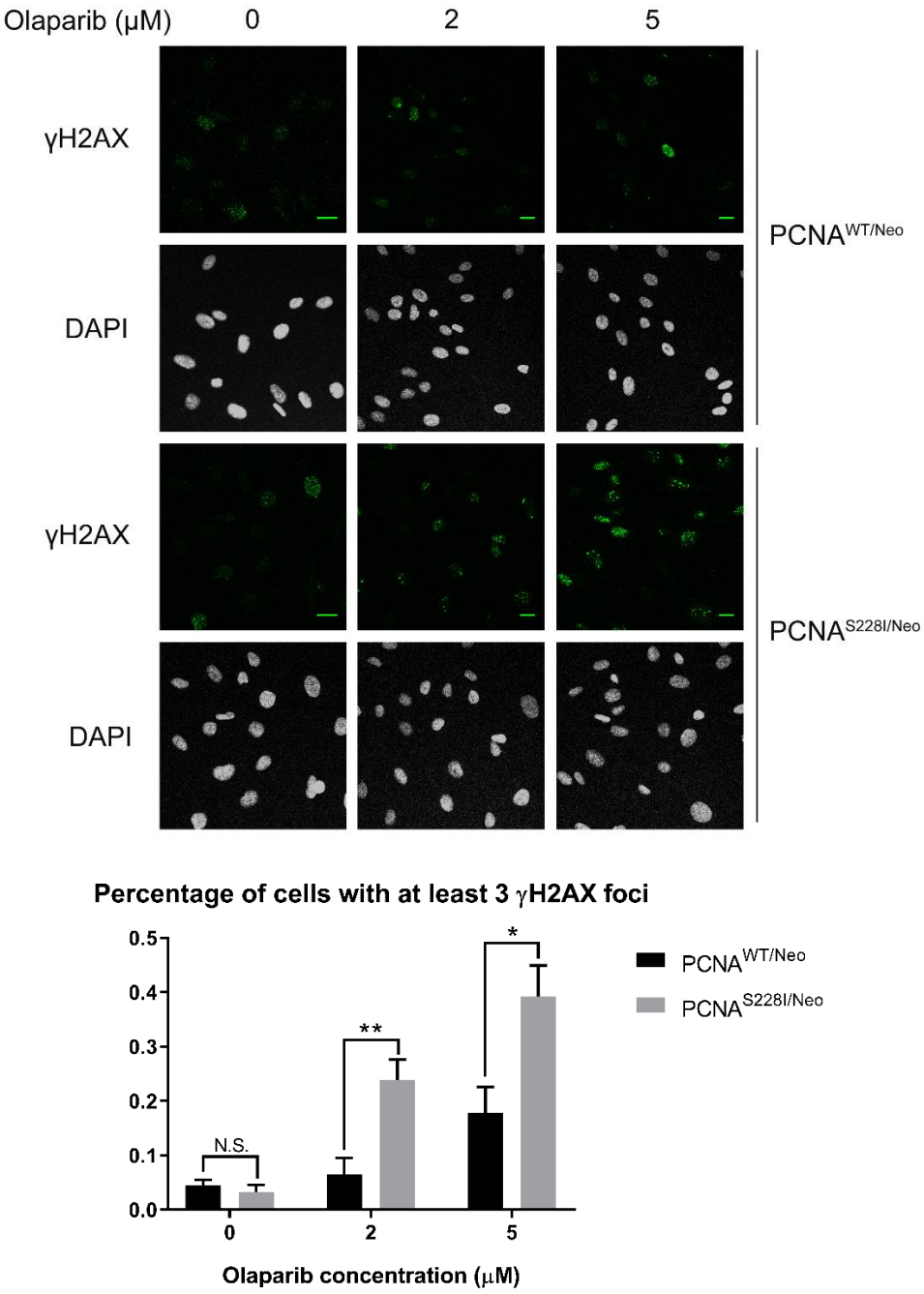


Figure 4.5B Immunofluorescence against γH2AX was performed in RPE-1 cells treated with olaparib for 24 hours. Cells with more than 3 γH2AX foci were counted by Cell Profiler software and the percentage was calculated in each single repeat. N=4. Scale bar = 28μm. Error bars represent SEM. N.S. no significance, * $p<0.05$, ** $p<0.01$, two-tail student's t-test.

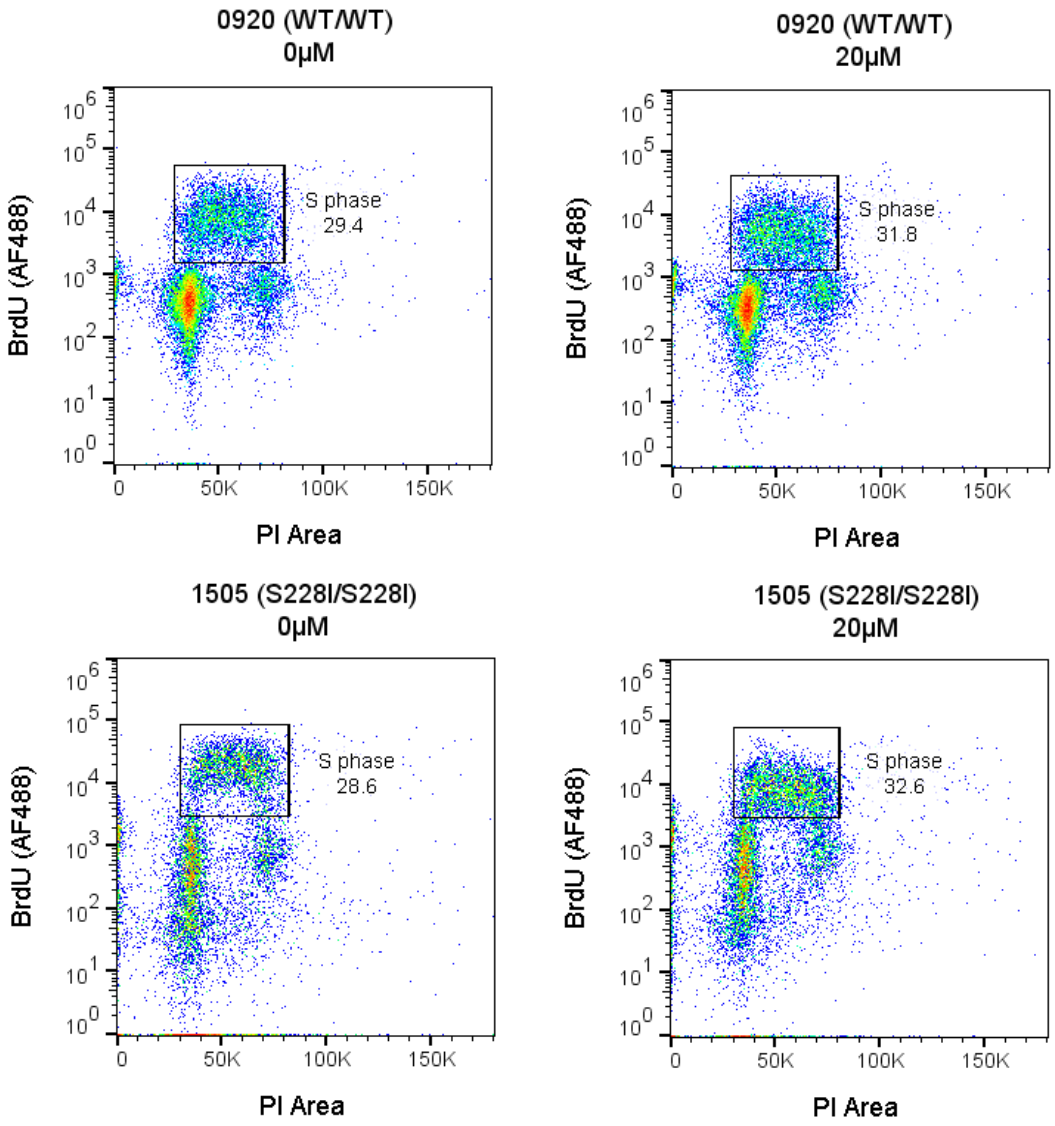


Figure 4.6A FACS cell cycle analysis after 6 hr olaparib treatment in lymphoblastoid cells derived from unaffected (WT/WT) and affected (S228I/S228I) individuals. The dot plots are from one single FACS analysis plotting DNA content (PI) against BrdU (AF488) to determine different cell cycle phases. The S phase cell percentage was shown in the plot.

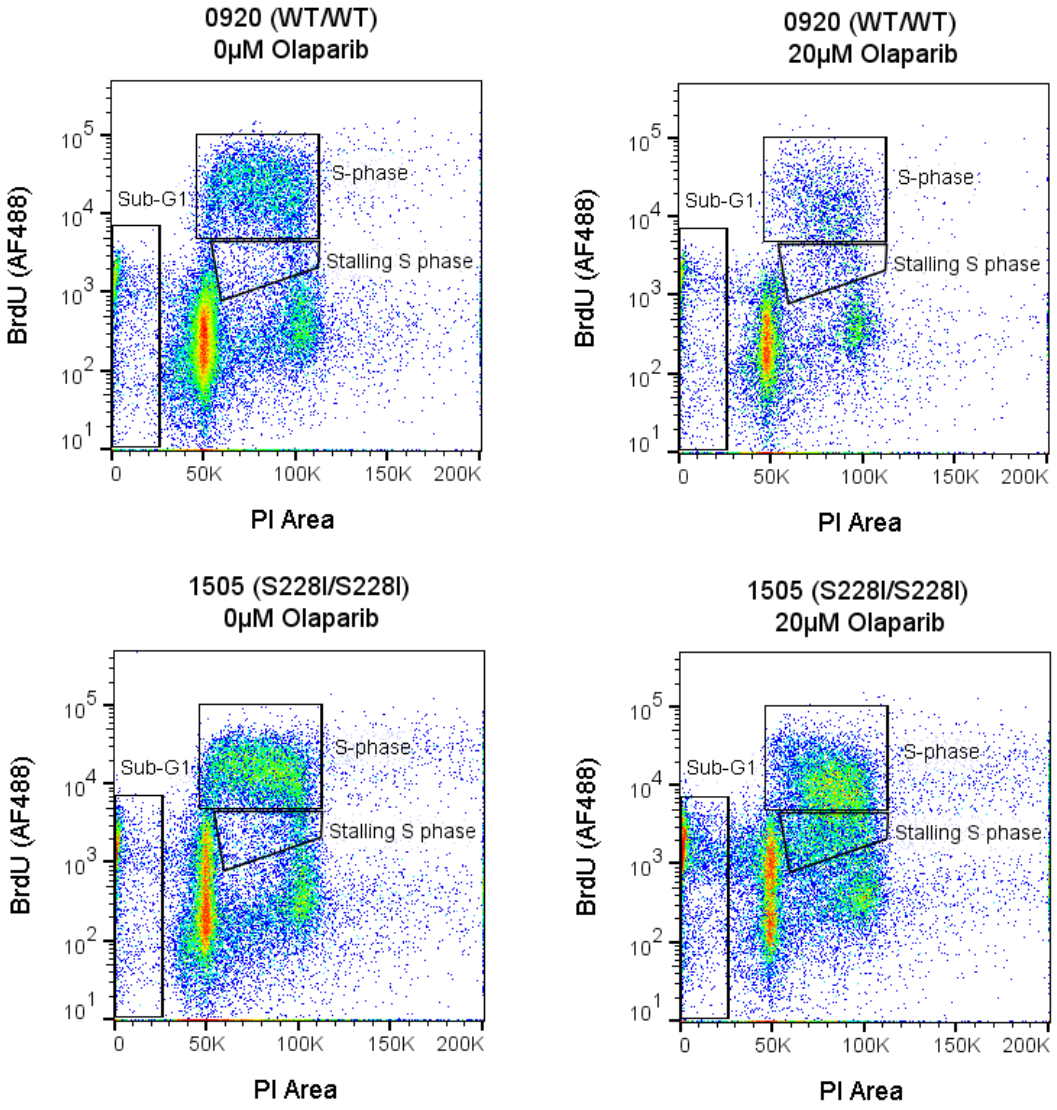


Figure 4.6B FACS cell cycle analysis after 24 hr olaparib treatment in lymphoblastoid cells derived from unaffected (0920, WT/WT) and affected (1505, S228I/S228I) individuals. The dot plots are representatives from three independent FACS analysis on these two cell lines plotting DNA content (PI) against BrdU (AF488) to determine different cell cycle phases. A sub-population of cells have a DNA content between the G1 and G2 populations, without associated ongoing DNA synthesis, this is labelled as stalling S phase. Percentage of each population is summarized in Table 4.6A.

Cell type	Olaparib conc. (μM)	S phase (%)	Stalling S phase (%)	Sub-G1 phase (%)
0920 (WT/WT)	0	16.3	2.37	5.42
	20	11.2	4.17	7.41
1505 (S228I/S228I)	0	24.2	4.28	5.28
	20	21.1	12.4	11.1

Table 4.6A Cell percentages summary for each population in Fig. 4.6B.

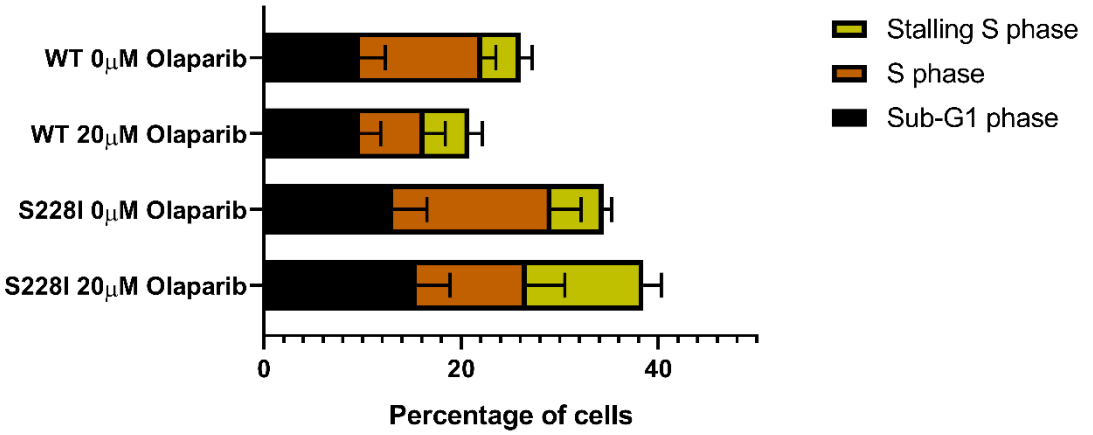


Figure 4.6C Average cell cycle proportions in lymphoblastoid cells after 24 hr olaparib treatment. Each average percentage was calculated from three independent FACS analysis of 0920 (WT/WT) and 1505 (S228I/S228I), and one more repeat in 0924 (WT/WT) and 1779 (S228I/S228I), to generate average cell cycle proportions for each genotype. Error bars represent SEM.

and G2 phase which are however not incorporating any nucleotides. We presume that the former population, with sub-G1 DNA content, represents cells undergoing some form of cell death, which is consistent with the olaparib sensitivity seen in these cells. The second population we have termed “stalling S phase cells” as they are apparently in S phase but not synthesizing DNA. This population only exists to any significant extent in the $PCNA^{S228I}$ lymphoblastoid cells after olaparib treatment (Table 4.6A and Fig. 4.6C). I therefore hypothesise that PARP inhibition triggers stalling of S phase, which

eventually leads to cell death, in EBV-transformed lymphoblastoid cells carrying the PCNA^{S228I} mutation. It is not clear from this data whether the strand breaks observed above arise before or after this S phase stalling. Besides, there is a clear reduction in S phase of WT lymphoblastoid cells after olaparib treatment, which cannot be seen in PCNA^{S228I} cells taking those stalled in S phase into consideration (Fig. 4.6B & C, Table 4.6A).

Similar experiments were performed in PCNA^{S228I} knock-in RPE-1 cells. The PCNA^{S228I} cells also showed a dramatic perturbation to their cell cycle profile upon 24-hour olaparib treatment. However, the effect was different to that seen in the lymphoblastoid cells. In RPE-1 PCNA^{S228I} cells stalling of S phase was not observed but instead a dramatic G2/M arrest was apparent (Fig. 4.6D1 & 2 and Table 4.6B1 & 2). These apparently contradictory results in the two cell types can probably be explained by the presence of different cell cycle checkpoint pathways operating in these two very different cell types. It is well known that a p53-dependent G2/M arrest results from G2/M checkpoint activation which can be triggered by DNA damage detected in S phase. RPE-1 cells have intact checkpoint pathways and thus the DNA damage caused by olaparib treatment (see Section 4.5) will trigger the G2/M arrest. On the other hand, EBV-immortalized lymphoblastoid cells, though having p53 expression, were reported to have abrogated activation of checkpoints in G2/M [296]. It seems likely then, that a failure to respond by arresting the cell cycle upon initial

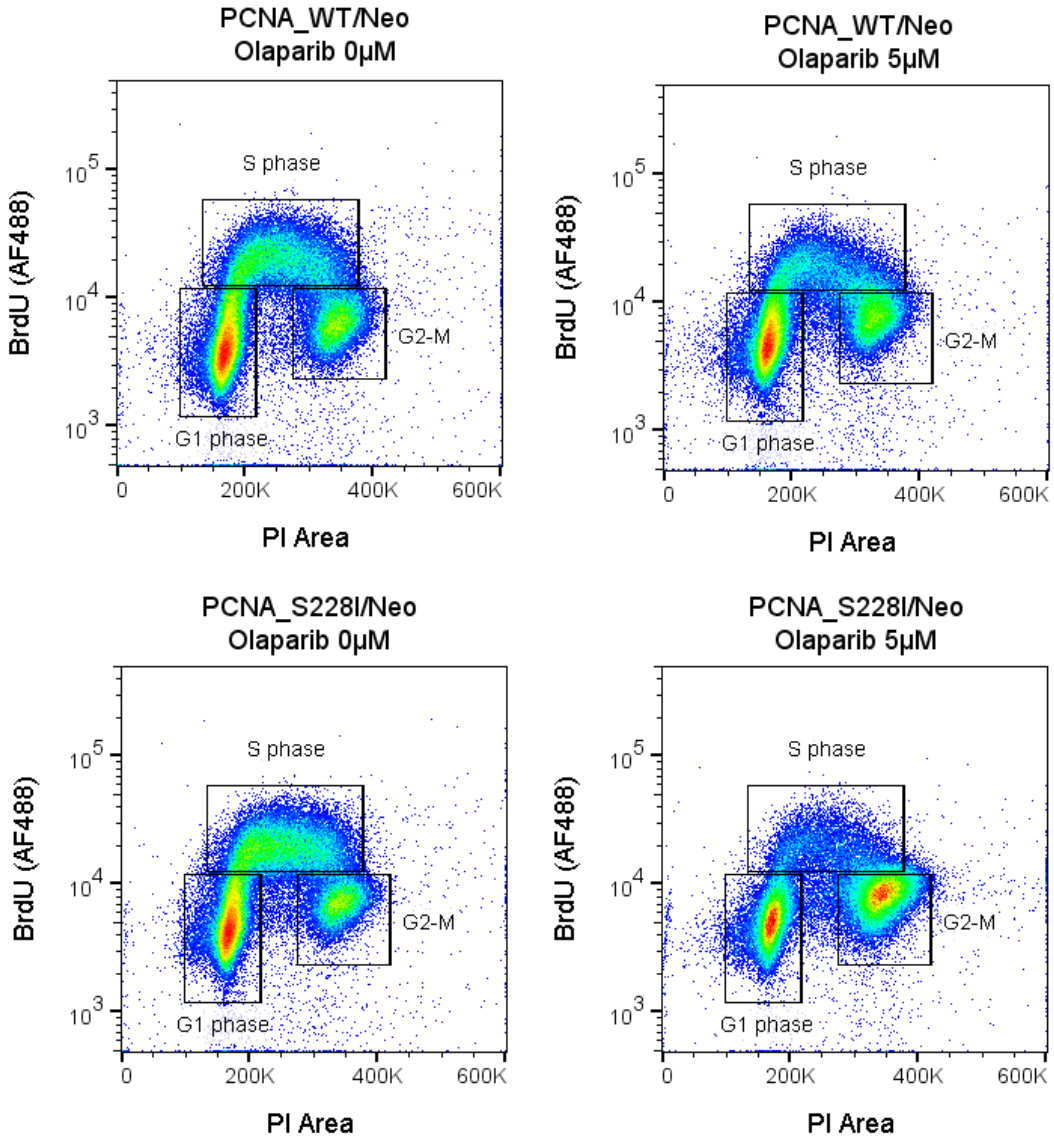


Figure 4.6D1 FACS cell cycle analysis after 24hr olaparib treatment in RPE-1 knock-in cells. The two dimensional dot plots are one of the two independent FACS analysis plotting DNA content (PI) against BrdU (AF488) to determine different cell cycle phases. Populations in different phases of the cell cycle are as indicated, and percentage of each population is summarized in Table 4.6B1.

Cell type	Olaparib conc. (μM)	G1 phase (%)	S phase (%)	G2 phase (%)
$PCNA^{WT/Neo}$	0	49.0	27.0	19.5
	5	55.2	17.3	21.4
$PCNA^{S228I/Neo}$	0	46.6	32.1	16.3
	5	37.1	10.8	46.1

Table 4.6B1 Cell percentages summary for each population in Fig. 4.6D1.

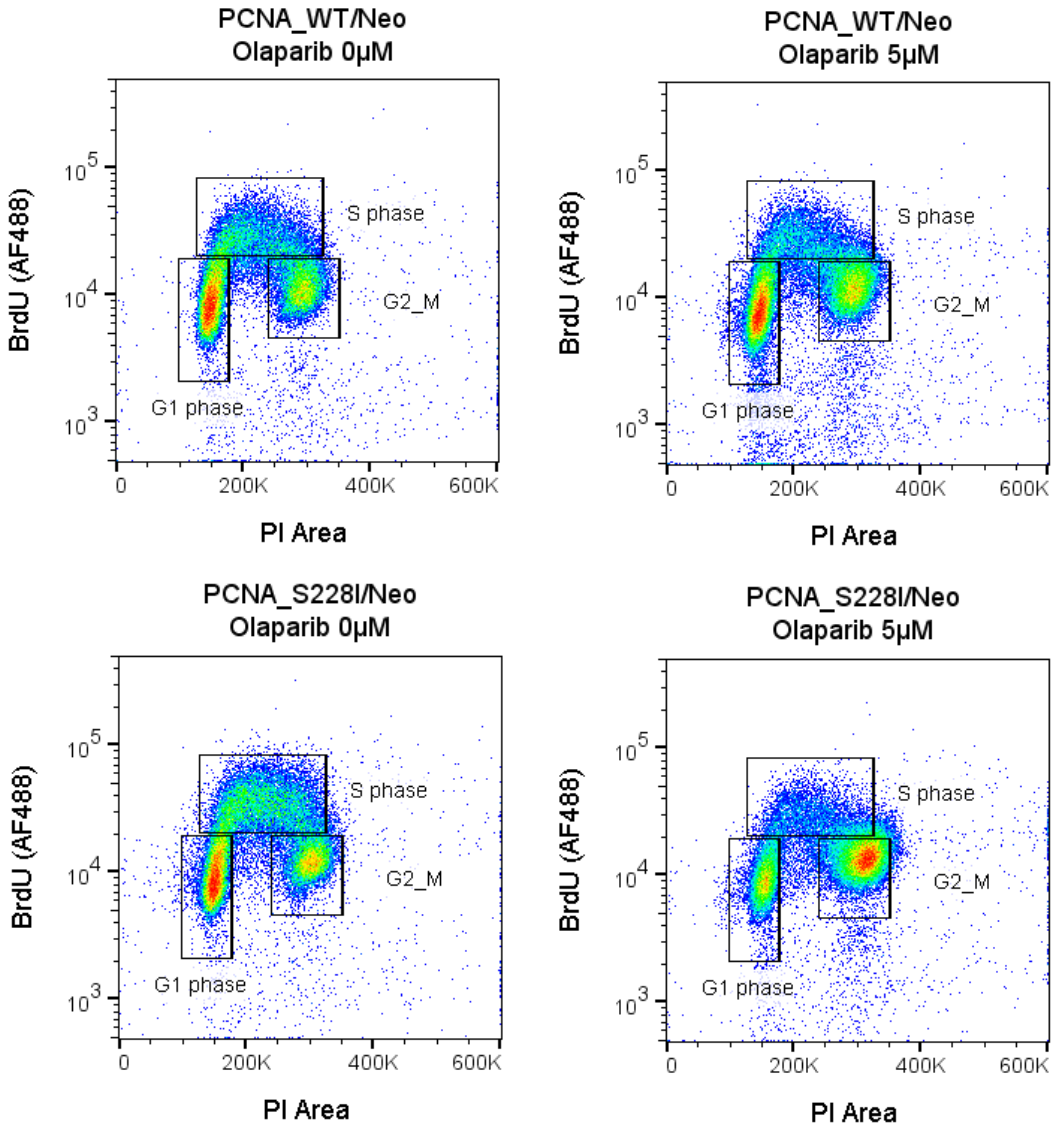


Figure 4.6D2 FACS cell cycle analysis after 24hr olaparib treatment in RPE-1 knock-in cells. The two dimensional dot plots are the other one of the two independent FACS analysis plotting DNA content (PI) against BrdU (AF488) to determine different cell cycle phases. Populations in different phases of the cell cycle are as indicated, and percentage of each population is summarized in Table 4.6B2.

Cell type	Olaparib conc. (μM)	G1 phase (%)	S phase (%)	G2 phase (%)
$PCNA^{WT/Neo}$	0	40.6	22.9	27.1
	5	42.2	15.0	31.4
$PCNA^{S228I/Neo}$	0	35.4	33.9	23.3
	5	23.7	12.0	52.5

Table 4.6B2 Cell percentages summary for each population in Fig. 4.6D2.

damage formation leads to exacerbation of the problems in the next cell cycle. So that the S phase stalling and subsequent generation of sub-G1 lymphoblastoid cells did not occur in the first cell cycle of olaparib treatment, but happened in the next round of S phase when coming across the unrepaired DNA damage escaping from the G2/M checkpoint of last cell cycle.

PCNA mono-ubiquitination functions in translesion synthesis to bypass DNA bulky lesions and is triggered by stalled replication forks [211]. We have previously reported that the S228I alteration of PCNA does not affect its mono-ubiquitination after UV-irradiation [246]. In contrast to this, I found a drastic decrease in the level of PCNA mono-ubiquitination after 24-hour treatment with olaparib in both $PCNA^{S228I}$ RPE-1 knock-in cells and lymphoblastoid cells derived from affected individuals (Fig. 4.6E). The decrease in mono-ubiquitinated PCNA in $PCNA^{S228I}$ RPE-1 cells can be explained by the sharp decrease in S phase cell number due to the G2/M arrest (Fig. 4.6 D1 & 2). The slight reduction in mono-ubiquitinated PCNA in WT lymphoblastoid cells can also be explained by the decrease in S phase cell number discovered after olaparib treatment (Fig. 4.6C). However, the $PCNA^{S228I}$ lymphblastoid cells do not show this G2/M arrest phenotype, but actually have more cells with apparently S phase DNA content after olaparib treatment. We can thus conclude that the stalling S phase cells are not generating a signal via PCNA

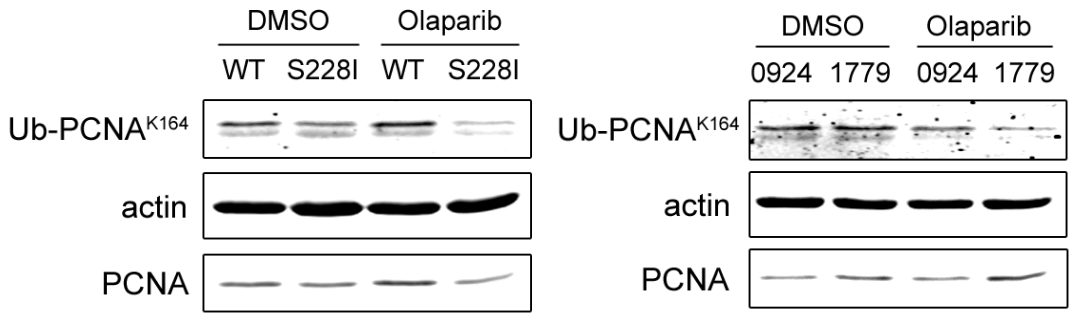


Figure 4.6E Western blot of RPE-1 (left) and lymphoblastoid cells (right, 0924: WT/WT, 1779: S228I/S228I) whole cell lysates harvested after 24 hr treatment of olaparib.

mono-ubiquitination. I hypothesise that replication forks have collapsed in these S phase stalling cells so that PCNA is no longer at the forks to receive a signal.

4.7 Discussion

In this chapter, I investigated the cellular consequences of PCNA^{S228I} mutation from various aspects. I have discovered for the first time that PARP inhibitor treatment is toxic to cells with the hypomorphic PCNA^{S228I} mutation. And by combined treatment of WT RPE-1 cells with PCNA inhibitor T3 and PARP inhibitor olaparib, I confirmed that compromised PCNA interactions can result in olaparib sensitivity. This result, if repeated in cancer cell lines, can actually give a hint on the cancer therapeutic strategy using combination of PARP inhibitors and PCNA inhibitors.

Besides, I have also shown that PARP inhibitor led to more DNA damage and thus cell cycle perturbations in PCNA^{S228I} cells. The elevated amount of γH2AX foci in PCNA^{S228I} RPE-1 cells after olaparib treatment indicates the activation of DNA damage response (DDR) pathways, and the corresponding G2/M arrest

in cell cycle suggests the activation of DNA damage checkpoint. The specific G2/M arrest implies that the DNA breaks after olaparib treatment are likely to come from S-G2 phase. In EBV-immortalized lymphoblastoid cells as discussed above, however, the G2/M checkpoint is inactive so we hypothesised that the DNA synthesis of PCNA^{S228I} lymphoblastoid cells in the next round of cell cycle will stop when encountering the unrepaired DNA damage escaping from the G2/M checkpoint of last cell cycle, which explains the increase in the number of cells stalling at S phase after olaparib treatment. The challenge in cell cycle synchronization of lymphoblastoid cells makes it difficult to prove this hypothesis, but the decrease in PCNA mono-ubiquitination in PCNA^{S228I} lymphoblastoid cells after olaparib treatment showed these cells stalling at S phase are not activating PCNA mono-ubiquitination dependent DNA damage tolerance pathway. To prove our hypothesis that the replication forks are actually collapsed in these cells stalling at S phase, neutral comet assay investigating DSBs after olaparib treatment can be applied in the future.

Given that PCNA^{S228I} lymphoblastoid cells did not show significant sensitivity to ionizing radiation (IR) (see Appendix Fig. E2), the S228I alteration of PCNA is unlikely to cause an HR defect, at least at a level which can be detected by decreased cell viability after IR. Thus, it seems likely that there is an alternative explanation for the PARP inhibitor sensitivity of PCNA^{S228I} cells, rather than the known synthetic lethality with HR-deficiency. The following chapter will

investigate this new mechanism for PARP inhibitor sensitivity, as it may give a potential novel application of PARP inhibitors in the cancer clinic.

Chapter 5: The mechanism of olaparib sensitivity in PCNA^{S228I} cells

5.1 Overview

The previous chapters have shown that olaparib leads to DNA damage and thus disrupts the cell cycle in PCNA^{S228I} cells. I next wanted to develop a model to explain the mechanism of olaparib sensitivity in PCNA^{S228I} cells. PARP inhibitors are known to inhibit PARP1 catalytic functions as well as trap the PARP1 enzymes at DNA damage sites [287]. Therefore, it was important to determine whether olaparib sensitizes PCNA^{S228I} cells through PARP1 function inhibition, PARP trapping or both. It was also unclear why PCNA^{S228I} cells generate DNA damage after olaparib treatment. The most straightforward hypothesis was that PCNA^{S228I} may have compromised SSB repair pathways so that the endogenous SSBs cannot be repaired in a timely fashion, leading to their accumulation through multiple cell cycles until they reach a threshold level which is exacerbated by PARP inhibition. Importantly however, a recent paper from Caldecott lab gave a new insight into a cellular role of PARP1 at the replication fork: in the monitoring and repair of unligated Okazaki fragments [283]. This led me to develop the hypothesis that the impaired interaction of FEN1 and LIG1 with PCNA^{S228I} can affect Okazaki fragment maturation which then becomes dependent on the PARP1-dependent machinery of SSB repair. PARPi blocks this alternative pathway so that the unligated Okazaki fragments

will turn into permanent SSBs in PCNA^{S228I} cells, a novel example of cellular synthetic lethality. In this chapter, I present studies devised to test these hypotheses and eventually propose a model to explain the mechanism of PCNA^{S228I} cell olaparib sensitivity.

5.2 Olaparib sensitizes PCNA^{S228I} cells through inhibition of PARP1 function instead of PARP trapping

To better understand the mechanisms of PARP inhibitor sensitivity in PCNA^{S228I} cells, I treated the RPE-1 knock-in cells with other PARP inhibitors including niraparib and veliparib. It has been reported that niraparib causes more PARP trapping while veliparib is less able to trap PARP1 [287]. Interestingly, PCNA^{S228I} cells were highly sensitive to niraparib but no significant sensitivity was observed with veliparib, which actually generated significant cellular toxicity at high doses even in WT cells (Fig. 5.2A). This correlation between trapping efficiency and cytotoxicity is suggesting a potential relationship between PARP trapping capacity and PARP inhibitor toxicity to PCNA^{S228I} cells. However, it is in fact complicated to distinguish the influence of PARP trapping from the PARP1 enzymatic activity, as the trapping of PARP1 at damage sites created by PARP inhibition can act to decrease the amount of functional PARP1 available in cells and consequently exacerbate the effect of the PARP inhibition. Besides, I am also aware that the concentrations of the PARP1 inhibitors used in the survival assay vary between each other, which can also affect the

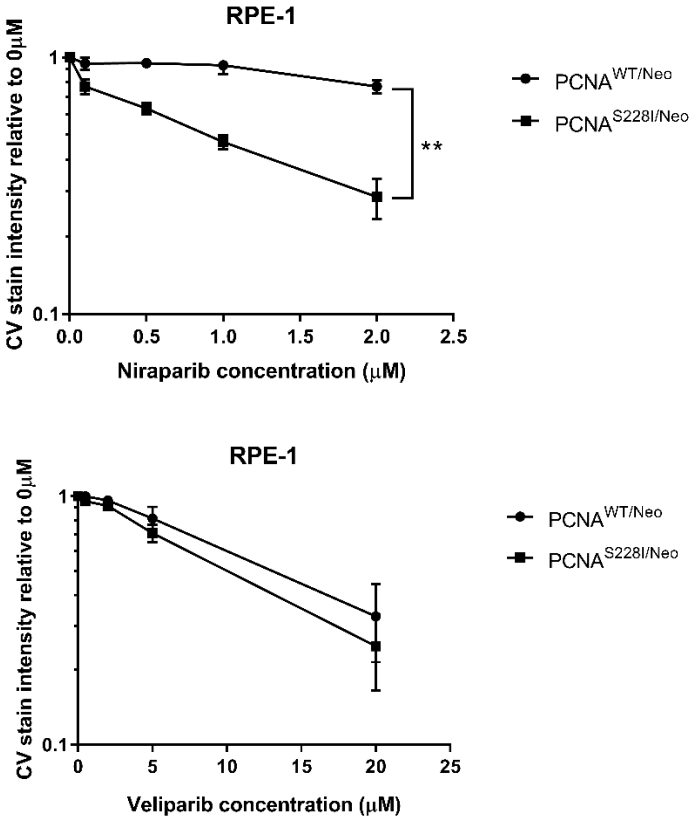


Figure 5.2A Niraparib and veliparib cytotoxicity to RPE-1 knock-in cells. Cells were treated with niraparib or veliparib as indicated 24 hr after seeded and stained with crystal violet 6 days after drug treatment. N=3. Error bars represent SEM. ** $p<0.01$, single-tail student's t-test.

contribution of PARP1 functional inhibition or PARP trapping to cellular sensitivity. In conclusion, the correlation between trapping capacity and cytotoxicity is insufficient to prove that the olaparib sensitivity of $PCNA^{S228I}$ cells is due to the PARP trapping capacity of the PARP inhibitor.

In order to find out whether $PCNA^{S228I}$ cell olaparib sensitivity is due to PARP1 functional inhibition or PARP trapping, I knocked down PARP1 in my knock-in cell lines using the siRNA from Sugimura *et al.* [297]. Western blot showed a significant decrease in PARP1 protein levels in both WT and S228I cells,

indicating that the depletion was successful (Fig. 5.2B). Apart from the knock-down efficiency, the results of Western blot also indicated an about two fold of endogenous PARP1 protein in PCNA^{S228I} knock-in cells compared with the WT control. Rather than this knockdown resulting in a less severe sensitivity to olaparib, as would be expected if the cellular toxicity was a result of PARP trapping, both cell lines in fact had an increased sensitivity to olaparib when PARP1 is depleted (Fig. 5.2C). This suggests that the olaparib sensitivity in PCNA^{S228I} RPE-1 cells is not due to PARP trapping, and in fact points to the fact that there is probably a threshold level of PARP1 activity which is required for cellular proliferation even in WT RPE-1 cells. In addition, simply knocking down of PARP1 without olaparib treatment led to a significant decrease in the survival of PCNA^{S228I} knock-in cells compared to WT controls (Fig. 5.2D), indicating that the function of PARP1 is important for the viability of PCNA^{S228I} cells. Therefore, I conclude that olaparib sensitizes PCNA^{S228I} cells through inhibition of PARP1 function and not through PARP trapping.

5.3 Perturbation in the repair of endogenous SSBs is not the reason for olaparib sensitivity in PCNA^{S228I} cells

Taken together, the experiments above suggest that PCNA^{S228I} cells depend on PARP activity for normal growth and proliferation, such that PCNA^{S228I} cells cannot survive if PARP is inhibited. What then is the reason for this dependency? It is known that PCNA, along with its partners, FEN1 and LIG1, are involved in

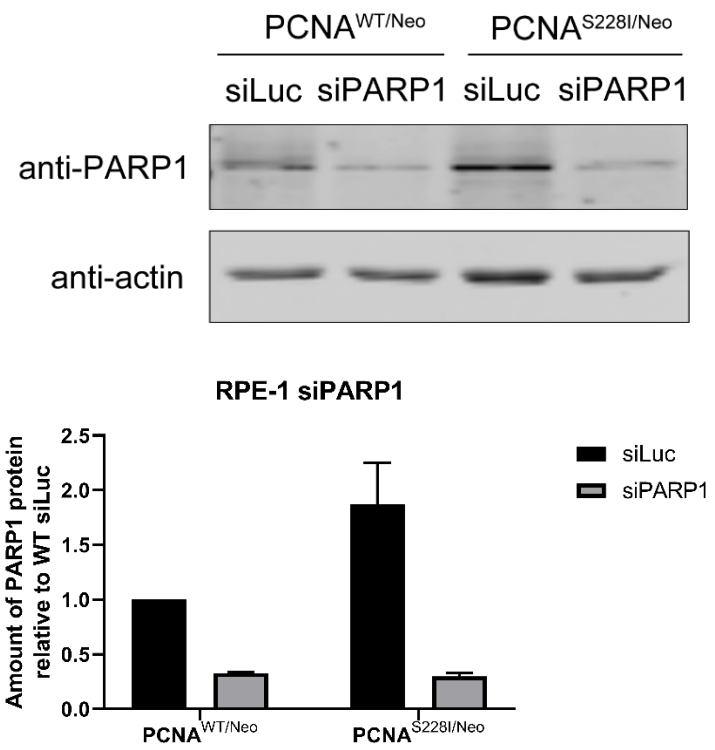


Figure 5.2B Western blot of RPE-1 cells transfected with siRNA against luciferase (siLuc) as control or against PARP1 (siPARP1). Anti-actin: loading control. The quantification was carried out from three independent Western blots. Histogram shows amount of PARP1 protein relative to WT control cells transfected with siLuc. Error bars represent SEM.

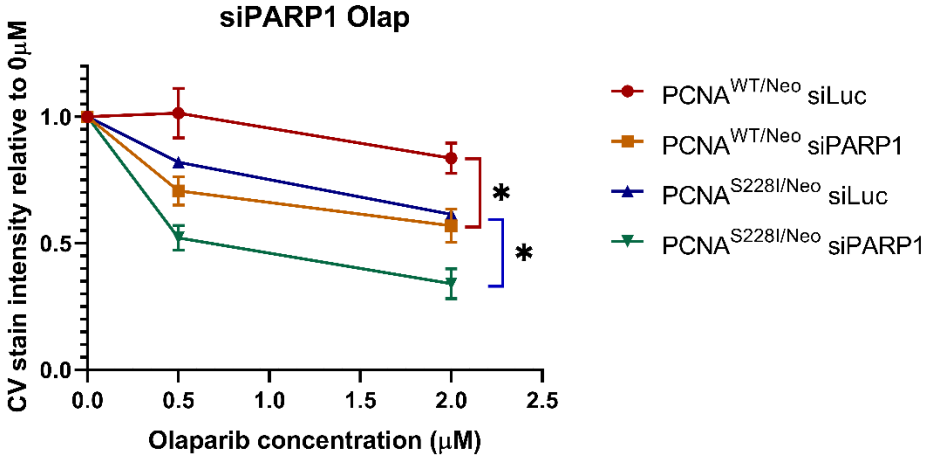


Figure 5.2C Olaparib cytotoxicity in PARP1 knock-down RPE-1 cells. Cells were first transfected with siRNAs for 48 hr and then seeded for the survival assay. Olaparib treatment was performed 24 hr after cells were seeded, and cells were stained with crystal violet (CV) 6 days after drug treatment. N=3. Error bars represent SEM. * $p<0.05$, two-tail paired student's t-test.

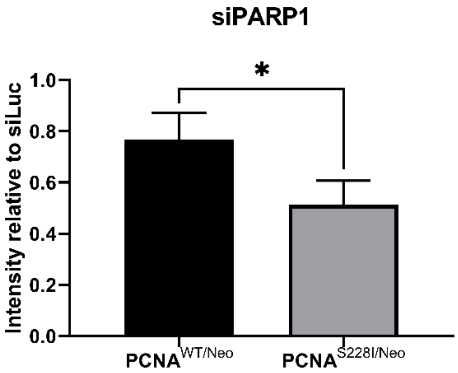


Figure 5.2D RPE-1 cell viability after PARP1 knock-down. Cells were transfected with siRNAs for 48 hr and then seeded with several numbers. After 7 days, cells were stained with crystal violet and the average intensity of PARP1 knock-down cells relative to the control luciferase knock-down cells (siLuc) was calculated as the viability. The rate was calculated in each single repeat. N=3. Error bars represent SEM. * $p<0.05$, single-tail paired student's t-test.

long-patch BER required for the repair of single stand breaks [108]. One hypothesis that I considered to be a likely explanation was that the S228I alteration of PCNA disrupts the BER pathway and delays SSB repair. The combination of this with inhibition of PARP1 would synergistically block the repair of SSBs generated from endogenous ROS or oxidative stress, and eventually these breaks accumulate to a lethal level in S228I cells upon PARP inhibition. To test this hypothesis, we challenged $PCNA^{S228I}$ cells with hydrogen peroxide (H_2O_2) to generate SSBs. Cells with genetic alterations that inactivate pathways of SSB repair are sensitive to this treatment [298]. However, we did not find a detectable sensitivity of H_2O_2 in $PCNA^{S228I}$ lymphoblastoid cells from the results of Dr Rose Wilson's survival assays (Fig. 5.3A). Furthermore, by comet assay we showed that $PCNA^{S228I}$ lymphoblastoid cells repair H_2O_2-

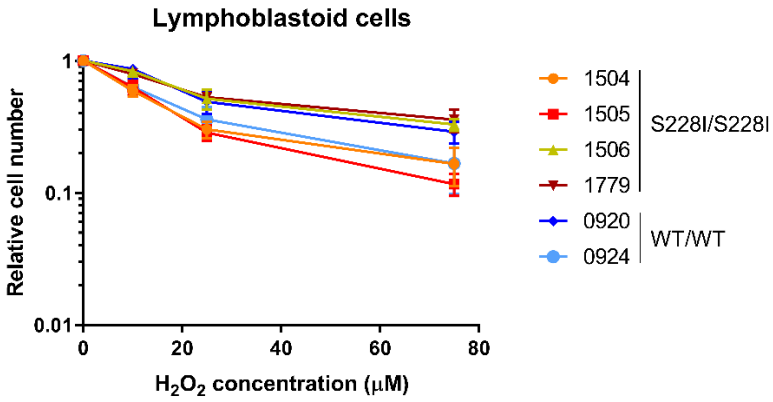


Figure 5.3A H_2O_2 cytotoxicity to lymphoblastoid cells derived from unaffected (WT/WT) and affected (S228I/S228I) individuals. Cells were counted before and after 72hr treatment with H_2O_2 and cell numbers were relative to vehicle treatment. N=4. Error bars represent SEM. (R. Wilson personal communication)

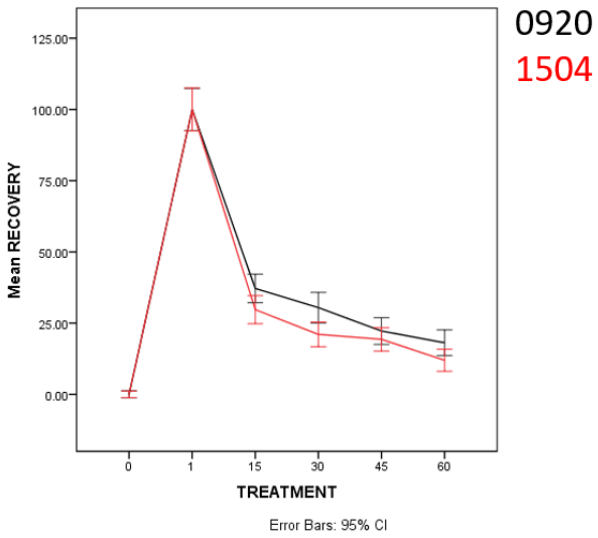


Figure 5.3B Results of comet assay showing the kinetics of DNA repair after H_2O_2 treatment. Lymphoblastoid cells were treated with 150µM H_2O_2 for 1 min and released in complete medium for desired time points (min) indicated in treatment axis of the graph. The recovery showed relative percentages of comet tail length compared with untreated (0 min) and no repair (1 min) samples. 0920: WT/WT, 1504: S228I/S228I. (R. Wilson and A. Legrand personal communication)

generated SSBs at a similar rate to WT control cells (R. Wilson and A. Legrand personal communication) (Fig. 5.3B). Thus, it appears that $PCNA^{S228I}$ cells have normal SSB repair pathways, and that the $PCNA^{S228I}$ alteration does not

impinge significantly on any role for PCNA in SSB repair. In addition to these data, while I found that culturing PCNA^{S228I} RPE-1 cells in low oxygen (3%), in order to reduce endogenous oxidative damage, had the effect of reducing the overall sensitivity of both WT and S228I cells to olaparib, but this did not eliminate the relative sensitivity of the S228I cells (Fig. 5.3C), leading to the conclusion that the unrepaired endogenous SSBs are not the reason for olaparib sensitivity in PCNA^{S228I} cells. Moreover, the results showed even higher relative olaparib sensitivity in the low oxygen condition compared to the normal oxygen condition. This can be explained by the fact that cells under hypoxia generate less NAD^+ in mitochondria due to slowing of electron transport [299] and effectively lead to inhibition of PARP1 activity. Therefore, the increasing relative olaparib sensitivity in PCNA^{S228I} cells under hypoxia also supports the previous conclusion that it is the inhibition of PARP1 activity by olaparib that results in sensitivity in PCNA^{S228I} cells. Together, these data suggest that the specific increase in olaparib sensitivity seen in PCNA^{S228I} cells is not due to compromised pathways of repairing SSBs generated endogenously from oxidative stress.

5.4 PAR chains are detected at replication forks in PCNA^{S228I} cells

The essential function of PCNA's interaction with FEN1 and LIG1 is to facilitate Okazaki fragment maturation. It was recently reported that unligated Okazaki

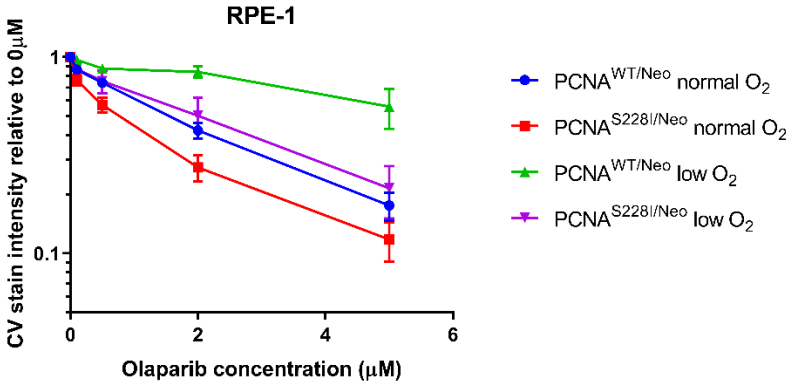


Figure 5.3C Olaparib cytotoxicity to RPE-1 knock-in cells with low O_2 incubation. Cells incubated with 3% oxygen were treated exactly the same as it was performed in olaparib survival assay before, and the result shared the same graph with that in Fig. 4.4B (normal O_2). N=3. Error bars represent SEM.

fragments (generated by inhibition of FEN1 or LIG1) can be sensed by PARP1 and repaired via the SSB repair machinery [283]. Therefore, I hypothesised that PCNA^{S228I} cells, with potentially defective recruitment of FEN1 and LIG1 to replication forks, might have to rely more heavily on SSB repair pathways signalled by PARP1 to deal with the unligated Okazaki fragments. To test whether PARP1 is hyper-activated in proliferating S228I cells, I performed a FACS analysis using an antibody specific for poly(ADP)ribose (PAR) chains. No detectable differences were observed in the level of PAR chains between untreated WT and S228I knock-in cells. However, upon treatment of cells with a PARG inhibitor (PARGi) for only 30 minutes to block the degradation of PAR polymers, a sharp increase in PAR chains was detected, and this increase was largely confined to PCNA^{S228I} knock-in cells that were in S phase as determined by DNA content (Fig. 5.4A1 & 2). This suggested that PCNA^{S228I} cells, though

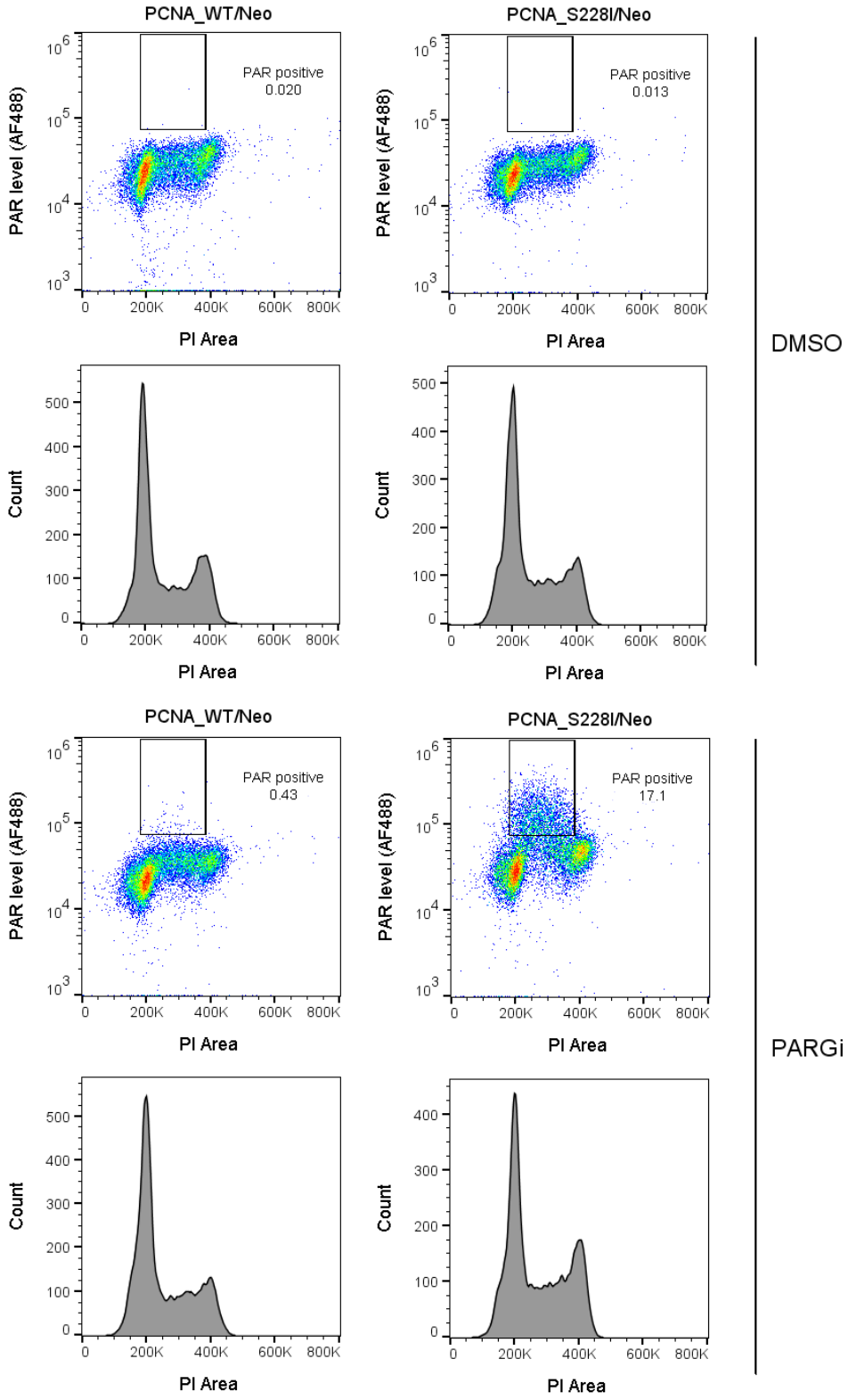


Figure 5.4A1 Two color flow cytometry, analyzing DNA content (PI area) and the PARylation level. DMSO: vehicle; PARGi: 10 μM treated for 30 minutes. One FACS analysis result from two independent repeats. The PAR positive population indicates cells with elevated amount of PARylation.

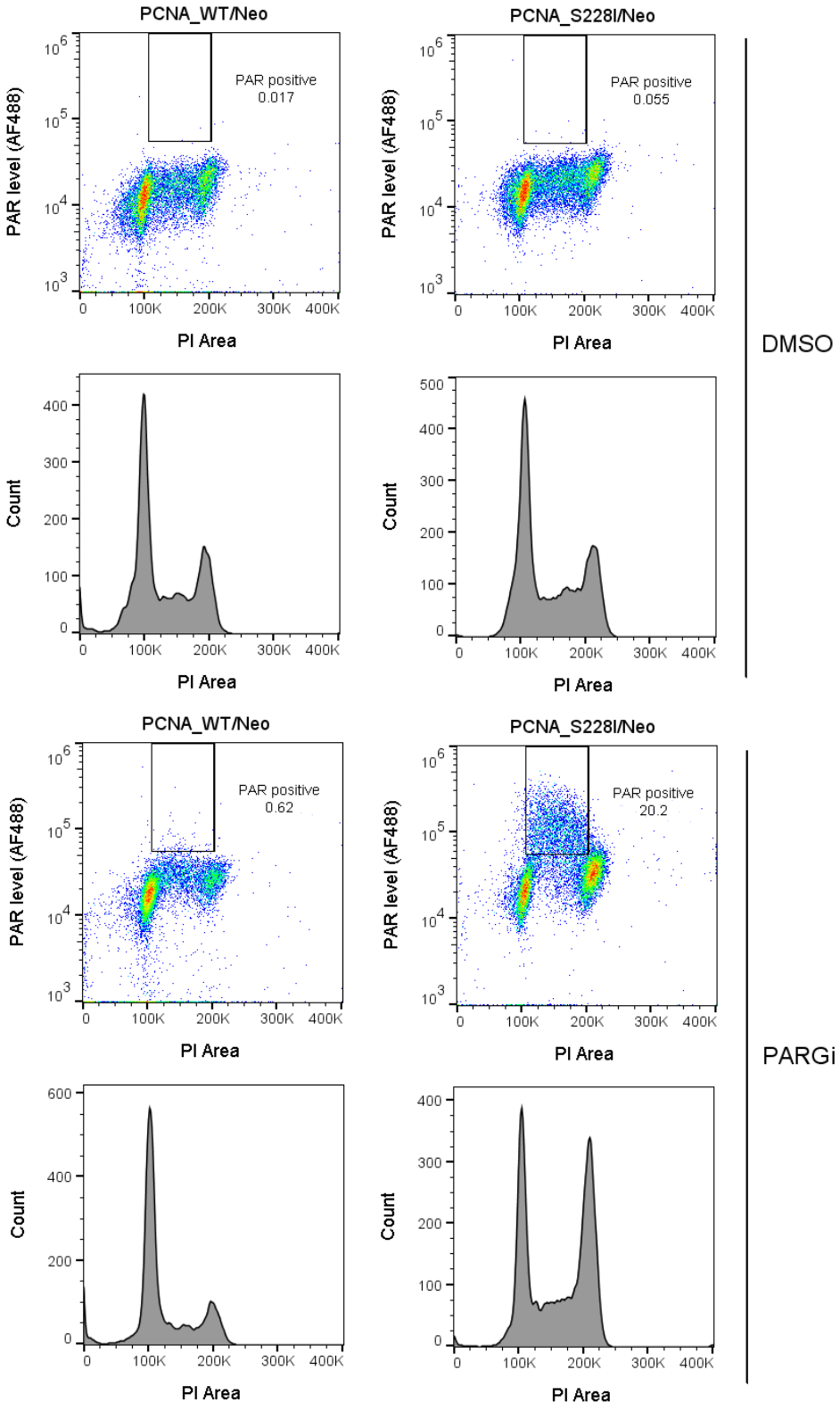


Figure 5.4A2 Two color flow cytometry, analyzing DNA content (PI area) and the PARylation level. DMSO: vehicle; PARGi: 10 μM treated for 30 minutes. The other FACS analysis result from two independent repeats. The PAR positive population indicates cells with elevated amount of PARylation.

apparently progressing normally through the cell cycle, are actually generating an elevated amount of active PARP1 signalling during S phase. I then applied immunofluorescence microscopy to investigate the localization of these PAR chains in S phase and used the Cell Profiler software to measure and calculate the relative intensity of PAR chain foci. This showed that there is a dramatic increase in the intensity of PAR chain foci in PCNA^{S228I} cells upon PARGi treatment, consistent with the FACS results (Fig. 5.4B). In addition, the PAR chains formed foci colocalizing with the PCNA foci during S phase, indicating that the PAR chains are formed at, or near to replication forks (Fig. 5.4C). Therefore, I can conclude that PCNA^{S228I} mutation triggers PARP signalling at replication forks. In other words, the process of DNA replication in PCNA^{S228I} cells is probably abnormal, and it leads to the formation of SSBs that depend on the PARP1 signalled SSB repair machinery to maintain cell viability.

It has been suggested that chronic treatment with PARGi will destroy the dynamic balance of NAD^+ and PAR, leading to a lack of NAD^+ for PARylation and generating similar results to PARP inhibition. Predictably therefore, PCNA^{S228I} RPE-1 knock-in cells showed sensitivity to PARGi according to the results of survival assays (Fig. 5.4D). It is also possible that this sensitivity is a result of a combination of effects, both indirectly through PARP inhibition and directly through the harmful accumulation of PAR chains at replication forks. In

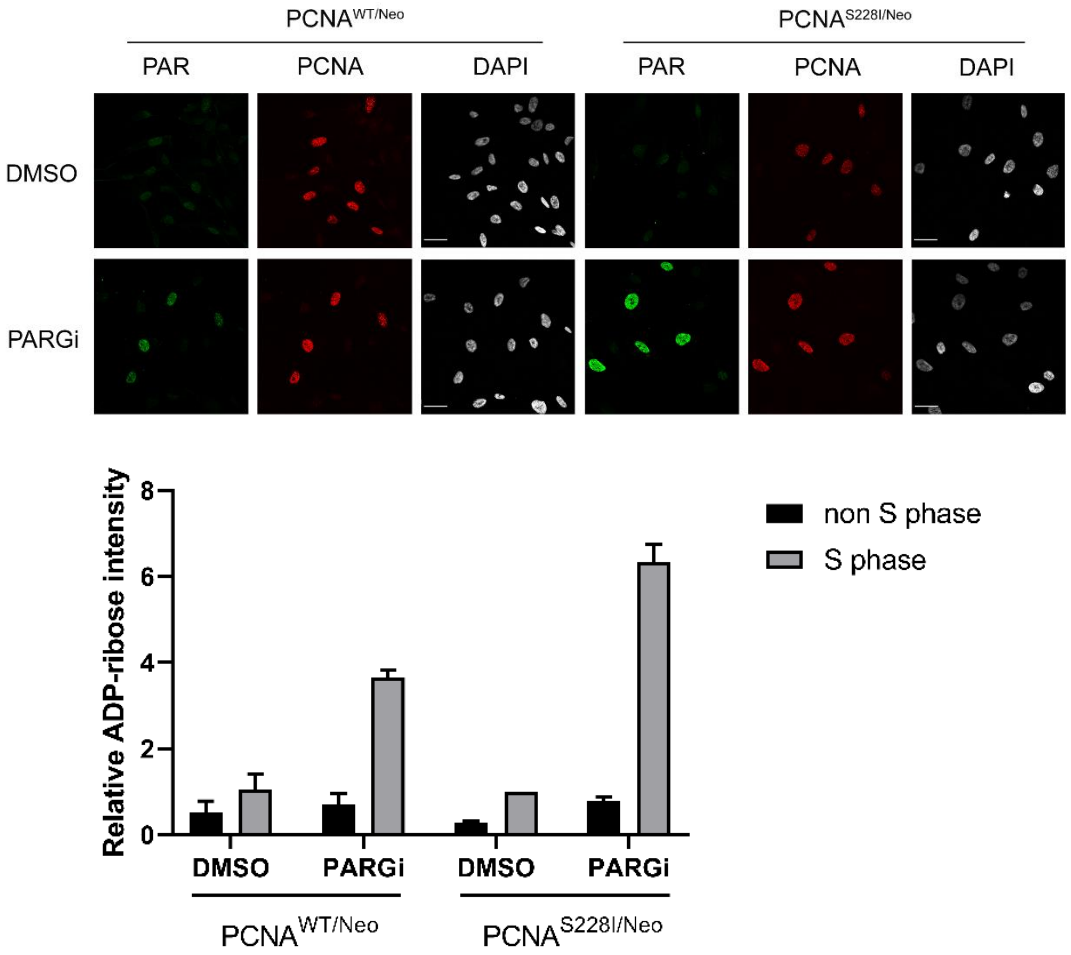


Figure 5.4B Immunofluorescence against PAR chains was performed in RPE-1 knock-in cells treated with 10 μM PARGi for 30 minutes. Cells were pretreated with triton extraction, so the S phase can be determined by PCNA labelling. The intensity of ADP-ribose was measured by Cell Profiler software, and the relative intensity was calculated in each repeat against PCNA$^{S228I/Neo}$ cells with DMSO treatment. Scale bar = 28 μm. N=3. Error bars represent SEM.

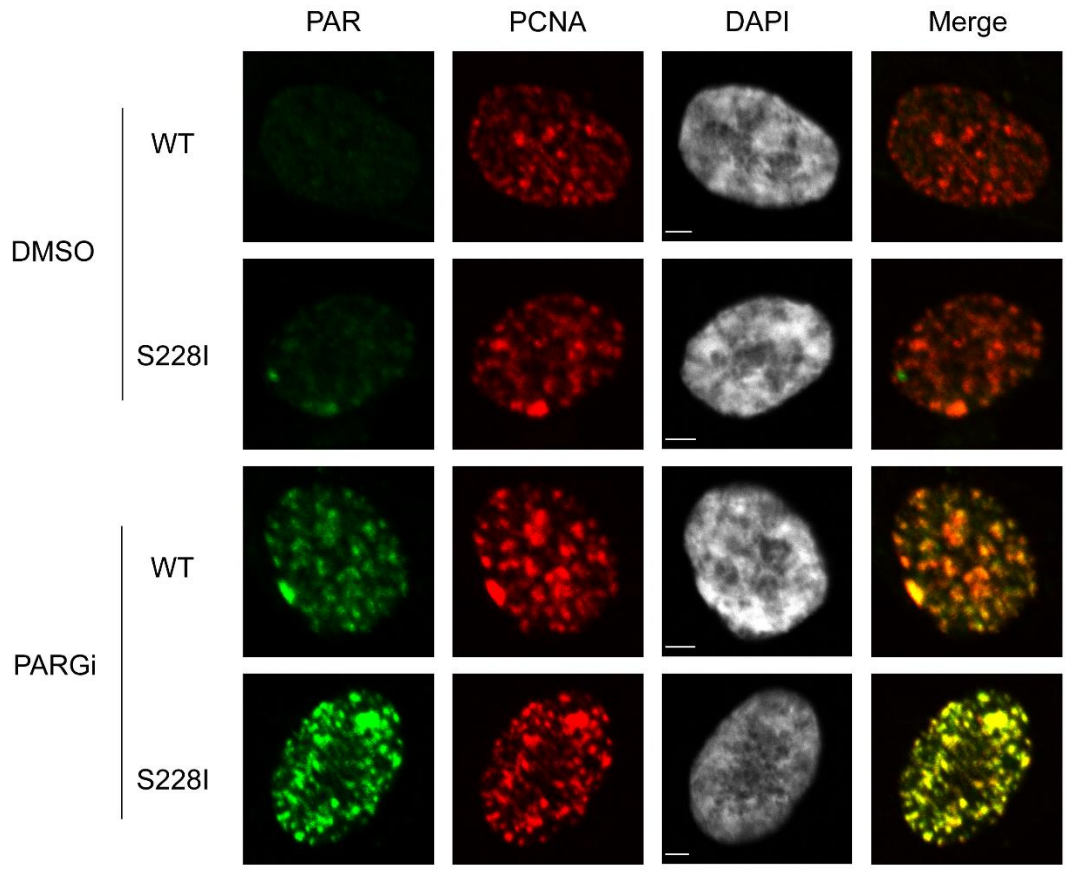


Figure 5.4C Immunofluorescence against PAR chains was performed in RPE-1 knock-in cells treated with 10 μM PARGi for 30 minutes (zoomed in). Cells were pretreated with triton extraction. Scale bar = 3 μm.

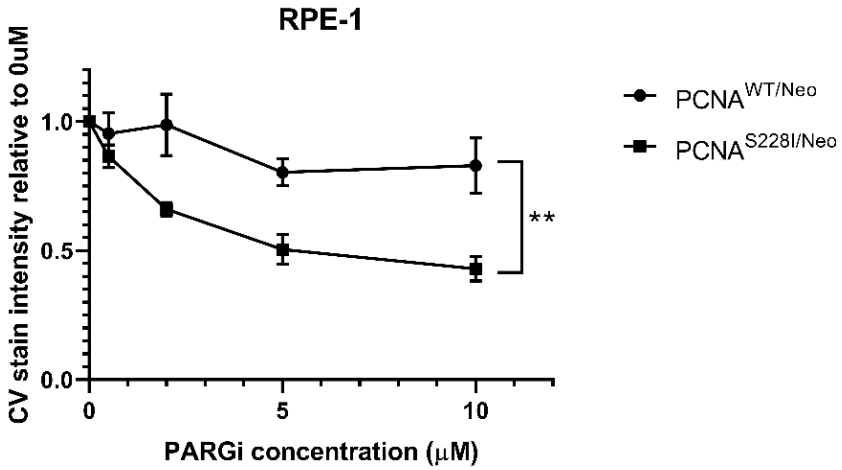


Figure 5.4D PARGi cytotoxicity to PCNA^{S228I} knock-in RPE-1 cells. Cells were treated with PARGi 24 hr after seeding and stained by crystal violet (CV) 6 days after drug treatment. N=4. Error bars represent SEM. ** $p<0.01$, two-tail student's t-test.

either case, this result further confirms that PCNA^{S228I} cells have to rely on PARP-dependent pathways to deal with problems arising from DNA replication.

5.5 Discussion

In this chapter, I first proved that the olaparib sensitivity of PCNA^{S228I} cells is due to inhibition of PARP1 function rather than PARP trapping. Then I ruled out the possibility that PCNA^{S228I} cells have problems in SSB repair, and finally arrived at the conclusion that PCNA^{S228I} cells generate SSBs during DNA replication and the need for PARP1 to signal SSB repair pathways accounts for the sensitivity of these cells to the inhibition of PARP1 function. Interestingly, I discovered an about two-fold of elevated endogenous PARP1 protein amount in PCNA^{S228I} cells compared with the WT controls when trying to knock down PARP1 expression (Fig. 5.2B). This gives an implication that PCNA^{S228I} cells require more PARP1 for their proliferation and viability, which is consistent with the result of synthetic lethality for PCNA^{S228I} and PARP1 depletion, although the mechanism for the upregulation of PARP1 in PCNA^{S228I} cells still remains to be elucidated.

It is widely known that PCNA mainly functions on the lagging strand to increase the processivity of Polδ as well as facilitate ligation of Okazaki fragments by recruiting FEN1 and LIG1 during DNA replication. PCNA^{S228I}, however, was

reported to have a lower affinity for both FEN1 and LIG1 and thus potentially it could have problems in Okazaki fragment maturation. However, before this work we had, perhaps surprisingly, not detected any perturbations to DNA replication in cells with PCNA^{S228I} [242] [246]. I have now shown that PCNA^{S228I} cells have more active PARP signalling at replication forks, which suggests that they are likely to generate more DNA nicks during DNA replication. Therefore, I can propose a model to explain the sensitivity of PCNA^{S228I} cells to PARP inhibition: the S228I alteration of PCNA results in impaired recruitment of FEN1 and LIG1 during DNA replication, which causes problems in Okazaki fragment maturation. Single stranded gaps remain between unligated Okazaki fragments, which can be sensed by PARP1 and repaired by the PARP1-dependent SSB repair machinery as an alternative pathway for Okazaki fragment maturation. The inhibition of PARP1 function blocks this alternative pathway, and the unligated Okazaki fragments remain as SSBs which activate the G2/M checkpoint in RPE-1 cells, or generate DSBs and replication fork collapse in the S phase of next cell cycle in EBV-immortalized lymphoblastoid cells, finally leading to cell death (Fig. 5.5).

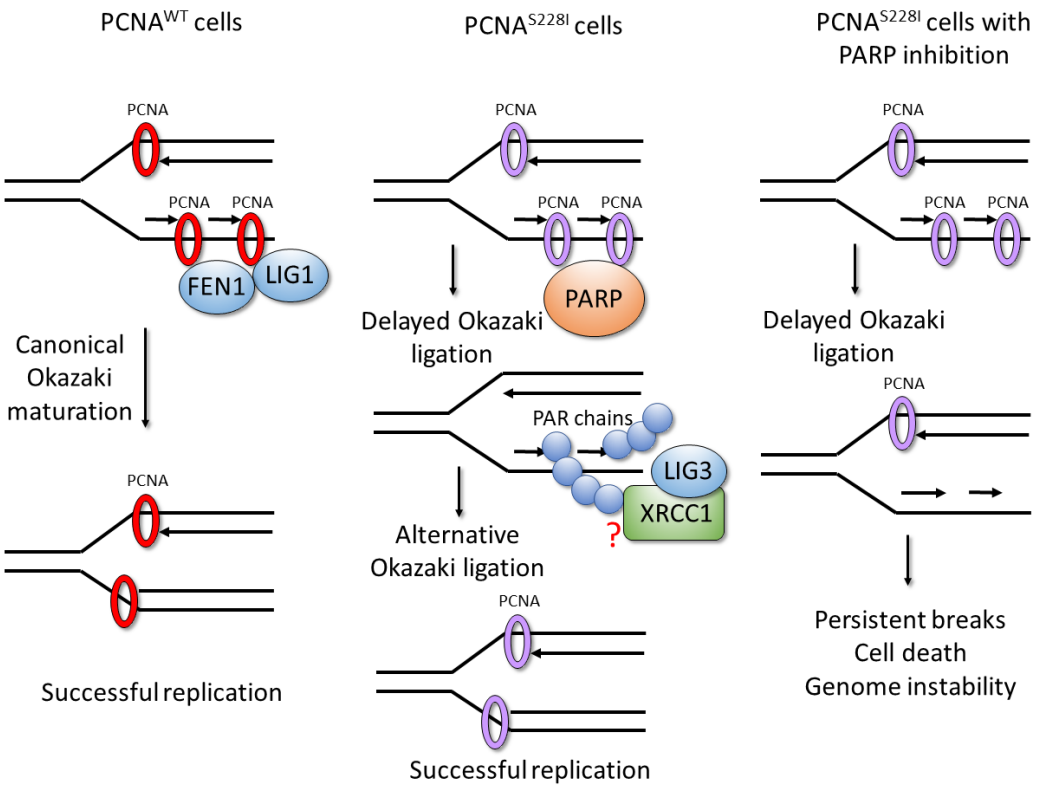


Figure 5.5 The model explaining the sensitivity of PCNA^{S228I} cells to PARP inhibition. In WT cells, the intact PCNA function ensures efficient Okazaki fragment processing. In contrast, the lower affinity of PCNA^{S228I} for both FEN1 and LIG1 can delay the Okazaki fragment maturation, which is sensed by PARP and repaired by XRCC1-dependent SSB repair machinery (not confirmed in this thesis). Therefore, PCNA^{S228I} cells are still able to carry out robust DNA replication. However, if the function of PARP is inhibited, the unligated Okazaki fragments generated during DNA replication in PCNA^{S228I} cells will lead to persistent DNA breaks and thereby genome instability and cell death.

Chapter 6: Discussion and future work

6.1 Discussion

As was described in Chapter 1, the functions of PCNA and the pathways in which it is involved have been well characterized in the past decades. It is widely accepted that PCNA interacts with its partners in a transient and dynamic way to function in multiple pathways [206], but the question of how cells regulate these multiple PCNA interactions in different conditions still remains largely unclear. Some PCNA interactions are apparently less essential that others, perhaps due to the existence of alternative recruitment mechanisms or other unknown pathways; these include the PCNA-Polε interaction for leading strand synthesis [219] and PCNA-DNMT1 in epigenetic inheritance [96]. Therefore, the mechanisms by which cells might tolerate impaired PCNA interactions are also hotspots of current research on PCNA.

The finding that p.Ser228Ile of PCNA caused PCNA-associated DNA repair disorder (PARD) gave a new angle to the research of PCNA functions [242]. The aberrant IDCL structure of $PCNA^{S228I}$ leads to compromised interactions of PCNA with many of its partners [246], making this mutation an interesting disease model for studying the functions and regulation of PCNA interactions. A fuller understanding of the cellular consequences of this mutation might elucidate the mechanisms by which the clinical phenotypes of PARD are generated. The fact that $PCNA^{S228I}$ cells from affected individuals sufficiently

tolerate the dramatic perturbations in PCNA client interactions which have been reported from biochemical studies [246] make this mutation of great interest, which might reveal mechanisms of cell tolerance to disrupted PCNA interactions.

In the work presented in this thesis, I have generated an isogenic PCNA^{S228I} knock-in RPE-1 cell line (Chapter 3) which was utilized as a disease model to address pathways involved in the disease pathology as well as to distinguish the regulation and robustness of various functions of PCNA which operate through different client interactions. By treatment of PCNA^{S228I} cells with the PARP inhibitor olaparib, I observed severe consequences of the S228I mutation (Chapter 4) which led me to propose an alternative pathway that maintains the robustness of DNA replication under the perturbations of PCNA client interaction caused by S228I mutation (Chapter 5).

My results demonstrated that:

1. The PCNA^{S228I} mutation does not affect overall DNA replication and only has subtle influence, if any, on the S phase progression, even though the interactions with key factors during replication such as FEN1 and LIG1 are perturbed.

2. The PCNA^{S228I} mutation sensitizes cells to the PARP inhibitor olaparib by leading to more DNA breaks and cell cycle disruption.

3. The function of PARP1 is important for PCNA^{S228I} cell viability.

4. The PCNA^{S228I} mutation results in more active PARP1 signalling at replication forks during S phase.

Therefore, I propose that a PARP1-signalled pathway, most likely to be the SSB repair pathway, is an alternative pathway that resolves defects in Okazaki fragment processing that arise due to impaired PCNA^{S228I} interaction with FEN1 and LIG1.

6.1.1 PARP1-signalled alternative pathway for Okazaki fragment processing

I think the most important finding from my work was the confirmation of PARP1 as an alternative factor to resolve defects in DNA replication in the context of PCNA^{S228I} mutation. As discussed in Section 5.5, DNA replication defects in PCNA^{S228I} cells are most likely to come from the maturation of Okazaki fragments during lagging strand synthesis, which, according to what Caldecott's group reported recently, require processing by a PARP1 and XRCC1 dependent "backup" pathway [283]. The reliance of PCNA^{S228I} cells on PARP1 functions have been proven in my thesis from several aspects including synthetic lethality and PAR polymers generated at replication forks. The roles of XRCC1 in this alternative pathway have not been investigated, but future confirmation of the XRCC1 involvement in the downstream of this pathway will

definitively strengthen the argument of PARP1-signalled SSB repair pathway as an alternative mechanism in Okazaki fragment processing when functions of FEN1/LIG1 are challenged.

Interestingly, as PARP1 is thought to be absent in yeast, there is actually evidence that PCNA^{S228I} mutation showed synthetic lethality with Dna2 mutation in *S. pombe* (Felicity Watts personal communication). Given that Dna2-catalysed long flap pathway is a well-known alternative pathway for Okazaki fragment processing [69], this result provides supportive evidence for defective short flap Okazaki fragment processing pathway in yeast with PCNA^{S228I} mutation, and also on the other hand suggests the importance of PARP1 as another backup factor in higher eukaryotic cells. Since there are two alternative pathways mediated by Dna2 or PARP1 in human cells to deal with replication intermediates, how they are regulated in different conditions still remains unclear and is an important question to better understand the crosstalk between DNA SSB repair pathway and lagging strand synthesis.

6.1.2 PCNA^{S228I} and the pathology of PARD

As was described in Chapter 1, PARD has features of short stature, premature aging, neurodegeneration and photosensitivity [242]. NER is defective in PCNA^{S228I} cells derived from affected individuals, and this explains the photosensitivity [242]. Short stature can arise as a developmental problem, which is likely to result from the problematic DNA replication caused by

PCNA^{S228I} mutation. Although the overall DNA replication is not significantly influenced by the S228I mutation, presumably because of a robust PARP1 mediated repair pathway, I did observe a slight increase in S phase percentage in PCNA^{S228I} cells. This might suggest that the alternative pathway probably requires additional time, or is suboptimal in some way. This subtle change in cell cycle progression might result in the accumulation of problems during development because the progress of development is strictly regulated.

The mechanisms which underlie premature aging and neurodegeneration phenotypes are likely to be more complicated. Among the hallmarks of aging [4], genome instability, epigenetic alterations and stem cell exhaustion are the three hallmarks that are most likely to be related to PARD. Genome instability could arise from defective NER, which makes the cells of affected individuals vulnerable not only to damage caused by environmental agents including UV light, but also to other helix distorting bulky base lesions, possibly including crosslinks that could be generated endogenously [161]. In addition, although my data suggest that the defects in DNA replication (Okazaki fragment processing) can be efficiently processed by PARP1 mediated pathways, there is still likely to be an increased basal level of SSBs arising during replication in the cells of affected individuals. This increase in damage is likely to have the consequence of increased genome instability. There is also a potential effect of PCNA^{S228I} on epigenetic alteration because PCNA^{S288I} was reported to have

lower binding affinity for DNMT1 [246]. However, the role that PCNA plays in epigenetic maintenance still remains unclear, and as such this remains an important avenue for future research. Stem cell exhaustion can also occur as a result of defective DNA replication. Though mostly resolved via the PARP pathway, the defects in DNA replication of PCNA^{S228I} cells do result in a persistent activation of PARP1 during DNA replication, which implies a persistent activation of DNA damage signalling. This is supported by the fact that I observed more p21 in the whole cell extract of PCNA^{S228I} knock-in RPE-1 cells when compared to WT cells (Fig. 6.1.1). However, from the data described in Section 3.2.3, this elevated expression of p21 did not lead to any cell cycle arrest. And there is also no evidence of DNA damage checkpoint activation in PCNA^{S228I} lymphoblastoid cells [242]. Therefore, we don't think the increasing p21 protein level in PCNA^{S228I} cells is a result of checkpoint activation, but it is instead a consequence of DNA damage signalling. And PCNA^{S228I} cells are also likely to activate some other pathways to overcome the inhibitory functions of p21 on cell cycle progression. Taken together, it is possible that stem cell exhaustion might occur as the result of a cascade of cellular pathways activated by overexpression of cell cycle inhibitory proteins like p21 due to persistent activation of DNA damage signalling. This might also in some way account for neurodegeneration in PARD, as it is widely known that the human neuron system requires the activity of neuronal stem cells. Oxidative stress has been widely accepted as a causative agent in neurodegeneration,

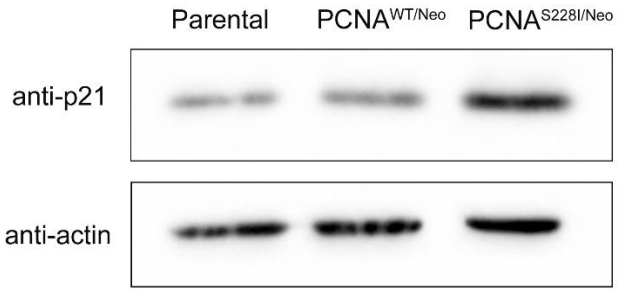


Figure 6.1.1 Anti-p21 Western blot of the whole cell lysate of the knock-in cell lines. Parental: RPE-1 parental cells as control. Anti-actin is loading control.

particularly in DNA repair disorders [300]. However, since I have demonstrated that PCNA^{S228I} cells have normal SSB repair pathways (Section 5.3), it appears less likely that the neurodegeneration in PARD results from compromised response to oxidative stress leading to neuronal cell death. I would thus favour the hypothesis that neuronal stem cell exhaustion owing to persistent activation of DNA damage signalling is a major reason for the neurodegeneration seen in PARD.

6.1.3 PCNA^{S228I}-PARPi synthetic lethality and cancer chemotherapy

From the results I have generated, I conclude that PCNA^{S228I} cells are sensitive to olaparib because the function of PARP1 is crucial to their viability as it resolves defects in DNA replication caused by the mutation of PCNA. In other words, PCNA^{S228I} and PARPi show synthetic lethality. PARG inhibitor is also toxic to PCNA^{S228I} cells, possibly because it destroys the balance of NAD^+ and PAR and so limits the synthesis of PAR chains, or the accumulation of PAR

chains at replication forks is harmful per se. Therefore, treatment with PARG inhibitor has similar consequences to PARP inhibitors in suppressing PARP1 function.

Considering the use of PARPi in BRCA-deficient cancers and potential treatment in wider HR-deficient cancers ('BRCAness'), my findings give an additional new potential application of PARPi in the cancer clinic. According to the model proposed here, defects in Okazaki fragment processing generate a reliance on PARP1-mediated pathways to resolve replication problems and ensure cell viability. Therefore, cancers with aberrant Okazaki fragment maturation can also be the targets of PARPi, or PARG inhibitor if a clinically utilisable version is generated. From database searches to date there are no cancers carrying $PCNA^{S228I}$ mutation, but it is inevitable that genes relevant to Okazaki fragment maturation, such as FEN1 and LIG1, can have hypomorphic mutations as "passengers" in some cancers due to the high mutation rate in cancer cells. Thus, any mutations causing similar consequences as $PCNA^{S228I}$ – called 'S228Iness' – can be a new potential application of PARP inhibitors. Moreover, as cancer cells are often subject to replication stress and are highly proliferative, PARPi treatment in combination with other drugs targeting the Okazaki fragment maturation such as the PCNA inhibitor T3 or the FEN1 inhibitor can also be a novel therapeutic strategy for some specific cancers. Also admittedly, targeting PARP1 as well as Okazaki fragment processing

simultaneously can be harmful to normal cells according to the model I proposed. Therefore, the strategy of such a combinational chemotherapy still requires more clinical investigations.

6.2 Ongoing and future work

The model that a PARP1-dependent process resolves defects in Okazaki fragment processing, caused by a failure of PCNA^{S228I} to properly interact with FEN1 and LIG1, is proposed to explain the overall robust DNA replication observed in PCNA^{S228I} cells. This would explain how DNA replication appears robust in PCNA^{S228I} cells, even though we have demonstrated that crucial interactions at the replication fork are dramatically perturbed [246]. However, this model is not yet completely proven by the results presented in this thesis. There are several questions that require further investigation. Below I will summarize the ongoing and future work that aims to address these questions.

1. Confirmation of a direct relationship between defective PCNA interactions with FEN1/LIG1 and the generation of replication-related nicks

So far, we have shown that the S228I mutation of PCNA leads to a lower affinity for FEN1 and LIG1, and that PCNA^{S228I} cells generate DNA nicks which are processed by PARP1 signalling at replication forks in S phase. However,

whether the DNA nicks at replication forks result from perturbations of PCNA interactions with FEN1 and LIG1, or different clients, has not been confirmed. To address this, the Green lab will attempt to rescue the over-PARylation in S phase of PCNA^{S228I} cells by expressing an exogenous version of FEN1 or LIG1 in which the PIP box has been swapped to the PIP box of p21 ("SuperPIP"). These domain swap experiments have been used to prove that the ability of p21 to retain the affinity for PCNA^{S228I} indeed lies in the PIP box sequence itself [246]. If the "SuperPIP" versions of FEN1 or LIG1 are able to restore binding to PCNA^{S228I} we might expect fewer unligated Okazaki fragments and less PARP signalling. This should also reduce PARPi/PARGi sensitivity. The aim of these rescue experiments using SuperPIP FEN1 and LIG1 is to confirm that reduced PCNA interaction with FEN1 and LIG1 is the reason for all the phenotypes that were observed in this thesis.

2. Visualization of DNA replication defects in PCNA^{S228I} cells

As highlighted in Chapter 3, the overall cell cycle profile of PCNA^{S228I} cells is unperturbed with only a subtle increase in S phase cells, which indicates that bulk DNA replication defects have not been observed in PCNA^{S228I} cells. Given that I now propose the model that PARP1 resolves replication defects in PCNA^{S228I} cells, we might expect to detect compromised DNA replication when PARP1 function is inhibited. Indeed, Ms Bernice Chan, a student working with me on an MSc dissertation, has generated some initial results using DNA fibre

assays, showing that PARG inhibitor treatment can significantly slow down the progression of DNA replication in PCNA^{S228I} cells compared to WT controls (Appendix Fig. F). This contributed to the model that PCNA^{S228I} mutation leads to defects in DNA replication which have to be processed by PARP1 signalling. I will repeat the experiment to confirm this result.

To fully confirm the model, we would like to monitor directly defects in Okazaki fragment processing in PCNA^{S228I} cells. We have made many attempts to visualize the Okazaki fragments from our cell lines by electrophoresis in alkaline agarose gels, without success. This may be due to the relatively small proportion of replicating cells in our cultures and the rapid nature of Okazaki fragments processing. I also tried to visualize the unexcised RNA primers in Okazaki fragments using 5-Ethynyluridine (EU) pulse labelling. However, EU can never form foci at replication forks (data not shown), possibly because the length of RNA primers (usually ~ 10 ribonucleotides) [52] as well as their distribution on the replicating DNA (every ~ 200 nucleotides according to the length of Okazaki fragments) [43] make it difficult to form EU foci. Alternatively, RPA labelling can be an indirect way of showing defective Okazaki fragment maturation in PCNA^{S228I} cells. If Okazaki fragments are not processed properly, more 5′ flaps will be generated, and therefore more RPA will localize at replication forks to bind to the flaps and facilitate Dna2-mediated incision [301], which will form RPA foci and be visualized by immunofluorescence microscopy.

3. Deciphering PARP1 signalled downstream pathways at replication forks

In my model, I suggested the SSB repair machinery as the pathway downstream of the PARP1 signalling to resolve the defective Okazaki fragment maturation because XRCC1 dependent SSB repair is the most common pathway that is recruited and activated by PARP1 signalling and also the unligated Okazaki fragments display DNA nicks with very similar structure to SSBs. However, this has not been proven in this thesis. Immunofluorescence microscopy will be used to visualize the localization of XRCC1 in PCNA^{S228I} knock-in cells after treatment of PARG inhibitor. Besides, XRCC1 knock-down through siRNA will also be carried out to measure the viability of PCNA^{S228I} cells. From these experiments I can investigate the importance of XRCC1 in the viability of PCNA^{S228I} cells and address the activity of SSB repair machinery at replication forks. Other SSB repair machinery proteins such as Polβ and LIG3 can also be investigated if necessary.

4. Investigation on other pathways that might be influenced by PCNA^{S228I} mutation

As described earlier, PCNA is involved in many cellular pathways and although I have here uncovered an effect of S228I on DNA replication there are still aspects of PCNA function that have not been assessed in the context of this mutation. Using lymphocytes from affected individuals, we previously showed

that p21 and Cdt1 steady state levels, or turnover after UV-irradiation, is not affected [246]. However, other PIP degron partners such as SET8 have not been assessed, nor has the influence of S228I on chromatin assembly or epigenetic inheritance been investigated. Even slight perturbations to such pathways might influence the development or disease progression of individuals affected with PARD, and thus these aspects remain worthy of future investigation.

Appendix A Karyotyping of hTERT RPE-1 cells

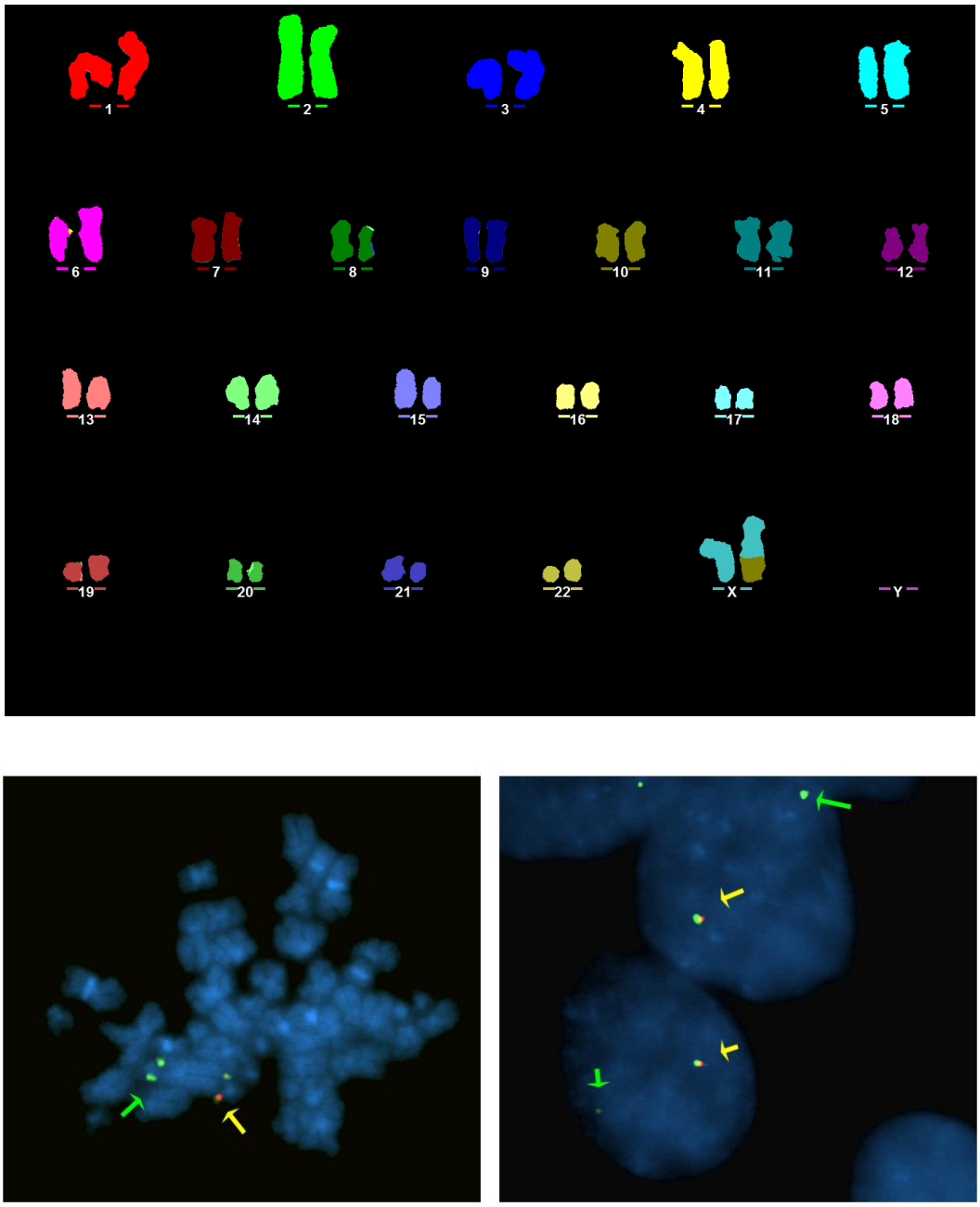


Figure A FISH karyotyping results of the parental hTERT RPE-1 cells. The picture on the top displays an example of the MFISH karyotyping. They contain no major rearrangements, apart from the pre-existent rearrangement in RPE-1 cells of chromosome X and chromosome 10. The picture on the bottom show the copy number of the PCNA gene by FISH using BAC probes against the PCNA locus in metaphase (left) or interphase (right). PCNA locus was labelled as green colour and hTERT as red. The yellow arrow showed an overlap of the two colour in one chromosome. (D. Moralli personal communication)

Appendix B Plasmid maps



Figure B1 Map of pSpCas9(BB)-2A-GFP plasmid with sgRNA cloned.

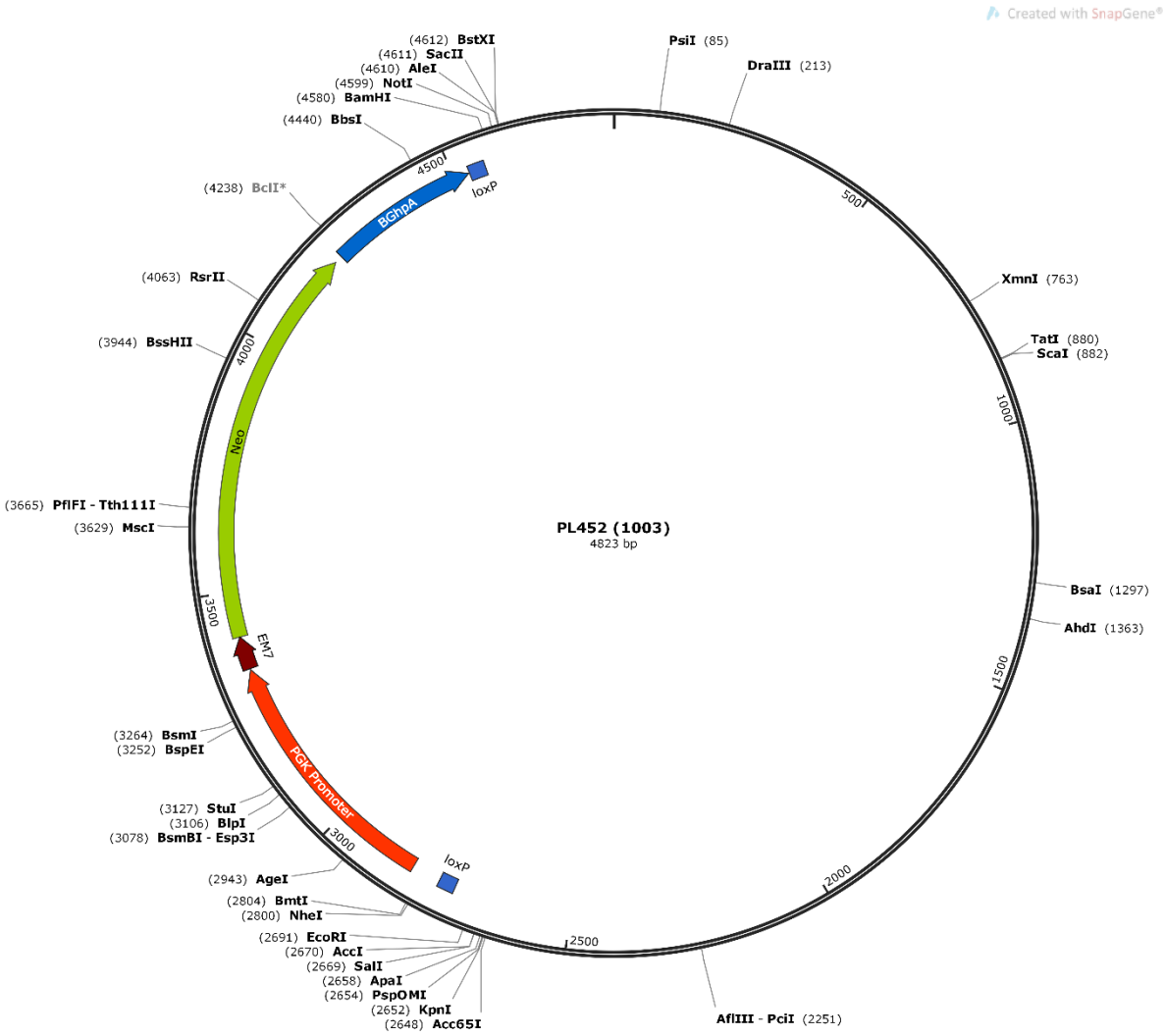


Figure B2 Map of the PL452 plasmid containing the PGK-Neo selection cassette. Restriction sites are also shown in the map.

Appendix C MFISH on knock-in RPE-1 cells

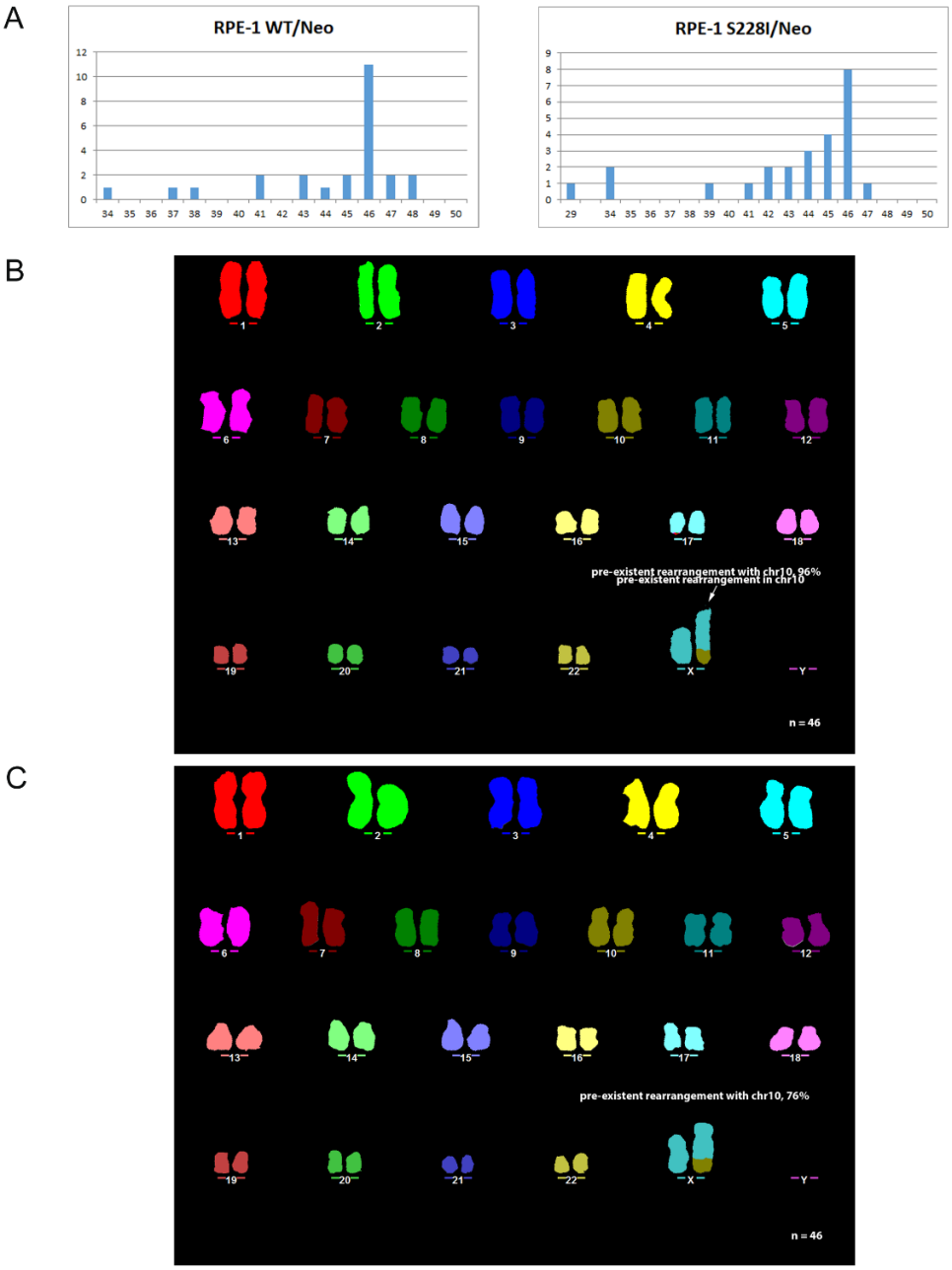


Figure C MFISH karyotyping results on RPE-1 knock-in cells. **(A)** Spreadsheet of the MFISH analysis on both WT control and PCNA^{S228I} knock-in cells. **(B and C)** A karyotype example of each cell line. They contain no major rearrangements, apart from the pre-existent rearrangement in RPE-1 cells of chromosome X and chromosome 10. The sample preparation and data analysis were all carried out by Dr Daniela Moralli and Ms Mary-Anne Durin who are Green lab members. (D. Moralli and M. Durin personal communication)

Appendix D Full Mass spectrometry results of PCNA

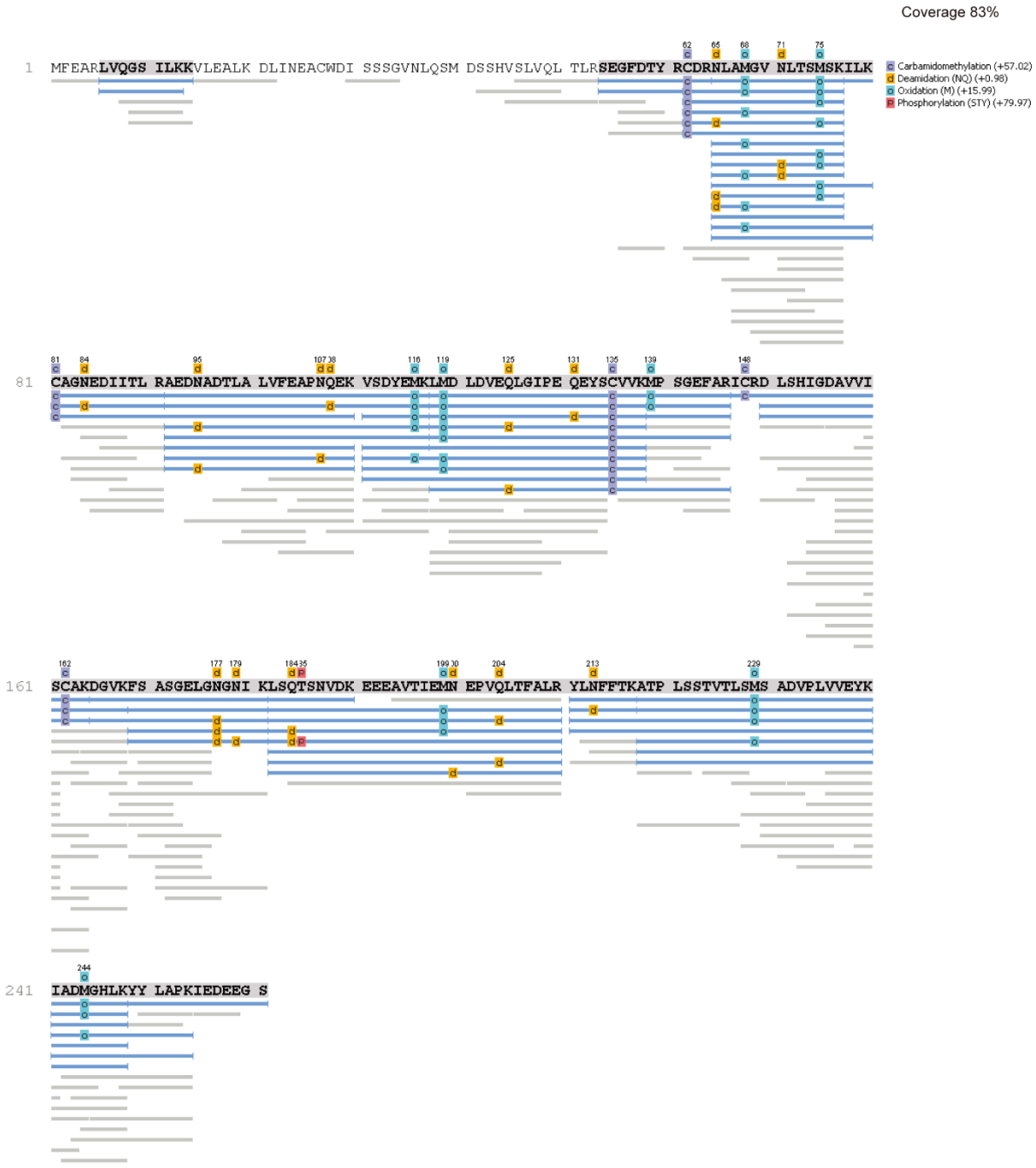


Figure D Full Mass Spec result of PCNA. Following Mass spectrometry analysis, modifications of PCNA was detected with a sequence coverage of 83% with only partial coverage of the N-terminus. S228 is covered by a series of tryptic peptides. We observed phosphorylation on T185 but not S228. The Mass Spec analysis was carried out by Dr Roman Fischer. The result has been published by Wilson, *et al.* [246].

Appendix E Results of the survival assay against different damaging agents in lymphoblastoid cells

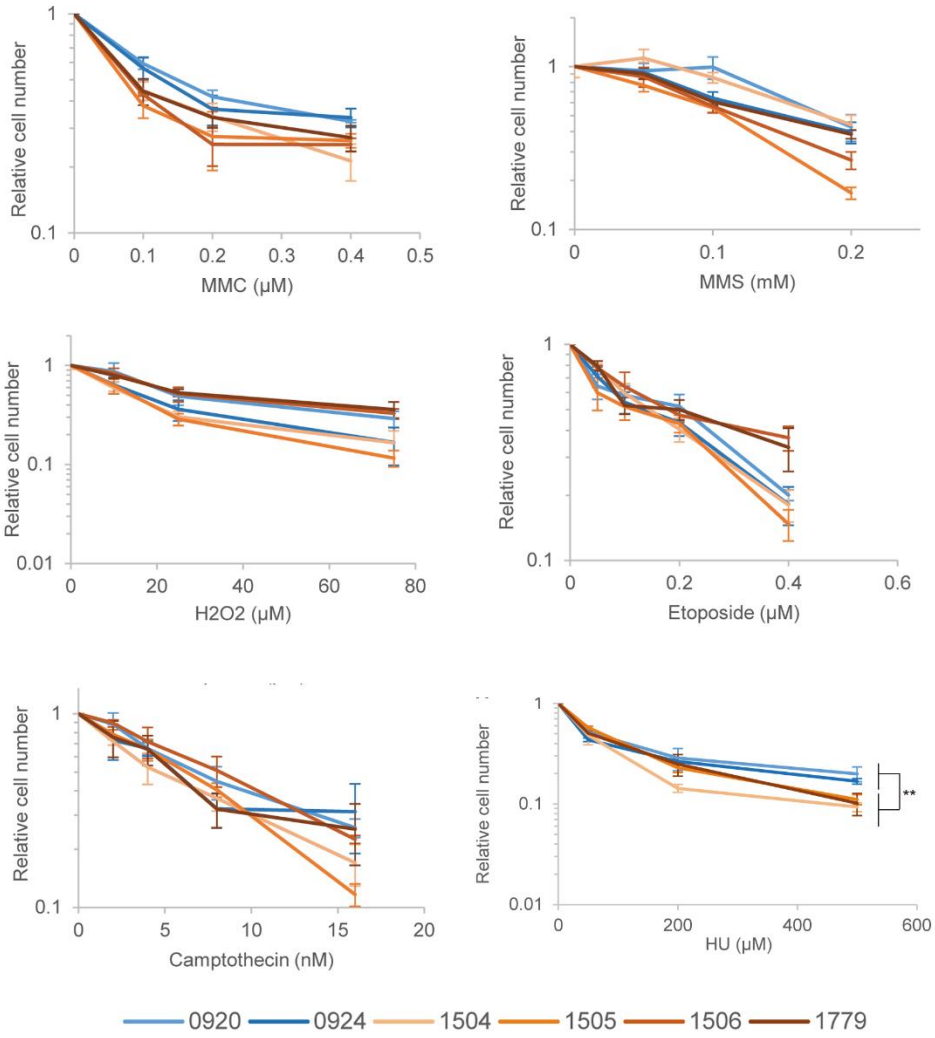


Figure E1 PCNA^{S228I} lymphoblastoid cells are not significantly more sensitive to many DNA damaging agents except HU at high doses. Graphs show relative cell number for PCNA$^{S228I/S228I}$ and PCNA$^{WT/WT}$ lymphoblasts treated with indicated treatments of certain chemical agents for three days, relative to vehicle treatment. n=3, error bars are SEM. ** $p<0.05$, student's t-test. (R. Wilson personal communication)

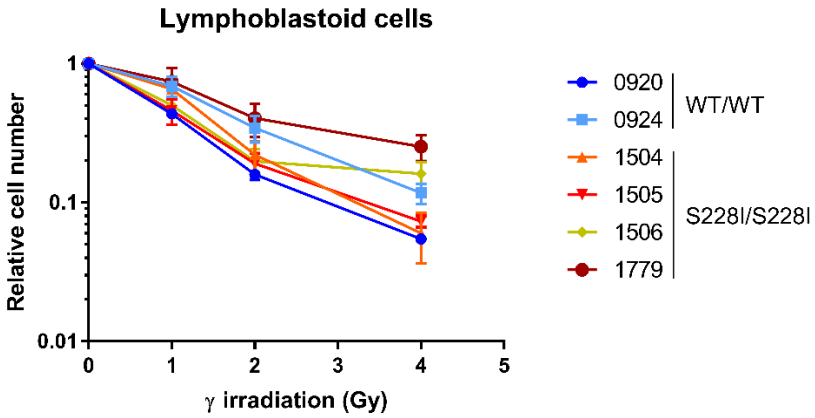


Figure E2 PCNA^{S228I} lymphoblastoid cells are not significantly more sensitive to IR. Graphs show relative cell number for PCNA$^{S228I/S228I}$ and PCNA$^{WT/WT}$ lymphoblasts treated with indicated treatment of gamma irradiation for five-day recovery, relative to vehicle treatment. n=3, error bars are SEM. (R. Wilson personal communication)

Appendix F Results of DNA fibre assay upon PARGi treatment

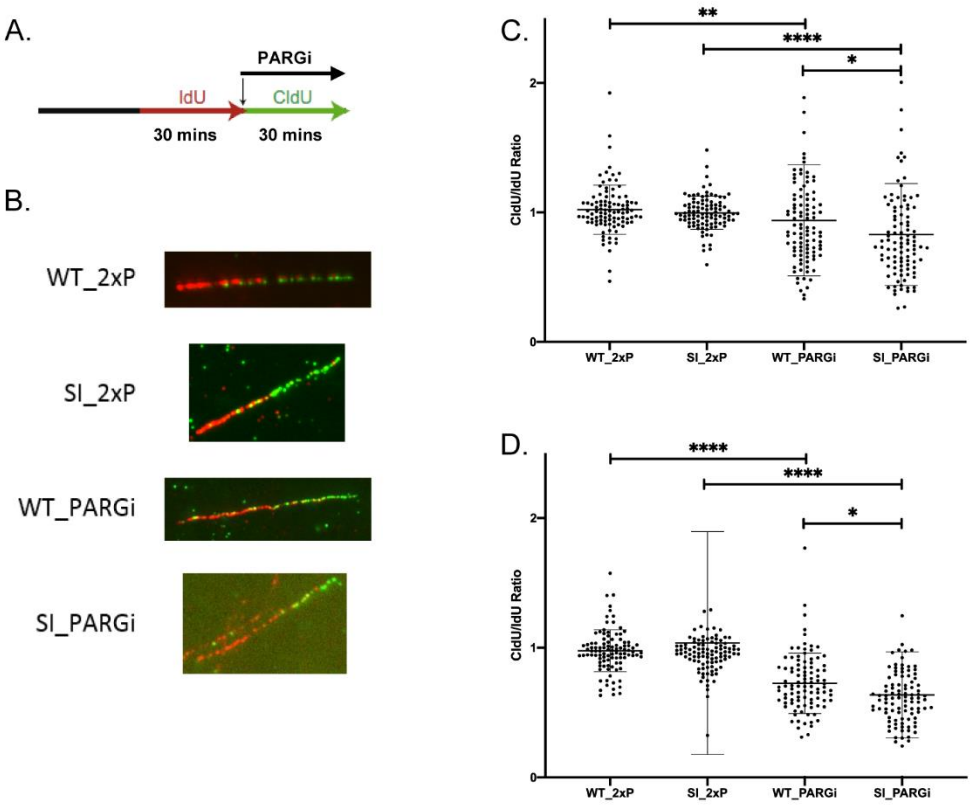


Figure F PCNA^{S228I} cells show slower DNA replication progression upon PARGi treatment. A) Graphical representation of the conditions of the DNA fibre assays with PARGi treatment. B) Images of average DNA fibre per each test. C and D) Dot plot with mean and standard deviation (SD) of two replicates. WT: wild-type control, SI: S228I. 2xP is the vehicle treatment. * $p<0.05$, ** $p<0.01$, **** $p<0.0001$. (Bernice Chan personal communication)

References

[1] Bell, S. P., & Dutta, A. (2002). DNA replication in eukaryotic cells. Annual review of biochemistry, 71(1), 333-374.

[2] Lord, C. J., & Ashworth, A. (2012). The DNA damage response and cancer therapy. Nature, 481(7381), 287.

[3] Hanahan, D., & Weinberg, R. A. (2011). Hallmarks of cancer: the next generation. cell, 144(5), 646-674.

[4] López-Otín, C., Blasco, M. A., Partridge, L., Serrano, M., & Kroemer, G. (2013). The hallmarks of aging. Cell, 153(6), 1194-1217.

[5] WATSON, J., & CRICK, F. (1953). Genetical Implications of the Structure of Deoxyribonucleic Acid. Nature, 171(4361), 964.

[6] Meselson, M., & Stahl, F. W. (1958). The replication of DNA in Escherichia coli. Proceedings of the national academy of sciences, 44(7), 671-682.

[7] Oka, A., Sugimoto, K., Takanami, M., & Hirota, Y. (1980). Replication origin of the Escherichia coli K-12 chromosome: the size and structure of the minimum DNA segment carrying the information for autonomous replication. Molecular and General Genetics MGG, 178(1), 9-20.

[8] Fuller, R. S., Funnell, B. E., & Kornberg, A. (1984). The dnaA protein complex with the E. coli chromosomal replication origin (oriC) and other DNA sites. Cell, 38(3), 889-900.

[9] Baker, T. A., Sekimizu, K., Funnell, B. E., & Kornberg, A. (1986). Extensive unwinding of the plasmid template during staged enzymatic initiation of DNA replication from the origin of the Escherichia coli chromosome. Cell, 45(1), 53-64.

[10] Arai, K. I., & Kornberg, A. (1981). Mechanism of dnaB protein action. III. Allosteric role of ATP in the alteration of DNA structure by dnaB protein in priming replication. Journal of Biological Chemistry, 256(10), 5260-5266.

[11] Huberman, J. A., Spotila, L. D., Nawotka, K. A., El-Assouli, S. M., & Davis, L. R. (1987). The in vivo replication origin of the yeast 2μm plasmid. Cell, 51(3), 473-481.

[12] Bell, S. P., & Stillman, B. (1992). ATP-dependent recognition of eukaryotic origins of DNA replication by a multiprotein complex. Nature, 357(6374), 128.

[13] Chuang, R. Y., & Kelly, T. J. (1999). The fission yeast homologue of Orc4p binds to replication origin DNA via multiple AT-hooks. Proceedings of the National Academy of Sciences, 96(6), 2656-2661.

[14] Okuno, Y., Satoh, H., Sekiguchi, M., & Masukata, H. (1999). Clustered adenine/thymine stretches are essential for function of a fission yeast replication origin. Molecular and cellular biology, 19(10), 6699-6709.

[15] Harland, R. M., & Laskey, R. A. (1980). Regulated replication of DNA microinjected into eggs of Xenopus laevis. Cell, 21(3), 761-771.

[16] Méchali, M. (2010). Eukaryotic DNA replication origins: many choices for appropriate answers. Nature reviews Molecular cell biology, 11(10), 728.

[17] Liang, C., Weinreich, M., & Stillman, B. (1995). ORC and Cdc6p interact and determine the frequency of initiation of DNA replication in the genome. Cell, 81(5), 667-676.

[18] Maiorano, D., Moreau, J., & Méchali, M. (2000). XCDT1 is required for the assembly of pre-replicative complexes in Xenopus laevis. Nature, 404(6778), 622.

[19] Donovan, S., Harwood, J., Drury, L. S., & Diffley, J. F. (1997). Cdc6p-dependent loading of Mcm proteins onto pre-replicative chromatin in budding yeast. Proceedings of the National Academy of Sciences, 94(11), 5611-5616.

[20] Diffley, J. F., Cocker, J. H., Dowell, S. J., & Rowley, A. (1994). Two steps in the assembly of complexes at yeast replication origins in vivo. Cell, 78(2), 303-316.

[21] Nguyen, V. Q., Co, C., & Li, J. J. (2001). Cyclin-dependent kinases prevent DNA re-replication through multiple mechanisms. Nature, 411(6841), 1068.

[22] Wohlschlegel, J. A., Dwyer, B. T., Dhar, S. K., Cvetic, C., Walter, J. C., & Dutta, A. (2000). Inhibition of eukaryotic DNA replication by geminin binding to Cdt1. Science, 290(5500), 2309-2312.

[23] Sheu, Y. J., & Stillman, B. (2010). The Dbf4–Cdc7 kinase promotes S phase by alleviating an inhibitory activity in Mcm4. Nature, 463(7277), 113.

[24] Randell, J. C., Fan, A., Chan, C., Francis, L. I., Heller, R. C., Galani, K., & Bell, S. P. (2010). Mec1 is one of multiple kinases that prime the Mcm2-7 helicase for phosphorylation by Cdc7. Molecular cell, 40(3), 353-363.

[25] Heller, R. C., Kang, S., Lam, W. M., Chen, S., Chan, C. S., & Bell, S. P. (2011). Eukaryotic origin-dependent DNA replication in vitro reveals sequential action of DDK and S-CDK kinases. Cell, 146(1), 80-91.

[26] Pacek, M., Tutter, A. V., Kubota, Y., Takisawa, H., & Walter, J. C. (2006). Localization of MCM2-7, Cdc45, and GINS to the site of DNA unwinding during eukaryotic DNA replication. Molecular cell, 21(4), 581-587.

[27] Bicknell, L. S., Bongers, E. M., Leitch, A., Brown, S., Schoots, J., Harley, M. E., ... & Van Bokhoven, H. (2011). Mutations in the pre-replication complex cause Meier-Gorlin syndrome. Nature genetics, 43(4), 356.

[28] Hughes, C. R., Guasti, L., Meimaridou, E., Chuang, C. H., Schimenti, J. C., King, P. J., ... & Metherell, L. A. (2012). MCM4 mutation causes adrenal failure, short stature, and natural killer cell deficiency in humans. The Journal of clinical investigation, 122(3), 814-820.

[29] Kornberg, A., Lehman, I. R., Bessman, M. J., & Simms, E. S. (1956). Enzymic synthesis of deoxyribonucleic acid. Biochimica et Biophysica Acta, 21(1), 197-198.

[30] Moyer, S. E., Lewis, P. W., & Botchan, M. R. (2006). Isolation of the Cdc45/Mcm2–7/GINS (CMG) complex, a candidate for the eukaryotic DNA replication fork helicase. Proceedings of the National Academy of Sciences, 103(27), 10236-10241.

[31] Snedeker, J., Wooten, M., & Chen, X. (2017). The inherent asymmetry of DNA replication. Annual review of cell and developmental biology, 33, 291-318.

[32] Pursell, Z. F., Isoz, I., Lundström, E. B., Johansson, E., & Kunkel, T. A. (2007). Yeast DNA polymerase ε participates in leading-strand DNA replication. Science, 317(5834), 127-130.

[33] Aria, V., & Yeeles, J. T. (2019). Mechanism of bidirectional leading-strand synthesis establishment at eukaryotic DNA replication origins. Molecular cell, 73(2), 199-211.

[34] Morrison, A., & Sugino, A. (1994). The 3′→ 5′ exonucleases of both DNA polymerases δ and ε participate in correcting errors of DNA replication in Saccharomyces cerevisiae. Molecular and General Genetics MGG, 242(3), 289-296.

[35] Sengupta, S., Van Deursen, F., de Piccoli, G., & Labib, K. (2013). Dpb2 integrates the leading-strand DNA polymerase into the eukaryotic replisome. Current Biology, 23(7), 543-552.

[36] Palles, C., Cazier, J. B., Howarth, K. M., Domingo, E., Jones, A. M., Broderick, P., ... & Sherborne, A. (2013). Germline mutations affecting the proofreading domains of POLE and POLD1 predispose to colorectal adenomas and carcinomas. Nature genetics, 45(2), 136.

[37] Hansen, M. F., Johansen, J., Bjørnevoll, I., Sylvander, A. E., Steinsbekk, K. S., Sætrom, P., ... & Sjursen, W. (2015). A novel POLE mutation associated with cancers of colon, pancreas, ovaries and small intestine. Familial cancer, 14(3), 437-448.

[38] Logan, C. V., Murray, J. E., Parry, D. A., Robertson, A., Bellelli, R., Tarnauskaitė, Ž., ... & Santoyo-Lopez, J. (2018). DNA polymerase epsilon deficiency causes IMAGe syndrome with variable immunodeficiency. The American Journal of Human Genetics, 103(6), 1038-1044.

[39] Sakabe, K., & Okazaki, R. (1966). A unique property of the replicating region of chromosomal DNA. Biochimica et Biophysica Acta (BBA)-Nucleic Acids and Protein Synthesis, 129(3), 651-654.

[40] Okazaki, R., Okazaki, T., Sakabe, K., Sugimoto, K., & Sugino, A. (1968). Mechanism of DNA chain growth. I. Possible discontinuity and unusual secondary structure of newly synthesized chains. Proceedings of the National Academy of Sciences of the United States of America, 59(2), 598.

[41] GAUTSCHI, J. R., & CLARKSON, J. M. (1975). Discontinuous DNA Replication in Mouse P-815 Cells. European journal of biochemistry, 50(2), 403-412.

[42] Tseng, B. Y., & Goulian, M. (1975). DNA synthesis in human lymphocytes: Intermediates in DNA synthesis, in vitro and in vivo. Journal of molecular biology, 99(2), 317-337.

[43] Smith, D. J., & Whitehouse, I. (2012). Intrinsic coupling of lagging-strand synthesis to chromatin assembly. Nature, 483(7390), 434.

[44] Marians, K. J. (1992). Prokaryotic DNA replication. Annual review of biochemistry, 61(1), 673-715.

[45] Meyer, R. R., & Laine, P. S. (1990). The single-stranded DNA-binding protein of Escherichia coli. Microbiology and Molecular Biology Reviews, 54(4), 342-380.

[46] Okazaki, R., Arisawa, M., & Sugino, A. (1971). Slow joining of newly replicated DNA chains in DNA polymerase I-deficient Escherichia coli mutants. Proceedings of the National Academy of Sciences, 68(12), 2954-2957.

[47] Tseng, B. Y., & Goulian, M. (1975). Evidence for covalent association of RNA with nascent DNA in human lymphocytes. Journal of molecular biology, 99(2), 339-346.

[48] Pellegrini, L. (2012). The Pol α-primase complex. In The eukaryotic replisome: a guide to protein structure and function (pp. 157-169). Springer, Dordrecht.

[49] Ricke, R. M., & Bielinsky, A. K. (2004). Mcm10 regulates the stability and chromatin association of DNA polymerase-α. Molecular cell, 16(2), 173-185.

[50] Zhu, W., Ukomadu, C., Jha, S., Senga, T., Dhar, S. K., Wohlschlegel, J. A., ... & Dutta, A. (2007). Mcm10 and And-1/CTF4 recruit DNA polymerase α to chromatin for initiation of DNA replication. Genes & development, 21(18), 2288-2299.

[51] Alberts, B. M., Barry, J., Bedinger, P., Formosa, T., Jongeneel, C. V., & Kreuzer, K. N. (1983, January). Studies on DNA Replication in the Bacteriophage T4 in vitro System. In Cold Spring Harbor symposia on quantitative biology (Vol. 47, pp. 655-668). Cold Spring Harbor Laboratory Press.

[52] Baranovskiy, A. G., Babayeva, N. D., Zhang, Y., Gu, J., Suwa, Y., Pavlov, Y. I., & Tahirov, T. H. (2016). Mechanism of concerted RNA-DNA primer synthesis by the human primosome. Journal of Biological Chemistry, 291(19), 10006-10020.

[53] Tsurimoto, T., & Stillman, B. (1991). Replication factors required for SV40 DNA replication in vitro. I. DNA structure-specific recognition of a primer-template junction by eukaryotic DNA polymerases and their accessory proteins. Journal of Biological Chemistry, 266(3), 1950-1960.

[54] Zhang, G., Gibbs, E., Kelman, Z., O'Donnell, M., & Hurwitz, J. (1999). Studies on the interactions between human replication factor C and human proliferating cell nuclear antigen. Proceedings of the National Academy of Sciences, 96(5), 1869-1874.

[55] Chen, S., Levin, M. K., Sakato, M., Zhou, Y., & Hingorani, M. M. (2009). Mechanism of ATP-driven PCNA clamp loading by S. cerevisiae RFC. Journal of molecular biology, 388(3), 431-442.

[56] Cai, J., Yao, N., Gibbs, E., Finkelstein, J., Phillips, B., O'Donnell, M., & Hurwitz, J. (1998). ATP hydrolysis catalyzed by human replication factor C requires participation of multiple subunits. Proceedings of the National Academy of Sciences, 95(20), 11607-11612.

[57] Prelich, G., Tan, C. K., Kostura, M., Mathews, M. B., So, A. G., Downey, K. M., & Stillman, B. (1987). Functional identity of proliferating cell nuclear antigen and a DNA polymerase-δ auxiliary protein. Nature, 326(6112), 517.

[58] Tsurimoto, T., & Stillman, B. (1991). Replication factors required for SV40 DNA replication in vitro. II. Switching of DNA polymerase alpha and delta during initiation of leading and lagging strand synthesis. Journal of Biological Chemistry, 266(3), 1961-1968.

[59] Perera, R. L., Torella, R., Klinge, S., Kilkenny, M. L., Maman, J. D., & Pellegrini, L. (2013). Mechanism for priming DNA synthesis by yeast DNA polymerase α. Elife, 2, e00482.

[60] Yuzhakov, A., Kelman, Z., Hurwitz, J., & O'Donnell, M. (1999). Multiple competition reactions for RPA order the assembly of the DNA polymerase δ holoenzyme. The EMBO Journal, 18(21), 6189-6199.

[61] Johansson, E., & Dixon, N. (2013). Replicative DNA polymerases. Cold Spring Harbor perspectives in biology, 5(6), a012799.

[62] Acharya, N., Klassen, R., Johnson, R. E., Prakash, L., & Prakash, S. (2011). PCNA binding domains in all three subunits of yeast DNA polymerase δ modulate its function in DNA replication. Proceedings of the National Academy of Sciences, 108(44), 17927-17932.

[63] Lessel, D., Hisama, F. M., Szakszon, K., Saha, B., Sanjuanelo, A. B., Salbert, B. A., ... & Plauchu, H. (2015). POLD1 germline mutations in patients initially diagnosed with Werner syndrome. Human mutation, 36(11), 1070-1079.

[64] Garg, P., Stith, C. M., Sabouri, N., Johansson, E., & Burgers, P. M. (2004). Idling by DNA polymerase δ maintains a ligatable nick during lagging-strand DNA replication. Genes & development, 18(22), 2764-2773.

[65] Qiu, J., Qian, Y., Frank, P., Wintersberger, U., & Shen, B. (1999). Saccharomyces cerevisiae RNase H (35) functions in RNA primer removal during lagging-strand DNA synthesis, most efficiently in cooperation with Rad27 nuclease. Molecular and cellular biology, 19(12), 8361-8371.

[66] Ishimi, Y., Claude, A., Bullock, P., & Hurwitz, J. (1988). Complete enzymatic synthesis of DNA containing the SV40 origin of replication. Journal of Biological Chemistry, 263(36), 19723-19733.

[67] Liu, Y., Kao, H. I., & Bambara, R. A. (2004). Flap endonuclease 1: a central component of DNA metabolism. Annual review of biochemistry, 73(1), 589-615.

[68] Murante, R. S., Rust, L., & Bambara, R. A. (1995). Calf 5′ to 3′

exo/endonuclease must slide from a 5′ end of the substrate to perform structure-specific cleavage. Journal of Biological Chemistry, 270(51), 30377-30383.

[69] Budd, M. E., & Campbell, J. L. (1997). A yeast replicative helicase, Dna2 helicase, interacts with yeast FEN-1 nuclease in carrying out its essential function. Molecular and cellular biology, 17(4), 2136-2142.

[70] Balakrishnan, L., Stewart, J., Polaczek, P., Campbell, J. L., & Bambara, R. A. (2010). Acetylation of Dna2 endonuclease/helicase and flap endonuclease 1 by p300 promotes DNA stability by creating long flap intermediates. Journal of Biological Chemistry, 285(7), 4398-4404.

[71] Stewart, J. A., Campbell, J. L., & Bambara, R. A. (2009). Dna2 is a structure-specific nuclease, with affinity for 5′-flap intermediates. Nucleic acids research, 38(3), 920-930.

[72] Bambara, R. A., Murante, R. S., & Henricksen, L. A. (1997). Enzymes and reactions at the eukaryotic DNA replication fork. Journal of Biological Chemistry, 272(8), 4647-4650.

[73] Hosfield, D. J., Mol, C. D., Shen, B., & Tainer, J. A. (1998). Structure of the DNA repair and replication endonuclease and exonuclease FEN-1: coupling DNA and PCNA binding to FEN-1 activity. Cell, 95(1), 135-146.

[74] Levin, D. S., McKenna, A. E., Motycka, T. A., Matsumoto, Y., & Tomkinson, A. E. (2000). Interaction between PCNA and DNA ligase I is critical for joining of Okazaki fragments and long-patch base-excision repair. Current Biology, 10(15), 919-S2.

[75] Zheng, L., Dai, H., Qiu, J., Huang, Q., & Shen, B. (2007). Disruption of the FEN-1/PCNA interaction results in DNA replication defects, pulmonary hypoplasia, pancytopenia, and newborn lethality in mice. Molecular and cellular biology, 27(8), 3176-3186.

[76] Dewar, J. M., & Walter, J. C. (2017). Mechanisms of DNA replication termination. Nature Reviews Molecular Cell Biology, 18(8), 507.

[77] Dimude, J., Midgley-Smith, S., Stein, M., & Rudolph, C. (2016). Replication termination: containing fork fusion-mediated pathologies in Escherichia coli. Genes, 7(8), 40.

[78] Duggin, I. G., Wake, R. G., Bell, S. D., & Hill, T. M. (2008). The replication fork trap and termination of chromosome replication. Molecular microbiology, 70(6), 1323-1333.

[79] Hiasa, H., & Marians, K. J. (1994). Tus prevents overreplication of oriC plasmid DNA. Journal of Biological Chemistry, 269(43), 26959-26968.

[80] Markovitz, A. (2005). A new in vivo termination function for DNA polymerase I of Escherichia coli K12. Molecular microbiology, 55(6), 1867-1882.

[81] McGuffee, S. R., Smith, D. J., & Whitehouse, I. (2013). Quantitative, genome-wide analysis of eukaryotic replication initiation and termination. Molecular cell, 50(1), 123-135.

[82] Maric, M., Maculins, T., De Piccoli, G., & Labib, K. (2014). Cdc48 and a ubiquitin ligase drive disassembly of the CMG helicase at the end of DNA replication. Science, 346(6208), 1253596.

[83] Moreno, S. P., Bailey, R., Campion, N., Herron, S., & Gambus, A. (2014). Polyubiquitylation drives replisome disassembly at the termination of DNA replication. Science, 346(6208), 477-481.

[84] Dewar, J. M., Budzowska, M., & Walter, J. C. (2015). The mechanism of DNA replication termination in vertebrates. Nature, 525(7569), 345.

[85] Dewar, J. M., Low, E., Mann, M., Räschle, M., & Walter, J. C. (2017). CRL2Lrr1 promotes unloading of the vertebrate replisome from chromatin during replication termination. Genes & development, 31(3), 275-290.

[86] Merlet, J., Burger, J., Tavernier, N., Richaudeau, B., Gomes, J. E., & Pintard, L. (2010). The CRL2LRR-1 ubiquitin ligase regulates cell cycle progression during C. elegans development. Development, 137(22), 3857-3866.

[87] Holliday, R. (1964). A mechanism for gene conversion in fungi. Genetics Research, 5(2), 282-304.

[88] Fishel, R. (2015). Mismatch repair. Journal of Biological Chemistry, 290(44), 26395-26403.

[89] McElhinny, S. A. N., Watts, B. E., Kumar, D., Watt, D. L., Lundström, E. B., Burgers, P. M., ... & Kunkel, T. A. (2010). Abundant ribonucleotide incorporation into DNA by yeast replicative polymerases. Proceedings of the National Academy of Sciences, 107(11), 4949-4954.

[90] McElhinny, S. A. N., Kumar, D., Clark, A. B., Watt, D. L., Watts, B. E., Lundström, E. B., ... & Kunkel, T. A. (2010). Genome instability due to ribonucleotide incorporation into DNA. Nature chemical biology, 6(10), 774.

[91] Sparks, J. L., Chon, H., Cerritelli, S. M., Kunkel, T. A., Johansson, E., Crouch, R. J., & Burgers, P. M. (2012). RNase H2-initiated ribonucleotide excision repair. Molecular cell, 47(6), 980-986.

[92] Bubeck, D., Reijns, M. A., Graham, S. C., Astell, K. R., Jones, E. Y., & Jackson, A. P. (2011). PCNA directs type 2 RNase H activity on DNA replication and repair substrates. Nucleic acids research, 39(9), 3652-3666.

[93] Crow, Y. J., Leitch, A., Hayward, B. E., Garner, A., Parmar, R., Griffith, E., ... & Baumann, C. (2006). Mutations in genes encoding ribonuclease H2 subunits cause Aicardi-Goutieres syndrome and mimic congenital viral brain infection. Nature genetics, 38(8), 910.

[94] Leonhardt, H., Page, A. W., Weier, H. U., & Bestor, T. H. (1992). A targeting sequence directs DNA methyltransferase to sites of DNA replication in mammalian nuclei. Cell, 71(5), 865-873.

[95] Chuang, L. S. H., Ian, H. I., Koh, T. W., Ng, H. H., Xu, G., & Li, B. F. (1997). Human DNA-(cytosine-5) methyltransferase-PCNA complex as a target for p21WAF1. Science, 277(5334), 1996-2000.

[96] Schermelleh, L., Haemmer, A., Spada, F., Rösing, N., Meilinger, D., Rothbauer, U., ... & Leonhardt, H. (2007). Dynamics of Dnmt1 interaction with the replication machinery and its role in postreplicative maintenance of DNA methylation. Nucleic acids research, 35(13), 4301-4312.

[97] Bostick, M., Kim, J. K., Estève, P. O., Clark, A., Pradhan, S., & Jacobsen, S. E. (2007). UHRF1 plays a role in maintaining DNA methylation in mammalian cells. Science, 317(5845), 1760-1764.

[98] Karagianni, P., Amazit, L., Qin, J., & Wong, J. (2008). ICBP90, a novel methyl K9 H3 binding protein linking protein ubiquitination with heterochromatin formation. Molecular and cellular biology, 28(2), 705-717.

[99] Verreault, A., Kaufman, P. D., Kobayashi, R., & Stillman, B. (1996). Nucleosome assembly by a complex of CAF-1 and acetylated histones H3/H4. Cell, 87(1), 95-104.

[100] Hoek, M., & Stillman, B. (2003). Chromatin assembly factor 1 is essential and couples chromatin assembly to DNA replication in vivo. Proceedings of the National Academy of Sciences, 100(21), 12183-12188.

[101] Shibahara, K. I., & Stillman, B. (1999). Replication-dependent marking of DNA by PCNA facilitates CAF-1-coupled inheritance of chromatin. Cell, 96(4), 575-585.

[102] Krawitz, D. C., Kama, T., & Kaufman, P. D. (2002). Chromatin assembly factor I mutants defective for PCNA binding require Asf1/Hir proteins for silencing. Molecular and cellular biology, 22(2), 614-625.

[103] Sancar, A., Lindsey-Boltz, L. A., Ünsal-Kaçmaz, K., & Linn, S. (2004). Molecular mechanisms of mammalian DNA repair and the DNA damage checkpoints. Annual review of biochemistry, 73(1), 39-85.

[104] McCullough, A. K., Dodson, M. L., & Lloyd, R. S. (1999). Initiation of base excision repair: glycosylase mechanisms and structures. Annual review of biochemistry, 68(1), 255-285.

[105] Satoh, M. S., & Lindahl, T. (1992). Role of poly (ADP-ribose) formation in DNA repair. Nature, 356(6367), 356.

[106] Caldecott, K. W. (2003). XRCC1 and DNA strand break repair. DNA repair, 2(9), 955-969.

[107] Ko, R., & Bennett, S. E. (2005). Physical and functional interaction of human nuclear uracil-DNA glycosylase with proliferating cell nuclear antigen. DNA repair, 4(12), 1421-1431.

[108] Klungland, A., & Lindahl, T. (1997). Second pathway for completion of human DNA base excision-repair: reconstitution with purified proteins and requirement for DNase IV (FEN1). The EMBO journal, 16(11), 3341-3348.

[109] Saleh-Gohari, N., Bryant, H. E., Schultz, N., Parker, K. M., Cassel, T. N., & Helleday, T. (2005). Spontaneous homologous recombination is induced by collapsed replication forks that are caused by endogenous DNA single-strand breaks. Molecular and cellular biology, 25(16), 7158-7169.

[110] Hoch, N. C., Hanzlikova, H., Rulten, S. L., Tétreault, M., Komulainen, E., Ju, L., ... & Staras, K. (2017). XRCC1 mutation is associated with PARP1 hyperactivation and cerebellar ataxia. Nature, 541(7635), 87.

[111] Chevillard, S., Radicella, J. P., Levalois, C., Lebeau, J., Poupon, M. F., Oudard, S., ... & Boiteux, S. (1998). Mutations in OGG1, a gene involved in the repair of oxidative DNA damage, are found in human lung and kidney tumours. Oncogene, 16(23), 3083.

[112] Sakumi, K., Tominaga, Y., Furuichi, M., Xu, P., Tsuzuki, T., Sekiguchi, M., & Nakabeppu, Y. (2003). Ogg1 knockout-associated lung tumorigenesis and its suppression by Mth1 gene disruption. Cancer research, 63(5), 902-905.

[113] Cheng, K. C., Cahill, D. S., Kasai, H., Nishimura, S., & Loeb, L. A. (1992). 8-Hydroxyguanine, an abundant form of oxidative DNA damage, causes G---- T and A----C substitutions. Journal of Biological Chemistry, 267(1), 166-172.

[114] Gillet, L. C., & Schärer, O. D. (2006). Molecular mechanisms of mammalian global genome nucleotide excision repair. Chemical reviews, 106(2), 253-276.

[115] Schärer, O. D. (2013). Nucleotide excision repair in eukaryotes. Cold Spring Harbor perspectives in biology, 5(10), a012609.

[116] Evans, E., Moggs, J. G., Hwang, J. R., Egly, J. M., & Wood, R. D. (1997). Mechanism of open complex and dual incision formation by human nucleotide excision repair factors. The EMBO journal, 16(21), 6559-6573.

[117] De Laat, W. L., Appeldoorn, E., Sugasawa, K., Weterings, E., Jaspers, N. G., & Hoeijmakers, J. H. (1998). DNA-binding polarity of human replication protein A positions nucleases in nucleotide excision repair. Genes & development, 12(16), 2598-2609.

[118] Fagbemi, A. F., Orelli, B., & Schärer, O. D. (2011). Regulation of endonuclease activity in human nucleotide excision repair. DNA repair, 10(7), 722-729.

[119] Staresincic, L., Fagbemi, A. F., Enzlin, J. H., Gourdin, A. M., Wijgers, N., Dunand-Sauthier, I., ... & Schärer, O. D. (2009). Coordination of dual incision and repair synthesis in human nucleotide excision repair. The EMBO journal, 28(8), 1111-1120.

[120] Marteijn, J. A., Lans, H., Vermeulen, W., & Hoeijmakers, J. H. (2014). Understanding nucleotide excision repair and its roles in cancer and ageing. Nature reviews Molecular cell biology, 15(7), 465.

[121] Lehmann, A. R., McGibbon, D., & Stefanini, M. (2011). Xeroderma pigmentosum. Orphanet journal of rare diseases, 6(1), 70.

[122] Masutani, C., Kusumoto, R., Yamada, A., Dohmae, N., Yokoi, M., Yuasa, M., ... & Hanaoka, F. (1999). The XPV (xeroderma pigmentosum variant) gene encodes human DNA polymerase η. Nature, 399(6737), 700.

[123] Karikkineth, A. C., Scheibye-Knudsen, M., Fivenson, E., Croteau, D. L., & Bohr, V. A. (2017). Cockayne syndrome: clinical features, model systems and pathways. Ageing research reviews, 33, 3-17.

[124] Lieber, M. R. (2010). The mechanism of double-strand DNA break repair by the nonhomologous DNA end-joining pathway. Annual review of biochemistry, 79, 181-211.

[125] Blier, P. R., Griffith, A. J., Craft, J., & Hardin, J. A. (1993). Binding of Ku protein to DNA. Measurement of affinity for ends and demonstration of binding to nicks. Journal of Biological Chemistry, 268(10), 7594-7601.

[126] Gu, J., Lu, H., Tippin, B., Shimazaki, N., Goodman, M. F., & Lieber, M. R. (2007). XRCC4: DNA ligase IV can ligate incompatible DNA ends and can ligate across gaps. The EMBO journal, 26(4), 1010-1023.

[127] Goodarzi, A. A., Yu, Y., Riballo, E., Douglas, P., Walker, S. A., Ye, R., ... & Lees-Miller, S. P. (2006). DNA-PK autophosphorylation facilitates Artemis endonuclease activity. The EMBO journal, 25(16), 3880-3889.

[128] Pryor, J. M., Waters, C. A., Aza, A., Asagoshi, K., Strom, C., Mieczkowski, P. A., ... & Ramsden, D. A. (2015). Essential role for polymerase specialization in cellular nonhomologous end joining. Proceedings of the National Academy of Sciences, 112(33), E4537-E4545.

[129] San Filippo, J., Sung, P., & Klein, H. (2008). Mechanism of eukaryotic homologous recombination. Annu. Rev. Biochem., 77, 229-257.

[130] Mailand, N., Bekker-Jensen, S., Faustrup, H., Melander, F., Bartek, J., Lukas, C., & Lukas, J. (2007). RNF8 ubiquitylates histones at DNA double-strand breaks and promotes assembly of repair proteins. Cell, 131(5), 887-900.

[131] Doil, C., Mailand, N., Bekker-Jensen, S., Menard, P., Larsen, D. H., Pepperkok, R., ... & Lukas, J. (2009). RNF168 binds and amplifies ubiquitin conjugates on damaged chromosomes to allow accumulation of repair proteins. Cell, 136(3), 435-446.

[132] Chen, L., Nievera, C. J., Lee, A. Y. L., & Wu, X. (2008). Cell cycle-dependent complex formation of BRCA1· CtIP· MRN is important for DNA double-strand break repair. Journal of Biological Chemistry, 283(12), 7713-7720.

[133] Zhang, F., Ma, J., Wu, J., Ye, L., Cai, H., Xia, B., & Yu, X. (2009). PALB2 links BRCA1 and BRCA2 in the DNA-damage response. Current Biology, 19(6), 524-529.

[134] Thorslund, T., & West, S. C. (2007). BRCA2: a universal recombinase regulator. Oncogene, 26(56), 7720.

[135] Li, X., Stith, C. M., Burgers, P. M., & Heyer, W. D. (2009). PCNA is required for initiation of recombination-associated DNA synthesis by DNA polymerase δ. Molecular cell, 36(4), 704-713.

[136] Petermann, E., Orta, M. L., Issaeva, N., Schultz, N., & Helleday, T. (2010). Hydroxyurea-stalled replication forks become progressively inactivated and require two different RAD51-mediated pathways for restart and repair. Molecular cell, 37(4), 492-502.

[137] van der Burg, M., van Veelen, L. R., Verkaik, N. S., Wiegant, W. W., Hartwig, N. G., Barendregt, B. H., ... & van Dongen, J. J. (2006). A new type of radiosensitive T–B–NK+ severe combined immunodeficiency caused by a LIG4 mutation. The Journal of clinical investigation, 116(1), 137-145.

[138] Noordzij, J. G., Verkaik, N. S., van der Burg, M., van Veelen, L. R., de Bruin-Versteeg, S., Wiegant, W., ... & van Gent, D. C. (2003). Radiosensitive SCID patients with Artemis gene mutations show a complete B-cell differentiation arrest at the pre–B-cell receptor checkpoint in bone marrow. Blood, 101(4), 1446-1452.

[139] Rosin, N., Elcioglu, N. H., Beleggia, F., Isgüven, P., Altmüller, J., Thiele, H., ... & Wollnik, B. (2015). Mutations in XRCC4 cause primary microcephaly, short stature and increased genomic instability. Human molecular genetics, 24(13), 3708-3717.

[140] Easton, D. F., Ford, D., & Bishop, D. T. (1995). Breast and ovarian cancer incidence in BRCA1-mutation carriers. Breast Cancer Linkage Consortium. American journal of human genetics, 56(1), 265.

[141] Deans, A. J., & West, S. C. (2011). DNA interstrand crosslink repair and cancer. Nature reviews cancer, 11(7), 467.

[142] Sasaki, M. S. (1975). Is Fanconi's anaemia defective in a process essential to the repair of DNA cross links?. Nature, 257(5526), 501.

[143] Moldovan, G. L., & D'Andrea, A. D. (2009). How the fanconi anemia pathway guards the genome. Annual review of genetics, 43, 223-249.

[144] Somyajit, K., Subramanya, S., & Nagaraju, G. (2012). Distinct roles of Fanco/RAD51C protein in DNA damage signaling and repair implications for fanconi anemia and breast cancer susceptibility. Journal of Biological Chemistry, 287(5), 3366-3380.

[145] Stoepker, C., Hain, K., Schuster, B., Hilhorst-Hofstee, Y., Rooimans, M. A., Steltenpool, J., ... & Jaspers, N. G. (2011). SLX4, a coordinator of structure-

specific endonucleases, is mutated in a new Fanconi anemia subtype. Nature genetics, 43(2), 138.

[146] Bogliolo, M., Schuster, B., Stoepker, C., Derkunt, B., Su, Y., Raams, A., ... & Casado, J. A. (2013). Mutations in ERCC4, encoding the DNA-repair endonuclease XPF, cause Fanconi anemia. The American Journal of Human Genetics, 92(5), 800-806.

[147] Zadorozhny, K., Sannino, V., Beláň, O., Mlčoušková, J., Špírek, M., Costanzo, V., & Krejčí, L. (2017). Fanconi-anemia-associated mutations destabilize RAD51 filaments and impair replication fork protection. Cell reports, 21(2), 333-340.

[148] Sawyer, S. L., Tian, L., Kähkönen, M., Schwartzentruber, J., Kircher, M., Majewski, J., ... & Moilanen, J. S. (2015). Biallelic mutations in BRCA1 cause a new Fanconi anemia subtype. Cancer discovery, 5(2), 135-142.

[149] Hira, A., Yoshida, K., Sato, K., Okuno, Y., Shiraishi, Y., Chiba, K., ... & Ito, E. (2015). Mutations in the gene encoding the E2 conjugating enzyme UBE2T cause Fanconi anemia. The American Journal of Human Genetics, 96(6), 1001-1007.

[150] Park, J. Y., Virts, E. L., Jankowska, A., Wiek, C., Othman, M., Chakraborty, S. C., ... & Andreassen, P. R. (2016). Complementation of hypersensitivity to DNA interstrand crosslinking agents demonstrates that XRCC2 is a Fanconi anaemia gene. Journal of medical genetics, 53(10), 672-680.

[151] Bluteau, D., Masliah-Planchon, J., Clairmont, C., Rousseau, A., Ceccaldi, R., d'Enghien, C. D., ... & Leblanc, T. (2016). Biallelic inactivation of REV7 is associated with Fanconi anemia. The Journal of clinical investigation, 126(9), 3580-3584.

[152] Knies, K., Inano, S., Ramírez, M. J., Ishiai, M., Surrallés, J., Takata, M., & Schindler, D. (2017). Biallelic mutations in the ubiquitin ligase RFWD3 cause Fanconi anemia. The Journal of clinical investigation, 127(8), 3013-3027.

[153] Kim, J. M., Kee, Y., Gurtan, A., & D'Andrea, A. D. (2008). Cell cycle–dependent chromatin loading of the Fanconi anemia core complex by FANCM/FAAP24. Blood, 111(10), 5215-5222.

[154] Alpi, A. F., & Patel, K. J. (2009). Monoubiquitylation in the Fanconi anemia DNA damage response pathway. DNA repair, 8(4), 430-435.

[155] Gurtan, A. M., Stuckert, P., & D'Andrea, A. D. (2006). The WD40 repeats of FANCL are required for Fanconi anemia core complex assembly. Journal of Biological Chemistry, 281(16), 10896-10905.

[156] Douwel, D. K., Boonen, R. A., Long, D. T., Szypowska, A. A., Räschle, M., Walter, J. C., & Knipscheer, P. (2014). XPF-ERCC1 acts in Unhooking DNA interstrand crosslinks in cooperation with FANCD2 and FANCP/SLX4. Molecular cell, 54(3), 460-471.

[157] Ciccia, A., McDonald, N., & West, S. C. (2008). Structural and functional relationships of the XPF/MUS81 family of proteins. Annu. Rev. Biochem., 77, 259-287.

[158] Hanada, K., Budzowska, M., Modesti, M., Maas, A., Wyman, C., Essers, J., & Kanaar, R. (2006). The structure-specific endonuclease Mus81–Eme1 promotes conversion of interstrand DNA crosslinks into double-strands breaks. The EMBO journal, 25(20), 4921-4932.

[159] Svendsen, J. M., Smogorzewska, A., Sowa, M. E., O'Connell, B. C., Gygi, S. P., Elledge, S. J., & Harper, J. W. (2009). Mammalian BTBD12/SLX4 assembles a Holliday junction resolvase and is required for DNA repair. Cell, 138(1), 63-77.

[160] Howlett, N. G., Harney, J. A., Rego, M. A., Kolling, F. W., & Glover, T. W. (2009). Functional interaction between the Fanconi Anemia D2 protein and proliferating cell nuclear antigen (PCNA) via a conserved putative PCNA interaction motif. Journal of Biological Chemistry, 284(42), 28935-28942.

[161] Stingele, J., Bellelli, R., & Boulton, S. J. (2017). Mechanisms of DNA–protein crosslink repair. Nature Reviews Molecular Cell Biology, 18(9), 563.

[162] Pommier, Y., Shar-yin, N. H., Gao, R., Das, B. B., Murai, J., & Marchand, C. (2014). Tyrosyl-DNA-phosphodiesterases (tdp1 and tdp2). DNA repair, 19, 114-129.

[163] Hartsuiker, E., Neale, M. J., & Carr, A. M. (2009). Distinct requirements for the Rad32^{Mre11} nuclease and Ctp1^{CtIP} in the removal of covalently bound topoisomerase I and II from DNA. Molecular cell, 33(1), 117-123.

[164] Stingele, J., Bellelli, R., Alte, F., Hewitt, G., Sarek, G., Maslen, S. L., ... & Skehel, J. M. (2016). Mechanism and regulation of DNA-protein crosslink repair by the DNA-dependent metalloprotease SPRTN. Molecular cell, 64(4), 688-703.

[165] Vaz, B., Popovic, M., Newman, J. A., Fielden, J., Aitkenhead, H., Halder, S., ... & Drobnitzky, N. (2016). Metalloprotease SPRTN/DVC1 orchestrates replication-coupled DNA-protein crosslink repair. Molecular cell, 64(4), 704-719.

[166] Centore, R. C., Yazinski, S. A., Tse, A., & Zou, L. (2012). Spartan/C1orf124, a reader of PCNA ubiquitylation and a regulator of UV-induced DNA damage response. Molecular cell, 46(5), 625-635.

[167] Lessel, D., Vaz, B., Halder, S., Lockhart, P. J., Marinovic-Terzic, I., Lopez-Mosqueda, J., ... & Cabrera, E. (2014). Mutations in SPRTN cause early onset hepatocellular carcinoma, genomic instability and progeroid features. Nature genetics, 46(11), 1239.

[168] Nyberg, K. A., Michelson, R. J., Putnam, C. W., & Weinert, T. A. (2002). Toward maintaining the genome: DNA damage and replication checkpoints. Annual review of genetics, 36(1), 617-656.

[169] Shiloh, Y. (1997). Ataxia-telangiectasia and the Nijmegen breakage syndrome: related disorders but genes apart. Annual review of genetics, 31.

[170] O'Driscoll, M., Ruiz-Perez, V. L., Woods, C. G., Jeggo, P. A., & Goodship, J. A. (2003). A splicing mutation affecting expression of ataxia–telangiectasia and Rad3–related protein (ATR) results in Seckel syndrome. Nature genetics, 33(4), 497.

[171] Smith, G. C., Cary, R. B., Lakin, N. D., Hann, B. C., Teo, S. H., Chen, D. J., & Jackson, S. P. (1999). Purification and DNA binding properties of the ataxia-telangiectasia gene product ATM. Proceedings of the National Academy of Sciences, 96(20), 11134-11139.

[172] Banin, S., Moyal, L., Shieh, S. Y., Taya, Y., Anderson, C. W., Chessa, L., ... & Ziv, Y. (1998). Enhanced phosphorylation of p53 by ATM in response to DNA damage. Science, 281(5383), 1674-1677.

[173] Bakkenist, C. J., & Kastan, M. B. (2003). DNA damage activates ATM through intermolecular autophosphorylation and dimer dissociation. Nature, 421(6922), 499.

[174] Ünsal-Kaçmaz, K., Makhov, A. M., Griffith, J. D., & Sancar, A. (2002). Preferential binding of ATR protein to UV-damaged DNA. Proceedings of the National Academy of Sciences, 99(10), 6673-6678.

[175] Abraham, R. T. (2001). Cell cycle checkpoint signaling through the ATM and ATR kinases. Genes & development, 15(17), 2177-2196.

[176] Zou, L., & Elledge, S. J. (2003). Sensing DNA damage through ATRIP recognition of RPA-ssDNA complexes. Science, 300(5625), 1542-1548.

[177] Zhao, H. U. I., & Piwnica-Worms, H. (2001). ATR-mediated checkpoint pathways regulate phosphorylation and activation of human Chk1. Molecular and cellular biology, 21(13), 4129-4139.

[178] Falck, J., Mailand, N., Syljuåsen, R. G., Bartek, J., & Lukas, J. (2001). The ATM–Chk2–Cdc25A checkpoint pathway guards against radioresistant DNA synthesis. Nature, 410(6830), 842.

[179] Shieh, S. Y., Ikeda, M., Taya, Y., & Prives, C. (1997). DNA damage-induced phosphorylation of p53 alleviates inhibition by MDM2. Cell, 91(3), 325-334.

[180] Xiong, Y., Hannon, G. J., Zhang, H., Casso, D., Kobayashi, R., & Beach, D. (1993). p21 is a universal inhibitor of cyclin kinases. Nature, 366(6456), 701.

[181] Waga, S., Hannon, G. J., Beach, D., & Stillman, B. (1994). The p21 inhibitor of cyclin-dependent kinases controls DNA replication by interaction with PCNA. Nature, 369(6481), 574.

[182] Burma, S., Chen, B. P., Murphy, M., Kurimasa, A., & Chen, D. J. (2001). ATM phosphorylates histone H2AX in response to DNA double-strand breaks. Journal of Biological Chemistry, 276(45), 42462-42467.

[183] Mathews, M. B., Bernstein, R. M., Franza Jr, B. R., & Garrels, J. I. (1984). Identity of the proliferating cell nuclear antigen and cyclin. Nature, 309(5966), 374.

[184] Tan, C. K., Castillo, C., So, A. G., & Downey, K. M. (1986). An auxiliary protein for DNA polymerase-delta from fetal calf thymus. Journal of Biological Chemistry, 261(26), 12310-12316.

[185] Moldovan, G. L., Pfander, B., & Jentsch, S. (2007). PCNA, the maestro of the replication fork. Cell, 129(4), 665-679.

[186] Kong, X. P., Onrust, R., O'Donnell, M., & Kuriyan, J. (1992). Three-dimensional structure of the β subunit of E. coli DNA polymerase III holoenzyme: a sliding DNA clamp. Cell, 69(3), 425-437.

[187] Stukenberg, P. T., Studwell-Vaughan, P. S., & O'Donnell, M. (1991). Mechanism of the sliding beta-clamp of DNA polymerase III holoenzyme. Journal of Biological Chemistry, 266(17), 11328-11334.

[188] Krishna, T. S., Kong, X. P., Gary, S., Burgers, P. M., & Kuriyan, J. (1994). Crystal structure of the eukaryotic DNA polymerase processivity factor PCNA. Cell, 79(7), 1233-1243.

[189] De March, M., Merino, N., Barrera-Vilarmau, S., Crehuet, R., Onesti, S., Blanco, F. J., & De Biasio, A. (2017). Structural basis of human PCNA sliding on DNA. Nature communications, 8, 13935.

[190] Ayyagari, R., Impellizzeri, K. J., Yoder, B. L., Gary, S. L., & Burgers, P. M. (1995). A mutational analysis of the yeast proliferating cell nuclear antigen indicates distinct roles in DNA replication and DNA repair. Molecular and Cellular Biology, 15(8), 4420-4429.

[191] Bowman, G. D., O'Donnell, M., & Kuriyan, J. (2004). Structural analysis of a eukaryotic sliding DNA clamp–clamp loader complex. Nature, 429(6993), 724.

[192] Naryzhny, S. N., Zhao, H., & Lee, H. (2005). Proliferating cell nuclear antigen (PCNA) may function as a double homotrimer complex in the mammalian cell. Journal of Biological Chemistry, 280(14), 13888-13894.

[193] Warbrick, E., Lane, D. P., Glover, D. M., & Cox, L. S. (1995). A small peptide inhibitor of DNA replication defines the site of interaction between the cyclin-dependent kinase inhibitor p21WAF1 and proliferating cell nuclear antigen. Current Biology, 5(3), 275-282.

[194] Gulbis, J. M., Kelman, Z., Hurwitz, J., O'Donnell, M., & Kuriyan, J. (1996). Structure of the C-terminal region of p21WAF1/CIP1 complexed with human PCNA. Cell, 87(2), 297-306.

[195] Warbrick, E., Lane, D. P., Glover, D. M., & Cox, L. S. (1997). Homologous regions of Fen1 and p21 Cip1 compete for binding to the same site on PCNA: a potential mechanism to co-ordinate DNA replication and repair. Oncogene, 14(19), 2313.

[196] Montecucco, A., Rossi, R., Levin, D. S., Gary, R., Park, M. S., Motycka, T. A., ... & Tomkinson, A. E. (1998). DNA ligase I is recruited to sites of DNA replication by an interaction with proliferating cell nuclear antigen: identification of a common targeting mechanism for the assembly of replication factories. The EMBO journal, 17(13), 3786-3795.

[197] Gary, R., Ludwig, D. L., Cornelius, H. L., MacInnes, M. A., & Park, M. S. (1997). The DNA repair endonuclease XPG binds to proliferating cell nuclear antigen (PCNA) and shares sequence elements with the PCNA-binding regions of FEN-1 and cyclin-dependent kinase inhibitor p21. Journal of Biological Chemistry, 272(39), 24522-24529.

[198] Warbrick, E., Lane, D. P., Glover, D. M., & Heatherington, W. (1998). PCNA binding proteins in Drosophila melanogaster: the analysis of a conserved PCNA binding domain. Nucleic acids research, 26(17), 3925-3932.

[199] Hishiki, A., Hashimoto, H., Hanafusa, T., Kamei, K., Ohashi, E., Shimizu, T., ... & Sato, M. (2009). Structural basis for novel interactions between human

translesion synthesis polymerases and proliferating cell nuclear antigen. Journal of Biological Chemistry, 284(16), 10552-10560.

[200] Armstrong, A. A., Mohideen, F., & Lima, C. D. (2012). Recognition of SUMO-modified PCNA requires tandem receptor motifs in Srs2. Nature, 483(7387), 59.

[201] Xu, H., Zhang, P., Liu, L., & Lee, M. Y. (2001). A novel PCNA-binding motif identified by the panning of a random peptide display library. Biochemistry, 40(14), 4512-4520.

[202] Gilljam, K. M., Feyzi, E., Aas, P. A., Sousa, M. M., Müller, R., Vågbø, C. B., ... & Krokan, H. E. (2009). Identification of a novel, widespread, and functionally important PCNA-binding motif. The Journal of cell biology, 186(5), 645-654.

[203] Shell, S. S., Putnam, C. D., & Kolodner, R. D. (2007). The N terminus of Saccharomyces cerevisiae Msh6 is an unstructured tether to PCNA. Molecular cell, 26(4), 565-578.

[204] Mailand, N., Gibbs-Seymour, I., & Bekker-Jensen, S. (2013). Regulation of PCNA–protein interactions for genome stability. Nature reviews Molecular cell biology, 14(5), 269.

[205] Dovrat, D., Stodola, J. L., Burgers, P. M., & Aharoni, A. (2014). Sequential switching of binding partners on PCNA during in vitro Okazaki fragment maturation. Proceedings of the National Academy of Sciences, 111(39), 14118-14123.

[206] Fridman, Y., Palgi, N., Dovrat, D., Ben-Aroya, S., Hieter, P., & Aharoni, A. (2010). Subtle alterations in PCNA-partner interactions severely impair DNA replication and repair. PLoS biology, 8(10), e1000507.

[207] Bruning, J. B., & Shamoo, Y. (2004). Structural and thermodynamic analysis of human PCNA with peptides derived from DNA polymerase-δ p66 subunit and flap endonuclease-1. Structure, 12(12), 2209-2219.

[208] Wang, S. C., Nakajima, Y., Yu, Y. L., Xia, W., Chen, C. T., Yang, C. C., ... & Hung, M. C. (2006). Tyrosine phosphorylation controls PCNA function through protein stability. Nature cell biology, 8(12), 1359.

[209] Cazzalini, O., Sommatis, S., Tillhon, M., Dutto, I., Bachi, A., Rapp, A., ... & Stivala, L. A. (2014). CBP and p300 acetylate PCNA to link its degradation with nucleotide excision repair synthesis. Nucleic acids research, 42(13), 8433-8448.

[210] Hoege, C., Pfander, B., Moldovan, G. L., Pyrowolakis, G., & Jentsch, S. (2002). RAD6-dependent DNA repair is linked to modification of PCNA by ubiquitin and SUMO. Nature, 419(6903), 135.

[211] Kannouche, P. L., Wing, J., & Lehmann, A. R. (2004). Interaction of human DNA polymerase η with monoubiquitinated PCNA: a possible mechanism for the polymerase switch in response to DNA damage. Molecular cell, 14(4), 491-500.

[212] Bienko, M., Green, C. M., Crosetto, N., Rudolf, F., Zapart, G., Coull, B., ... & Hofmann, K. (2005). Ubiquitin-binding domains in Y-family polymerases regulate translesion synthesis. Science, 310(5755), 1821-1824.

[213] Davies, A. A., Huttner, D., Daigaku, Y., Chen, S., & Ulrich, H. D. (2008). Activation of ubiquitin-dependent DNA damage bypass is mediated by replication protein a. Molecular cell, 29(5), 625-636.

[214] Huang, T. T., Nijman, S. M., Mirchandani, K. D., Galardy, P. J., Cohn, M. A., Haas, W., ... & D'Andrea, A. D. (2006). Regulation of monoubiquitinated PCNA by DUB autocleavage. Nature cell biology, 8(4), 341.

[215] Unk, I., Hajdú, I., Fátyol, K., Hurwitz, J., Yoon, J. H., Prakash, L., ... & Haracska, L. (2008). Human HLTF functions as a ubiquitin ligase for proliferating cell nuclear antigen polyubiquitination. Proceedings of the National Academy of Sciences, 105(10), 3768-3773.

[216] Motegi, A., Liaw, H. J., Lee, K. Y., Roest, H. P., Maas, A., Wu, X., ... & Myung, K. (2008). Polyubiquitination of proliferating cell nuclear antigen by HLTF and SHPRH prevents genomic instability from stalled replication forks. Proceedings of the National Academy of Sciences, 105(34), 12411-12416.

[217] Ciccia, A., Nimonkar, A. V., Hu, Y., Hajdu, I., Achar, Y. J., Izhar, L., ... & Livingston, D. M. (2012). Polyubiquitinated PCNA recruits the ZRANB3 translocase to maintain genomic integrity after replication stress. Molecular cell, 47(3), 396-409.

[218] Dua, R., Levy, D. L., Li, C. M., Snow, P. M., & Campbell, J. L. (2002). In Vivo Reconstitution of Saccharomyces cerevisiae DNA Polymerase ε in Insect Cells PURIFICATION AND CHARACTERIZATION. Journal of Biological Chemistry, 277(10), 7889-7896.

[219] Hogg, M., Osterman, P., Bylund, G. O., Ganai, R. A., Lundström, E. B., Sauer-Eriksson, A. E., & Johansson, E. (2014). Structural basis for processive DNA synthesis by yeast DNA polymerase ε. Nature structural & molecular biology, 21(1), 49.

[220] Chilkova, O., Stenlund, P., Isoz, I., Stith, C. M., Grabowski, P., Lundström, E. B., ... & Johansson, E. (2007). The eukaryotic leading and lagging strand DNA polymerases are loaded onto primer-ends via separate mechanisms but have comparable processivity in the presence of PCNA. Nucleic acids research, 35(19), 6588-6597.

[221] Harper, J. W., Adami, G. R., Wei, N., Keyomarsi, K., & Elledge, S. J. (1993). The p21 Cdk-interacting protein Cip1 is a potent inhibitor of G1 cyclin-dependent kinases. Cell, 75(4), 805-816.

[222] Umar, A., Buermeyer, A. B., Simon, J. A., Thomas, D. C., Clark, A. B., Liskay, R. M., & Kunkel, T. A. (1996). Requirement for PCNA in DNA mismatch repair at a step preceding DNA resynthesis. Cell, 87(1), 65-73.

[223] Clark, A. B., Valle, F., Drotschmann, K., Gary, R. K., & Kunkel, T. A. (2000). Functional interaction of proliferating cell nuclear antigen with MSH2-MSH6 and MSH2-MSH3 complexes. Journal of Biological Chemistry, 275(47), 36498-36501.

[224] Rowbotham, S. P., Barki, L., Neves-Costa, A., Santos, F., Dean, W., Hawkes, N., ... & Green, C. M. (2011). Maintenance of silent chromatin through replication requires SWI/SNF-like chromatin remodeler SMARCAD1. Molecular cell, 42(3), 285-296.

[225] Spada, F., Haemmer, A., Kuch, D., Rothbauer, U., Schermelleh, L., Kremmer, E., ... & Leonhardt, H. (2007). DNMT1 but not its interaction with the replication machinery is required for maintenance of DNA methylation in human cells. The Journal of cell biology, 176(5), 565-571.

[226] Shivji, M. K., Kenny, M. K., & Wood, R. D. (1992). Proliferating cell nuclear antigen is required for DNA excision repair. Cell, 69(2), 367-374.

[227] Shivji, M. K., Podust, V. N., Huebscher, U., & Wood, R. D. (1995). Nucleotide Excision Repair DNA Synthesis by DNA Polymerase. epsilon. in the Presence of PCNA, RFC, and RPA. Biochemistry, 34(15), 5011-5017.

[228] Fan, J., Otterlei, M., Wong, H. K., Tomkinson, A. E., & Wilson III, D. M. (2004). XRCC1 co-localizes and physically interacts with PCNA. Nucleic acids research, 32(7), 2193-2201.

[229] Otterlei, M., Warbrick, E., Nagelhus, T. A., Haug, T., Slupphaug, G., Akbari, M., ... & Krokan, H. E. (1999). Post-replicative base excision repair in replication foci. *The EMBO journal*, *18*(13), 3834-3844.

[230] Arias, E. E., & Walter, J. C. (2006). PCNA functions as a molecular platform to trigger Cdt1 destruction and prevent re-replication. Nature cell biology, 8(1), 84.

[231] Mansilla, S. F., Soria, G., Vallerga, M. B., Habif, M., Martínez-López, W., Prives, C., & Gottifredi, V. (2013). UV-triggered p21 degradation facilitates damaged-DNA replication and preserves genomic stability. Nucleic acids research, 41(14), 6942-6951.

[232] Saredi, G., Huang, H., Hammond, C. M., Alabert, C., Bekker-Jensen, S., Forne, I., ... & Cejka, P. (2016). H4K20me0 marks post-replicative chromatin and recruits the TONSL–MMS22L DNA repair complex. Nature, 534(7609), 714.

[233] Nakamura, K., Saredi, G., Becker, J. R., Foster, B. M., Nguyen, N. V., Beyer, T. E., ... & Chapman, J. R. (2019). H4K20me0 recognition by BRCA1-BARD1 directs homologous recombination to sister chromatids. Nat Cell Biol, 21(3), 311-318.

[234] Jørgensen, S., Eskildsen, M., Fugger, K., Hansen, L., Larsen, M. S. Y., Kousholt, A. N., ... & Sørensen, C. S. (2011). SET8 is degraded via PCNA-coupled CRL4 (CDT2) ubiquitylation in S phase and after UV irradiation. The Journal of cell biology, 192(1), 43-54.

[235] Havens, C. G., & Walter, J. C. (2011). Mechanism of CRL4Cdt2, a PCNA-dependent E3 ubiquitin ligase. Genes & development, 25(15), 1568-1582.

[236] Bruck, I., & O'Donnell, M. (2001). The ring-type polymerase sliding clamp family. Genome biology, 2(1), reviews3001-1.

[237] Lek, M., Karczewski, K. J., Minikel, E. V., Samocha, K. E., Banks, E., Fennell, T., ... & Tukiainen, T. (2016). Analysis of protein-coding genetic variation in 60,706 humans. Nature, 536(7616), 285.

[238] Waseem, N. H., Labib, K., Nurse, P., & Lane, D. P. (1992). Isolation and analysis of the fission yeast gene encoding polymerase delta accessory protein PCNA. The EMBO Journal, 11(13), 5111-5120.

[239] Henderson, D. S., Banga, S. S., Grigliatti, T. A., & Boyd, J. B. (1994). Mutagen sensitivity and suppression of position-effect variegation result from mutations in mus209, the Drosophila gene encoding PCNA. The EMBO Journal, 13(6), 1450-1459.

[240] Roa, S., Avdievich, E., Peled, J. U., MacCarthy, T., Werling, U., Kuang, F. L., ... & Edelmann, W. (2008). Ubiquitylated PCNA plays a role in somatic hypermutation and class-switch recombination and is required for meiotic

progression. Proceedings of the National Academy of Sciences, 105(42), 16248-16253.

[241] Langerak, P., Nygren, A. O., Krijger, P. H., van den Berk, P. C., & Jacobs, H. (2007). A/T mutagenesis in hypermutated immunoglobulin genes strongly depends on PCNAK164 modification. Journal of Experimental Medicine, 204(8), 1989-1998.

[242] Baple, E. L., Chambers, H., Cross, H. E., Fawcett, H., Nakazawa, Y., Chioza, B. A., ... & Muggenthaler, M. (2014). Hypomorphic PCNA mutation underlies a human DNA repair disorder. The Journal of clinical investigation, 124(7), 3137-3146.

[243] Perlman, S., Becker-Catania, S., & Gatti, R. A. (2003, September). Ataxia-telangiectasia: diagnosis and treatment. In Seminars in pediatric neurology (Vol. 10, No. 3, pp. 173-182). WB Saunders.

[244] DiGiovanna, J. J., & Kraemer, K. H. (2012). Shining a light on xeroderma pigmentosum. Journal of investigative dermatology, 132(3), 785-796.

[245] Duffy, C. M., Hilbert, B. J., & Kelch, B. A. (2016). A disease-causing variant in PCNA disrupts a promiscuous protein binding site. Journal of molecular biology, 428(6), 1023-1040.

[246] Wilson, R. H., Biasutto, A. J., Wang, L., Fischer, R., Baple, E. L., Crosby, A. H., ... & Green, C. M. (2017). PCNA dependent cellular activities tolerate dramatic perturbations in PCNA client interactions. DNA repair, 50, 22-35.

[247] Punchihewa, C., Inoue, A., Hishiki, A., Fujikawa, Y., Connelly, M., Evison, B., ... & Hashimoto, H. (2012). Identification of small molecule proliferating cell nuclear antigen (PCNA) inhibitor that disrupts interactions with PIP-box proteins and inhibits DNA replication. Journal of Biological Chemistry, 287(17), 14289-14300.

[248] Zhang, Z., Shibahara, K. I., & Stillman, B. (2000). PCNA connects DNA replication to epigenetic inheritance in yeast. Nature, 408(6809), 221.

[249] Eissenberg, J. C., Ayyagari, R., Gomes, X. V., & Burgers, P. M. (1997). Mutations in yeast proliferating cell nuclear antigen define distinct sites for interaction with DNA polymerase delta and DNA polymerase epsilon. Molecular and Cellular Biology, 17(11), 6367-6378.

[250] Lau, P. J., Flores-Rozas, H., & Kolodner, R. D. (2002). Isolation and characterization of new proliferating cell nuclear antigen (POL30) mutator mutants that are defective in DNA mismatch repair. Molecular and cellular biology, 22(19), 6669-6680.

[251] Amin, N. S., Nguyen, M. N., Oh, S., & Kolodner, R. D. (2001). exo1-Dependent mutator mutations: model system for studying functional interactions in mismatch repair. Molecular and cellular biology, 21(15), 5142-5155.

[252] Chambon, P., Weill, J. D., & Mandel, P. (1963). Nicotinamide mononucleotide activation of a new DNA-dependent polyadenylic acid synthesizing nuclear enzyme. Biochemical and biophysical research communications, 11(1), 39-43.

[253] Okayama, H., Edson, C. M., Fukushima, M., Ueda, K., & Hayaishi, O. (1977). Purification and properties of poly (adenosine diphosphate ribose) synthetase. Journal of Biological Chemistry, 252(20), 7000-7005.

[254] Amé, J. C., Rolli, V., Schreiber, V., Niedergang, C., Apiou, F., Decker, P., ... & de Murcia, G. (1999). PARP-2, A novel mammalian DNA damage-dependent poly (ADP-ribose) polymerase. Journal of Biological Chemistry, 274(25), 17860-17868.

[255] Chaudhuri, A. R., & Nussenzweig, A. (2017). The multifaceted roles of PARP1 in DNA repair and chromatin remodelling. Nature reviews Molecular cell biology, 18(10), 610.

[256] Jungmichel, S., Rosenthal, F., Altmeyer, M., Lukas, J., Hottiger, M. O., & Nielsen, M. L. (2013). Proteome-wide identification of poly(ADP-Ribosyl)ation targets in different genotoxic stress responses. Molecular cell, 52(2), 272-285.

[257] Barkauskaite, E., Jankevicius, G., & Ahel, I. (2015). Structures and mechanisms of enzymes employed in the synthesis and degradation of PARP-dependent protein ADP-ribosylation. Molecular cell, 58(6), 935-946.

[258] Koh, D. W., Lawler, A. M., Poitras, M. F., Sasaki, M., Wattler, S., Nehls, M. C., ... & Dawson, T. M. (2004). Failure to degrade poly (ADP-ribose) causes increased sensitivity to cytotoxicity and early embryonic lethality. Proceedings of the National Academy of Sciences, 101(51), 17699-17704.

[259] Kameshita, I., Matsuda, Z., Taniguchi, T., & Shizuta, Y. (1984). Poly (ADP-Ribose) synthetase. Separation and identification of three proteolytic fragments as the substrate-binding domain, the DNA-binding domain, and the automodification domain. Journal of biological chemistry, 259(8), 4770-4776.

[260] Berger, N. A., Sikorski, G. W., Petzold, S. J., & Kurohara, K. K. (1979). Association of poly (adenosine diphosphoribose) synthesis with DNA damage and repair in normal human lymphocytes. The Journal of clinical investigation, 63(6), 1164-1171.

[261] Durkacz, B. W., Omidiji, O., Gray, D. A., & Shall, S. (1980). (ADP-ribose) n participates in DNA excision repair. Nature, 283(5747), 593.

[262] Gradwohl, G., de Murcia, J. M., Molinete, M., Simonin, F., Koken, M., Hoeijmakers, J. H., & de Murcia, G. (1990). The second zinc-finger domain of poly (ADP-ribose) polymerase determines specificity for single-stranded breaks in DNA. Proceedings of the National Academy of Sciences, 87(8), 2990-2994.

[263] Satoh, M. S., & Lindahl, T. (1992). Role of poly (ADP-ribose) formation in DNA repair. Nature, 356(6367), 356.

[264] Masson, M., Niedergang, C., Schreiber, V., Muller, S., Menissier-de Murcia, J., & de Murcia, G. (1998). XRCC1 is specifically associated with poly (ADP-ribose) polymerase and negatively regulates its activity following DNA damage. Molecular and cellular biology, 18(6), 3563-3571.

[265] Pleschke, J. M., Kleczkowska, H. E., Strohm, M., & Althaus, F. R. (2000). Poly (ADP-ribose) binds to specific domains in DNA damage checkpoint proteins. Journal of Biological Chemistry, 275(52), 40974-40980.

[266] Dantzer, F., de la Rubia, G., Ménissier-de Murcia, J., Hostomsky, Z., de Murcia, G., & Schreiber, V. (2000). Base excision repair is impaired in mammalian cells lacking Poly (ADP-ribose) polymerase-1. Biochemistry, 39(25), 7559-7569.

[267] El-Khamisy, S. F., Masutani, M., Suzuki, H., & Caldecott, K. W. (2003). A requirement for PARP-1 for the assembly or stability of XRCC1 nuclear foci at sites of oxidative DNA damage. *Nucleic acids research*, *31*(19), 5526-5533.

[268] Ruscetti, T., Lehnert, B. E., Halbrook, J., Le Trong, H., Hoekstra, M. F., Chen, D. J., & Peterson, S. R. (1998). Stimulation of the DNA-dependent protein kinase by poly (ADP-ribose) polymerase. Journal of Biological Chemistry, 273(23), 14461-14467.

[269] Haince, J. F., Kozlov, S., Dawson, V. L., Dawson, T. M., Hendzel, M. J., Lavin, M. F., & Poirier, G. G. (2007). Ataxia telangiectasia mutated (ATM) signaling network is modulated by a novel poly (ADP-ribose)-dependent pathway in the early response to DNA-damaging agents. Journal of Biological Chemistry, 282(22), 16441-16453.

[270] Aguilar-Quesada, R., Muñoz-Gámez, J. A., Martín-Oliva, D., Peralta, A., Valenzuela, M. T., Matínez-Romero, R., ... & Oliver, F. J. (2007). Interaction between ATM and PARP-1 in response to DNA damage and sensitization of ATM deficient cells through PARP inhibition. BMC molecular biology, 8(1), 29.

[271] Li, M., & Yu, X. (2013). Function of BRCA1 in the DNA damage response is mediated by ADP-ribosylation. Cancer cell, 23(5), 693-704.

[272] Lehmann, A. R., Kirk-Bell, S., Shall, S., & Whish, W. J. D. (1974). The relationship between cell growth, macromolecular synthesis and poly ADP-ribose polymerase in lymphoid cells. Experimental cell research, 83(1), 63-72.

[273] Anachkova, B., Russev, G., & Poirier, G. G. (1989). DNA replication and poly (ADP-ribosyl) ation of chromatin. Cytobios, 58(236), 19-28.

[274] Simbulan-Rosenthal, C. M., Rosenthal, D. S., Boulares, A. H., Hickey, R. J., Malkas, L. H., Coll, J. M., & Smulson, M. E. (1998). Regulation of the expression or recruitment of components of the DNA synthesome by poly (ADP-ribose) polymerase. Biochemistry, 37(26), 9363-9370.

[275] Frouin, I., Maga, G., Denegri, M., Riva, F., Savio, M., Spadari, S., ... & Scovassi, A. I. (2003). Human proliferating cell nuclear antigen, poly (ADP-ribose) polymerase-1, and p21waf1/cip1 a dynamic exchange of partners. Journal of Biological Chemistry, 278(41), 39265-39268.

[276] Yang, Y. G., Cortes, U., Patnaik, S., Jasin, M., & Wang, Z. Q. (2004). Ablation of PARP-1 does not interfere with the repair of DNA double-strand breaks, but compromises the reactivation of stalled replication forks. Oncogene, 23(21), 3872.

[277] Bryant, H. E., Petermann, E., Schultz, N., Jemth, A. S., Loseva, O., Issaeva, N., ... & Helleday, T. (2009). PARP is activated at stalled forks to mediate Mre11-dependent replication restart and recombination. The EMBO journal, 28(17), 2601-2615.

[278] Dungrawala, H., Rose, K. L., Bhat, K. P., Mohni, K. N., Glick, G. G., Couch, F. B., & Cortez, D. (2015). The replication checkpoint prevents two types of fork collapse without regulating replisome stability. Molecular cell, 59(6), 998-1010.

[279] Haince, J. F., McDonald, D., Rodrigue, A., Déry, U., Masson, J. Y., Hendzel, M. J., & Poirier, G. G. (2008). PARP1-dependent kinetics of recruitment of MRE11 and NBS1 proteins to multiple DNA damage sites. Journal of Biological Chemistry, 283(2), 1197-1208.

[280] Ying, S., Hamdy, F. C., & Helleday, T. (2012). Mre11-dependent degradation of stalled DNA replication forks is prevented by BRCA2 and PARP1. Cancer research, 72(11), 2814-2821.

[281] Chaudhuri, A. R., Hashimoto, Y., Herrador, R., Neelsen, K. J., Fachinetti, D., Bermejo, R., ... & Lopes, M. (2012). Topoisomerase I poisoning results in

PARP-mediated replication fork reversal. Nature structural & molecular biology, 19(4), 417.

[282] Berti, M., Chaudhuri, A. R., Thangavel, S., Gomathinayagam, S., Kenig, S., Vujanovic, M., ... & Marino, F. (2013). Human RECQ1 promotes restart of replication forks reversed by DNA topoisomerase I inhibition. Nature structural & molecular biology, 20(3), 347.

[283] Hanzlikova, H., Kalasova, I., Demin, A. A., Pennicott, L. E., Cihlarova, Z., & Caldecott, K. W. (2018). The importance of poly (ADP-ribose) polymerase as a sensor of unligated Okazaki fragments during DNA replication. Molecular cell, 71(2), 319-331.

[284] Farmer, H., McCabe, N., Lord, C. J., Tutt, A. N., Johnson, D. A., Richardson, T. B., ... & Martin, N. M. (2005). Targeting the DNA repair defect in BRCA mutant cells as a therapeutic strategy. Nature, 434(7035), 917.

[285] Zaremba, T., & Curtin, N. J. (2007). PARP inhibitor development for systemic cancer targeting. Anti-Cancer Agents in Medicinal Chemistry (Formerly Current Medicinal Chemistry-Anti-Cancer Agents), 7(5), 515-523.

[286] Kedar, P. S., Stefanick, D. F., Horton, J. K., & Wilson, S. H. (2012). Increased PARP-1 association with DNA in alkylation damaged, PARP-inhibited mouse fibroblasts. Molecular Cancer Research, 10(3), 360-368.

[287] Murai, J., Shar-yin, N. H., Das, B. B., Renaud, A., Zhang, Y., Doroshow, J. H., ... & Pommier, Y. (2012). Trapping of PARP1 and PARP2 by clinical PARP inhibitors. Cancer research, 72(21), 5588-5599.

[288] Xu, G., Chapman, J. R., Brandsma, I., Yuan, J., Mistrik, M., Bouwman, P., ... & Jaspers, J. E. (2015). REV7 counteracts DNA double-strand break resection and affects PARP inhibition. Nature, 521(7553), 541.

[289] Ghezraoui, H., Oliveira, C., Becker, J. R., Bilham, K., Moralli, D., Anzilotti, C., ... & Bonham, S. (2018). 53BP1 cooperation with the REV7–shieldin complex underpins DNA structure-specific NHEJ. Nature, 560(7716), 122.

[290] Lord, C. J., & Ashworth, A. (2016). BRCAness revisited. Nature Reviews Cancer, 16(2), 110.

[291] Zimmermann, M., Murina, O., Reijns, M. A., Agathanggelou, A., Challis, R., Tarnauskaitė, Ž., ... & Yuan, W. (2018). CRISPR screens identify genomic ribonucleotides as a source of PARP-trapping lesions. Nature, 559(7713), 285.

[292] Deveau, H., Garneau, J. E., & Moineau, S. (2010). CRISPR/Cas system and its role in phage-bacteria interactions. Annual review of microbiology, 64, 475-493.

[293] Hsu, P. D., Scott, D. A., Weinstein, J. A., Ran, F. A., Konermann, S., Agarwala, V., ... & Cradick, T. J. (2013). DNA targeting specificity of RNA-guided Cas9 nucleases. Nature biotechnology, 31(9), 827.

[294] Ran, F. A., Hsu, P. D., Wright, J., Agarwala, V., Scott, D. A., & Zhang, F. (2013). Genome engineering using the CRISPR-Cas9 system. Nature protocols, 8(11), 2281.

[295] Liu, P., Jenkins, N. A., & Copeland, N. G. (2003). A highly efficient recombineering-based method for generating conditional knockout mutations. Genome research, 13(3), 476-484.

[296] Wade, M., & Allday, M. J. (2000). Epstein-Barr virus suppresses a G2/M checkpoint activated by genotoxins. Molecular and cellular biology, 20(4), 1344-1360.

[297] Sugimura, K., Takebayashi, S. I., Taguchi, H., Takeda, S., & Okumura, K. (2008). PARP-1 ensures regulation of replication fork progression by homologous recombination on damaged DNA. J Cell Biol, 183(7), 1203-1212.

[298] Fortini, P., & Dogliotti, E. (2007). Base damage and single-strand break repair: mechanisms and functional significance of short-and long-patch repair subpathways. DNA repair, 6(4), 398-409.

[299] Eales, K. L., Hollinshead, K. E. R., & Tennant, D. A. (2016). Hypoxia and metabolic adaptation of cancer cells. Oncogenesis, 5(1), e190.

[300] Uttara, B., Singh, A. V., Zamboni, P., & Mahajan, R. T. (2009). Oxidative stress and neurodegenerative diseases: a review of upstream and downstream antioxidant therapeutic options. Current neuropharmacology, 7(1), 65-74.

[301] Bae, S. H., Bae, K. H., Kim, J. A., & Seo, Y. S. (2001). RPA governs endonuclease switching during processing of Okazaki fragments in eukaryotes. Nature, 412(6845), 456.